universität wien

DISSERTATION / DOCTORAL THESIS

Titel der Dissertation /Title of the Doctoral Thesis

„The Functional Characterization of JMJ27 in

Arabidopsis thaliana“

verfasst von / submitted by

Atıl Çağdaş Saydere

angestrebter akademischer Grad / in partial fulfilment of the requirements for the degree of

Doctor of Philosophy (PhD)

Wien, 2017 / Vienna 2017

Studienkennzahl lt. Studienblatt / degree programme code as it appears on the student record sheet:	A 094 490
Dissertationsgebiet lt. Studienblatt / field of study as it appears on the student record sheet:	Molekulare Biologie
Betreut von / Supervisor:	Doz. Dipl.-Biol. Dr. Ortrun Mittelsten Scheid

Acknowledgements

First, I want to express my gratitude to Ortrun Mittelsten Scheid for offering her help and making it possible to finish my degree. I am thankful to her as my supervisor in the final phase of my PhD and for her helpful comments and the review of my thesis.

I am thankful to Ines Crisostomo for her guidance to finish my degree and her efforts in Vienna for the procedures to be completed.

I thank to Hisashi Tamaru for giving me the opportunity to be part of his team and do research in his lab with his scientific support.

I am grateful to my colleagues Nina Chumak, Vera Schoft, Lucyna Slusarz, Magdalena Mosiolek, Adriana Machlicova, Marcelina Garcia-Aguilar, Andrea Raganelli, Zsuzsanna Mérai, Janos Bindics, Stephanie Arnoux and Martin Xavier. Thank you all for sharing your knowledge with me from my first day in the lab until the last and helping me at various stages of my project. Thank you all for your friendship over the years. I miss our coffee breaks.

I would like to thank to my thesis committee members; Andreas Bachmair, Tim Clausen and Kazufumi Mochizuki for their comments and suggestions during my PhD.

I want to thank to Peter Schlögelhofer for his advice on the generation of expression constructs.

I am thankful to the service I received from the BioOptics Facility. My special thanks to Pawel Pasierbek for sharing his expertise and technical support on microscopy.

I thank to Protein Chemistry Facility for their Mass Spectrometry service. I am grateful to Karl Mechtler for his suggestions on the protocol. I thank to Susanne Opravil for the sample preparation and running the experiment, and Richard Imre for the bioinformatic analysis of the results.

I am grateful for the friendly environment and the stimulating intellectual atmosphere within the GMI. I thank to all members of GMI for creating a work place enjoyable and for maintaining the high-quality research. I will be always proud to be a part of the GMI family.

I thank to Ümit Seren and Fernando Rabanal for their friendship and all the laughs we shared. I miss our movie nights and having a drink together. A special thanks to Ümit for being the best DJ partner!

I thank to Derya Donertas for her support during difficult times and for everything we shared together.

I thank to my fellows in Pavia for making my student life less stressful and for keeping my mood positive. I thank to Anna Czcz for encouraging me to finish my thesis on time.

Finally, I want to thank my family for their continuous support and love through the years.

To my beloved grandparents;

Melek & Abdullah

Abstract

The dynamic structure of chromatin, switching between open euchromatin and compact heterochromatin state, enables the regulation of diverse cellular events. In contrast to the mechanisms known for heterochromatin formation and maintenance, little is known about the processes involved in heterochromatin dissociation and switches to a different state. Here, I use the model organism *Arabidopsis thaliana* that has a unique male gametophyte (pollen) structure with nuclei of different heterochromatin organization to understand these chromatin dynamics. Unlike animals, where the male gametophyte is produced at the end of meiosis, flowering plants generate pollen by two mitotic divisions following meiosis. Moreover, an asymmetric mitosis with incomplete cytokinesis gives rise to two cells: a generative (sperm) cell and a vegetative cell, with different chromatin condensation levels. Since a mitosis event differentiates these cells, it is likely that an active process is responsible for these differential chromatin states. Histone 3 lysine 9 di-methylation (H3K9me2) is known as a mark of constitutive heterochromatin. Not long ago, histone methylation events were believed to be irreversible, until a lysine-specific histone demethylase 1A (LSD1) was discovered. Later, a second class of histone demethylases (JmjC domain-containing protein family) was discovered, and the implications of heterochromatin on cell fate and metabolism were re-considered. One member of the JmjC domain-containing family, a putative histone demethylase JMJ27 (AT4G0099), was found to be involved in H3K9me2 demethylation and DNA hypomethylation at 45S rDNA promoters in *Arabidopsis thaliana* (Chumak 2012). A mutation in the *JMJ27* gene causes retaining of H3K9me2 that co-localizes with 45S rDNA repeats in pollen vegetative nuclei, concomitant with increased DNA methylation at 45S rDNA promoters. I contributed to that work by generating a construct encoding a fluorescent tagged JMJ27 that was used to test expression, subcellular localization and complementation.

In my study, I further created transgenic lines and utilized them to address several questions regarding the function of JMJ27. I tested the histone demethylation activity of JMJ27 by inducing a mutation at the catalytic site of the JmjC domain known to be essential for the histone demethylase activity of JmjC domain family members. Inspection of pollen vegetative nuclei revealed that JMJ27 has a functional JmjC domain and is required for H3K9me2 demethylase activity *in vivo*. An epitope-tagged JMJ27 line was used to perform co-immunoprecipitation coupled with mass spectrometry to identify possible interactors. This might elucidate the network of factors and the role of JMJ27 in modulating histone and DNA demethylation at 45S rDNA loci. Among a list of multiple candidates, nine proteins were highlighted by functional annotation clustering analysis to have a higher chance of cooperation with JMJ27. Cytology-based preliminary tests in pollen

showed supporting results for three of these candidates which were screened: EMB1644/LSM4, EMB1138 and CCR2/GRP7. However, future studies are needed to confirm any of these interactions by additional methods and evaluating the significance of such interactions with JMJ27 in a larger framework.

Zusammenfasung

Die dynamische Struktur des Chromatins, die zwischen offenem Euchromatin und komplettem Heterochromatin-Zustand umschaltet, ermöglicht die Regulierung diverser zellulärer Ereignisse. Im Gegensatz zu den Mechanismen, die für die Heterochromatinbildung und -pflege bekannt sind, ist wenig über die Prozesse bekannt, die an der Heterochromatin-Dissoziation beteiligt sind, und wechselt in einen anderen Zustand. Hier verwende ich den Modellorganismus *Arabidopsis thaliana*, der eine einzigartige männliche Gametophyten (Pollen) Struktur mit Kernen unterschiedlicher Heterochromatin-Organisation hat, um diese Chromatin-Dynamik zu verstehen. Im Gegensatz zu Tieren, wo der männliche Gametophyt am Ende der Meiose produziert wird, erzeugen Blütenpflanzen Pollen um zwei mitotische Spaltungen nach der Meiose. Darüber hinaus entsteht eine asymmetrische Mitose mit unvollständiger Zytokinese zu zwei Zellen: einer generativen (Spermien) und einer vegetativen Zelle mit unterschiedlichen Chromatin kondensationsniveaus. Da ein Mitoseereignis diese Zellen unterscheidet, ist es wahrscheinlich, dass ein aktiver Prozess für diese differentiellen Chromatin Zustände verantwortlich ist. Histon 3-Lysin-9-di-methylierung (H3K9me2) ist als Markierung von konstitutivem Heterochromatin bekannt. Vor nicht allzu langer Zeit wurde angenommen, dass Histon-Methylierungsereignisse irreversibel waren, bis eine Lysin-spezifische Histon-Demethylase 1A (LSD1) entdeckt wurde. Später wurde eine zweite Klasse von Histon-Demethylasen (JmjC-Domänen-haltige Proteinfamilie) entdeckt, und die Implikationen von Heterochromatin auf Zellschicksal und Metabolismus wurden erneut betrachtet. Ein Mitglied der JmjC-Domänen-haltigen Familie, eine mutmaßliche Histon-Demethylase JMJ27 (AT4G0099), wurde bei der H3K9me2-Demethylierung und der DNA-Hypomethylierung bei 45S-rDNA-Promotoren in *Arabidopsis thaliana* (Chumak 2012) gefunden. Eine Mutation im JMJ27-Gen bewirkt die Beibehaltung von H3K9me2, die mit 45S-rDNA-Repeats in Pollen-vegetativen Kernen koordiniert, begleitet mit einer erhöhten DNA-Methylierung bei 45S-rDNA-Promotoren. Ich habe zu dieser Arbeit beigetragen, indem ich ein Konstrukt kodiere, das für ein fluoreszierendes markiertes JMJ27 kodiert, das verwendet wurde, um die Expression, die subzelluläre Lokalisierung und die Komplementierung zu testen.

In meiner Studie schuf ich weiter transgene Linien und nutzte sie, um mehrere Fragen bezüglich der Funktion von JMJ27 zu behandeln. Ich habe die Histon-Demethylierungsaktivität von JMJ27 getestet, indem ich eine Mutation an der katalytischen Stelle der JmjC-Domäne induzierte, die als essentiell für die Histon-Demethylase-Aktivität von JmjC-Domänen-Familienmitgliedern bekannt ist. Die Untersuchung von Pollen-vegetativen Kernen zeigte, dass JMJ27 eine funktionelle JmjC-Domäne aufweist und für die H3K9me2-Demethylase-Aktivität in vivo erforderlich ist. Eine

Epitop-markierte JMJ27-Linie wurde verwendet, um eine Co-Immunpräzipitation durchzuführen, gepaart mit Massenspektrometrie, um mögliche Interaktoren zu identifizieren. Dies könnte das Netzwerk von Faktoren und die Rolle von JMJ27 bei der modulierenden Histon- und DNA-Demethylierung an 45S-rDNA-Loci erhellen. Unter einer Liste von mehreren Kandidaten wurden neun Proteine durch funktionale Annotations-Clustering-Analyse hervorgehoben, um eine höhere Chance der Zusammenarbeit mit JMJ27 zu haben. Zytologie-basierte vorläufige Tests in Pollen zeigten unterstützende Ergebnisse für drei dieser Kandidaten, die gescreent wurden: EMB1644 / LSM4, EMB1138 und CCR2 / GRP7. Allerdings sind zukünftige Studien erforderlich, um diese Interaktionen durch zusätzliche Methoden zu bestätigen und die Bedeutung solcher Wechselwirkungen mit JMJ27 in einem größeren Rahmen zu bewerten.

1 Introduction

1.1 Overview and Concepts of Epigenetics

Historically, the concept of epigenetics was developed at the boundaries of development and evolution to reflect how a single fertilized egg gives rise to a complex organism of diverse phenotypes. In 1940s, C.H. Waddington fathered the term "epigenetics" and defined it as the causal mechanisms by which the same genotypes bring about different phenotypic effects (Waddington 1942; Holliday 2006). Until the 1950s, epigenetics was used to explain developmental events from fertilization to mature organism. However, the term might have been much older, connected to the debate among embryologists in the late 19th century. Two views were favored among them to describe developmental steps of the fertilized egg; the first was "Preformationism" which was based on the belief that each cell contained preformed elements or parts of the organism that enlarged during development until the mature form is achieved; a homunculus, a tiny human, inside a human sperm growing up to be a baby. In contrast, the second view of "Epigenesis", whose origins could be traced back to Aristotle, proposed that interactions between components inside the embryo were responsible for organizing developmental stages and individual parts, which gradually form the whole organism. Later, the "epigenetics" evolved as a term to refer to these events (Waddington 1942). Now, in the modern era of science, the interplay between regulatory networks and the epigenetic events shaping the organism are better understood. These events are crucial for developmental stage and cell type-specific control of gene expression (Tarakhovsky 2010).

1.2 Epigenetics in Plants

Besides sharing common principles of life such as sexual propagation via meiosis and fertilization, plants and animals are also very similar in control of chromatin, the organization of euchromatin and heterochromatin, modification of DNA and histones (Pikaard & Mittelsten Scheid 2014). The sedentary life style of plants requires tight control and regulation of gene expression and chromatin organization upon environmental signals, and plants have mechanisms similar and often specifically extended compared to animals, to deal with conditional such changes. Having a similar epigenetic control and regulation of chromatin, in addition to ease of growth, breeding, and high numbers of progeny, make plants good models to study such mechanisms which could be conserved in animals. However, there are also important differences, for examples in gamete formation. While sperm and egg in mammals represent direct haploid products of the second meiotic division, higher

plants form gametophytes, as an extended haploid phase of their life cycle. Pollen, the male gametophyte, undergoes two mitotic divisions after meiosis, while the oocyte undergoes three mitotic divisions after meiosis to generate the embryo sac, the mature female gametophytes. These differences provide some unique characteristics to plants, and epigenetic modifications can be transmitted to next generation likely easier than in mammals, due to absence of a genome-wide erasure of all marks during gamete development characteristic for mammalian gametes (Pikaard & Mittelsten Scheid 2014). One major advantage of plants compared to mammals is the ease of genetic manipulation, generation of homozygous transgenic lines and mutant screens. Many of the components in epigenetic control pathways were revealed based on forward and reverse genetic screens in plants. Functional redundancy between gene families in plants further offers the possibility of analyzing mutants that could have deleterious effects otherwise.

1.3 Chromatin Organization

The basic unit of chromatin structure consists of nucleosomes, which are composed of octamers of histone proteins; dimers of H2A, H2B, H3 and H4 proteins with 146 bp of DNA wrapped around them (Luger et al. 1997). Histone proteins are highly conserved among eukaryotes and have a small size with protruding tails and overall basic charge. A complete nucleosome is assembled first with tetramerization of H3 and H4 dimers in contact with DNA, followed by joining of two sets of H2A-H2B dimers, making the compact structure. Several histone variants reserved for specific regions of DNA (e.g. centromeres) also exist. Protruding histone tails are the targets of many chemical modifications, although occasional modifications in histone bodies or globular domains are also observed. The “beads on a string” model illustrates the overall assembly of DNA and nucleosomes. Linker DNA regions between each nucleosome body are also bound by a class of histone proteins, called linker histones or H1, in which covalent modifications are also observed. There are several and partially functionally redundant isoforms of H1 proteins, making their characterization a difficult task. An important function of linker histones is believed to shield the negative charges of linker DNAs from uncoordinated interaction with nucleosomes. The overall diameter of the nucleosome string is approximately 11 nm, and forming a more compact structure requires the interaction of histones with chromatin-associated proteins such as HP1 or Polycomb group proteins, to obtain a compaction size around 30 nm diameter. Higher order compaction and loop formation are necessary to achieve three-dimensional chromatin organization. Nuclear envelope proteins like lamins are further involved in anchoring the compact loops into larger domains, resulting in a size of between 300 nm and 700 nm (Kornberg & Lorch 1999; Strahl & Allis 2000).

1.3.1 Euchromatin and Heterochromatin

Historically, the definition of euchromatin and heterochromatin stems from the observation of different staining patterns of the chromosomes. Giemsa staining produces two distinct types of bands on chromosomes based on the intensity of staining. Heterochromatin is characterized by intense, darker bands while euchromatin represents weakly stained parts of the chromosome (Heitz 1928; Strålfors & Ekwall 2011). Structurally, euchromatin is the less condensed, open or accessible conformation of chromatin while heterochromatin is the highly condensed and less accessible form. The euchromatic regions are gene- rich and more readily transcribed while in general, heterochromatic regions are gene-poor and typically not associated with transcription (Huisinga et al. 2006). Euchromatin and heterochromatin are enriched with different sets of molecules. Euchromatin is associated with acetylated histones H3 and H4 and methylated H3 at lysine 4 (H3K4me), while heterochromatin is enriched in methylated cytosines, hypoacetylated histones and H3K9me (Grewal & Jia 2007). Beside these structural and molecular differences, the spatial localization in the nucleus (distance to nuclear envelope or nucleolus) can also determine the euchromatic or heterochromatic nature of chromatin. Heterochromatic regions are often located close to the nuclear envelope (Van de Vosse et al. 2011).

Heterochromatin can be distinguished into constitutive or facultative heterochromatin, formed on the different regions of the genome. The regions rich in repetitive DNA elements such as centromeres, telomeres and transposons are kept condensed and silenced throughout the cell cycle and represent constitutive heterochromatin (Wang et al. 2016). Instead, the facultative heterochromatin signifies the condensed chromatin regions which can be transiently decondensed and transcribed within different contexts such as developmental state and cellular activity (Trojer & Reinberg 2007). In *Arabidopsis*, the heterochromatic repeat loci are spatially organized into structures called chromocenters. The centromeric and pericentromeric repeats, 5S rDNA and 45S rDNA repeat arrays are clustered together in these chromocenters which appear as intense foci by 4′,6′-diamidino-2-phenylindole (DAPI) staining (Del Prete et al. 2014). In response to developmental and environmental stimuli, chromocenters can undergo decondensation and re-organization which can be assessed with DAPI staining and fluorescence *in situ* hybridization (FISH) (Benoit et al. 2013; Probst & Mittelsten Scheid 2015). Thus, even constitutive heterochromatin is a dynamic structure crucial for the regulation of developmentally important loci, segregation of the chromosomes during cell division, protection of the chromosome ends and control of the transposable elements (TEs) (Grewal & Jia 2007). Indeed, one hypothesis is that heterochromatin has evolved as a defense mechanism to "parasitic" or invader TEs (Slotkin & Martienssen 2007; Fedoroff 2012). TEs invade the host genome by increasing their copy number

and insertion into new loci which result in deleterious effects for the host. Therefore, epigenetic silencing mechanisms have developed to silence these elements by keeping them in a transcriptionally inactive heterochromatin state.

Genome-wide maintenance of euchromatin and heterochromatin is necessary to secure the balance of transcription and silencing, with otherwise detrimental effects for cells. The active transcription process requires the coordinated interaction of many sub-complexes within euchromatic environment in a spatiotemporal manner (Berger 2007). Recruitment of chromatin modifier complexes to interact with active histone marks to alter the nearby nucleosome structures makes the region accessible to the RNA polymerase II complex and ensures the transcription start. Replacement of canonical histones with specific variants might be essential to sustain the integrity of chromatin as well as the persistence of the transcription machinery through the DNA sequence (Ahmad & Henikoff 2002). Although heterochromatin represents the compact and silent regions of chromatin, there are also several instances of which heterochromatic regions are actively transcribed (Yasuhara & Wakimoto 2006; Eymery et al. 2009). Several factors and the mechanisms involved in the process have been uncovered in various organisms. In Drosophila, HP1a mediates transcription of genes embedded in heterochromatin (Dimitri et al. 2009; Kwon & Workman 2011), whereas in fission yeast , Swi6/HP1 recruits Epe1, a JmjC domain protein, to enable transcription of repetitive elements (Zofall & S. Grewal 2006). Similarly, the *Arabidopsis* Epe1 homolog JMJ24 is required for the basal level transcription of endogenous silenced loci (Deng et al. 2015). In mammals, pericentromeric and centromeric DNA transcription is observed during embryonic development and cellular differentiation (Hall et al. 2012; Saksouk et al. 2015). Transcription in these regions during epithelial to mesenchymal transition is regulated by Snail1/LOXL2 in mice (Millanes-Romero et al. 2013). Thus, although the nature of heterochromatin might suggest it is not essential for any biological function, new roles are increasingly revealed. Most components of the regulatory network acting on different states of chromatin are well conserved among organisms. Some plants and mammals have similar ratios of euchromatin to heterochromatin, which is one of the reasons that make plants useful for studying chromatin dynamics (Pikaard & Mittelsten Scheid 2014).

1.4 DNA Methylation

DNA methylation is a covalent modification observed in both prokaryotes and eukaryotes. In eukaryotes, it is most frequently the process of adding a methyl group to the 5^{th} carbon atom of cytosine, to form 5-methylcytosine. In prokaryotes, DNA methylation is utilized as a basic mechanism of defense against foreign DNA of mostly viral origin (Murray 2002). In eukaryotes, it

is conserved in many organisms like mammals, insects, fungi and plants, but some common model organisms such as *Saccharomyces cerevisiae* and *Caenorhabditis elegans* represent exceptions (Suzuki & Bird 2008). In *Drosophila melanogaster,* although not completely lost, DNA methylation is restricted to certain developmental stages and found as a rare modification (Goll 2006; Kunert 2003). DNA methylation can be divided into two categories; *de novo* methylation that occurs as a previously unmethylated DNA sequence, and maintenance methylation that is restored during DNA replication and repair, usually based on the hemi-methylated state at symmetrical sequences of the complementary strand (Matzke & Mosher 2014). Unlike in mammals where almost all of the DNA methylation occurs at CG dinucleotides (with the exception of embryonic stem cells which can contain non-CG pattern as well (Ramsahoye et al. 2000)), DNA methylation in plants occurs in three different sequence context of CG, CHG and CHH, where H is either A, T or C but no G (Furner & Matzke 2011). Moreover, methylation at transposable elements is usually more pronounced and denser than that at gene bodies (Xiaoyu Zhang et al. 2006; Coleman-Derr & Zilberman 2013) While *de novo* methylation is found in all three contexts, the maintenance methylation is most efficient on CG and CHG contexts, as described by the symmetric occurrence of a C on the opposite strand (Law & Jacobsen 2010). Specific methylation at transposable elements and gene bodies requires a precise targeting and maintenance mechanism, and enzymes with different specificities play a central role. In mammals, maintenance of CG methylation is achieved by the DNA methyltransferase DNMT1 (DNA cytosine-5 methyltransferase 1), mediated by the cofactor UHRF1 (ubiquitin-like containing PHD and RING finger domains 1) which recognizes hemi-methylated DNA (Bostick et al. 2007; Sharif et al. 2007). Similar in structure to DNMT1, the members of DNMT3 (DNA methyltransferase 3) family establish *de novo* methylation in mammals. DNMT3 family consists of three members; DNMT3A, DNMT3B, and DNMT3L (DNMT3-like). The first two are active DNA methyltransferases and responsible for *de novo* methylation, while DNMT3L lacks catalytic activity but acts as a regulator of the other two members via direct interactions (Suetake et al. 2004; Hata et al. 2002). DNMT3L expression was found to be higher during embryonic development and needed for proper establishment of genomic imprinting (Bourc'his 2001; Hata et al. 2002). A recent study also showed that DNMT3L can bind to unmethylated lysine 4 of histone 3 tails via its ATRX-DNMT3-DNMT3L (ADD) domain and might be recruiting DNMT3A and DNMT3B to specific loci (Ooi et al. 2007; Otani et al. 2009)

In *Arabidopsis*, maintenance methylation of CG dinucleotides is catalyzed by a homolog of mammalian DNMT1 called MET1 (DNA METHYLTRANSFERASE 1), and, like the mammalian homolog, it is recruited to hemi-methylated sites by cofactors which are members of the VIM (VARIATION IN METHYLATION) family proteins (VIM1, VIM2 and VIM3) in *Arabidopsis*

(Woo et al. 2008). Maintenance methylation in CHG context is mediated by the plant-specific DNA methyltransferase CMT3 (CHROMOMETHYLASE 3) (Lindroth 2001). The third, non-symmetrical context CHH requires an active mechanism to re-establish methylation post replication. DRM (DOMAINS REARRANGED METHYLTRANSFERASES) family proteins, DRM1 and DRM2, which are homologues of mammalian DNMT3 methyltransferases, are the two *de novo* methyltransferases in *Arabidopsis* which can catalyze CHH methylation as well as CG and CHG methylation (Cao & Jacobsen 2002), yet their role in CHH methylation is prominent since they are the major de novo DNA methyltransferases, however assisted by CMT3 (Bartee et al. 2001). The DRM2 is part of a small RNA targeted *de novo* DNA methylation machinery in plants, a unique mechanism known as RNA-directed DNA methylation (RdDM), targeting and silencing DNA repeats, foreign DNA and transposable elements (Matzke & Mosher 2014). Eukaryotes have three common DNA-dependent RNA polymerases: RNA Pol I, RNA Pol II and RNA Pol III, each with specific functions. In plants exist two more additional polymerases which enable the RdDM machinery. In the core of this mechanism lie the plant-specific two DNA-dependent multisubunit RNA polymerases: RNA Pol IV and RNA Pol V, which are evolved from the RNA Pol II (Tucker et al. 2010). Although most of the 12 subunits are common between the polymerases, differences in their catalytic and carboxy terminal domains allow RNA Pol IV and RNA Pol V polymerase to interact with new partners such as Argonaute (AGO) family proteins, enabling siRNA-mediated epigenetic modifications (C. F. Li et al. 2006). In brief, Pol IV-transcribed single stranded RNAs are copied into double stranded RNA (dsRNA) molecules by RDR2 and processed by DICER-LIKE 3 (DCL3) into 24 nt small RNAs. In the cytoplasm, these are loaded onto AGO4 and target AGO4-containing RNA-induced silencing complex (RISC) to Pol V-transcribed regions for complementary binding. Upon recruiting DRM2 and several chromatin modifiers, cytosine bases at CHH, CHG and CG contexts are *de novo* methylated (Matzke & Mosher 2014). However, an RdDM-independent pathway for CHH methylation also exists. CMT2, a homolog of CMT3, is responsible for CHH methylation in a DDM1-mediated mechanism on targets distinct from RdDM targets (Zemach et al. 2013).

1.5 DNA Demethylation

Although it is a rather stable modification, both plants and mammals can lose DNA methylation, via passive or active mechanisms. Passive loss can occur upon replication due to any defect in maintenance methylation pathways leading to dilution of methylation in each replication (Furner & Matzke 2011). However, active loss is driven by several factors that can catalyze the removal of a methylated cytosine. In *Arabidopsis*, bi-functional DNA glycosylases can excise

methylated cytosines and then cleave the DNA backbone at abasic site, initiating a base excision repair cascade leading to replacing with an unmethylated cytosine (H Zhang & Zhu 2013). A family of DNA glycosylase domain-containing proteins in *Arabidopsis* is known to function in active DNA demethylation; DEMETER (DME), REPRESSOR OF SILENCING 1 (ROS1), DEMETER-LIKE 2 (DML2) and DEMETER-LIKE 3 (DML3) (Roldán-Arjona & Ariza 2009). DME was shown to be expressed in both male and female gametophytes, in the vegetative cell and the central cell, respectively, and it is essential for male fertility and establishing maternal allele gene imprinting (Choi et al. 2002; Schoft et al. 2011). Maternal alleles of Polycomb-group protein genes MEDEA (MEA) and FERTILIZATION INDEPENDENT SEED 2 (FIS2), and the homeodomain transcription factor gene FLOWERING WAGENINGEN (FWA) are known targets of DME (Hsieh et al. 2011). Furthermore, its role in reconfiguration of the methylation landscape in endosperm and vegetative cell of pollen was indicated by recent studies that identified genome wide demethylation of transposons and repeated sequences targeted by DME (Gehring et al. 2009; Hsieh et al. 2009; Schoft et al. 2011; Ibarra et al. 2012).

In contrast to DME which functions during gametogenesis, the other three DNA glycosylases ROS1, DML2 and DML3 were found to be more active in vegetative tissues (Penterman, Zilberman, et al. 2007). In addition, while DME activity is responsible for genome-wide decrease in CG methylation in endosperm, the single mutants of ROS1, DML2 and DML3 indicate that the corresponding proteins function redundantly, and triple mutants do not have a substantial increase in global methylation (Penterman, Zilberman, et al. 2007). However, their target loci were found enriched for transposons and repetitive elements. The majority of these loci are near transcribed genes, and methylation is concentrated more at 5' and 3' ends (Penterman, Zilberman, et al. 2007; Penterman, Uzawa, et al. 2007). A possible role of ROS1, DML2 and DML3 as antagonists to the RdDM pathway was suggested, protecting genes from silencing by small RNA-mediated methylation (Law & Jacobsen 2010). Reinforcing this idea, several components of the RdDM pathway were found in genetic screens for *ros1* suppressors, and decreased ROS1 expression was detected in RdDM mutants (Matzke & Mosher 2014). How DNA glycosylases are targeted to their specific loci is an open question. ROS3, a protein with an RNA recognition motif, was proposed to be involved in DNA demethylation target specificity of ROS1 (Zheng et al. 2008). ROS3 was shown to bind small single strand RNA (ssRNA) molecules (21-26nt) *in vivo* and *in vitro* in a sequence specific manner, and analysis of *ros3* and *ros1ros3* double mutants demonstrated that ROS3 acts in the same DNA demethylation pathway as ROS1. This suggests that they might be part of a bigger DNA demethylation complex (Zheng et al. 2008; H Zhang & Zhu 2013). However, ROS3 may not be cooperating with DME since it causes demethylation in a more genome-wide

manner and require less target specificity (Law & Jacobsen 2010). In another model, ROS1 is speculated to find its targets by randomly sliding along DNA (Ponferrada-Marín et al. 2012).

1.6 Histone Modifications:

The dynamic higher order organization of nucleosomes sets the active or repressed state of chromatin. Histone proteins, the basic unit of nucleosomes, provide the base for dynamic change in chromatin due to its flexible and charged protruding tails. Covalent post-translational modifications (PTMs) such as acetylation, methylation, phosphorylation, sumoylation, ubiquitination, carbonylation and glycateylation can change the overall charge of the structure allowing regulation on the DNA structure wrapped around them (Bannister & Kouzarides 2011). Moreover the position and degree of modification on histone tails can alter the nucleosome in diverse ways, creating complexity and building the hypothesis of a histone code (Strahl & Allis 2000; Jenuwein 2001). Histone modifications do not occur in isolation, but rather in combinatorial manner by interactions in cis, on the same histone, and in trans, on the adjacent histones either on the same nucleosome or in neighboring nucleosomes, catalyzed by unique enzymes for each distinct modification. Overall there is a coordinated network of histone modifiers, DNA modifiers and chromatin binding proteins generating the histone code. However, compared to the DNA code, the histone code is less universal for all organisms. Some modifications such as H3K9me3 can be an indication of heterochromatin in animals and fungi, but might be correlated with active transcription in plants. In contrast, H3K9me1 and H3K9me2 are associated with heterochromatin in plants but can be correlated with euchromatin in animals (Fuchs et al. 2006; Berger 2007). Nevertheless, genome-wide studies showed that there is an increased correlation of certain histone modifications with euchromatin/ transcriptionally active states and heterochromatin / transcriptionally silent states (Table 1). In general, acetylation and phosphorylation events are associated with transcriptional activation where the negative charges of these molecules help to neutralize or change the positive charge of histones, causing relaxation that makes the DNA accessible to a diverse array of factors. In contrast, methylation modifications can have either activating or repressing effects. Methyl groups are smaller than acetyl- and phospho- groups, and their addition to lysine or arginine residues does not alter the charge of nucleosomes. However, regulatory proteins can recognize and bind to these chemical groups which in turn alter chromatin depending on the modification site and level (Bannister & Kouzarides 2005). In contrast to smaller sized methyl groups, one very large modification is ubiquitination, as ubiquitin molecules (8.5 kDa) are nearly as big as histone proteins (11- 21 kDa). Addition of ubiquitin to histone tails results in a structural change due its volume and alters the distance between histone and DNA. However, the outcomes of this modification can also

be repressive or activating in terms of transcription (Berger 2007). Beside those well-studied modifications, the list of novel histone modifications is still growing (Tan et al. 2010). Besides a role of diverse modifications for transcriptional activity, others determine processes such as DNA repair, X chromosome inactivation, or stem cell pluripotency (Rothbart & Strahl 2014).

Modification Type	Mechanism	Modified Residue	Transcription Outcome
Ubiquitination	Distances histones from DNA (bulky moiety)	**H2A**: K5	Repression
		H2B: K143	Activation
Methylation	Recruitment of other chromatin regulators	**H3**: K4, R17, K36, K79 **H4**: R3	Activation
		H3: K9, K27 **H4**: K20	Repression
Acetylation	Charge change, recruitment of other chromatin regulators	**H2A**: K5, K144 **H2B**: K6, K11, K27, K32 **H3**: K9, K14, K18, K23 **H4**: K5, K8, K12, K16	Activation
Phosphorylation		**H2A**: S129 **H2B**: S15 **H3**: S10	Activation

Table 1: Summary of histone modifications (lysine (K), arginine (R), serine (S)) and their role in transcription. (Modified from (Berger 2007; Pfluger & Wagner 2007; Zhang et al. 2007)

1.6.1 Establishment and Interpretation of Histone Modifications

Components of epigenetic regulation through histone modification can be hypothetically categorized in three classes: writers, erasers and readers (Figure 1) (Tarakhovsky 2010). Nucleosome structure is altered due to the interplay between these components, with the outcome of either transcriptional activation or repression. Writer class components are the partners that generate modifications by attaching chemical groups such as methyl and acetyl groups to individual amino acid residues in histone tails. Recently, modifications in the histone core, of loops and secondary structure were also detected (Tessarz & Kouzarides 2014). Histone acetyl transferases (HAT), histone methyl transferases (HMT) and histone kinases constitute the writer group of proteins. Eraser class components work antagonistically to writers and remove the modifications from histones. Due to the nature of the covalent binding, phosphoryl and acetyl groups are easier to

remove compared to more stable methyl groups (Tarakhovsky 2010; Bannister & Kouzarides 2011). Histone deacetylases (HDAC), histone demethylases (HDM) and histone phosphatases represent the erasers. The third classification, readers, includes proteins with specific conserved domains such as bromodomain, chromodomain, PHD fingers or WD40 repeats that can selectively recognize histone modifications (Taverna et al. 2007). Bromodomains are found to be involved in recognizing acetylated lysine residues and help erasers like HDACs to find their targets. The chromodomain was named after chromatin organization modifiers and selectively recognizes methylated histones. It was shown to be associated with RNA-induced transcriptional silencing and heterochromatin formation. PHD finger domain-containing proteins show affinity to methylated histones in general, more specifically to tri-methylated histones. WD40 repeats are usually required to establish a scaffold for interaction between proteins involved in histone modifications. Most enzyme complexes such as chromatin remodelers may contain several of these putative "reader" domains, which suggest a possible combinatorial effect of several distinct histone modifications on each nucleosome or at adjacent nucleosomes. Furthermore, the methylation pattern of DNA can contribute to create even more versatility if it interacts with the complexity of histone modifications.

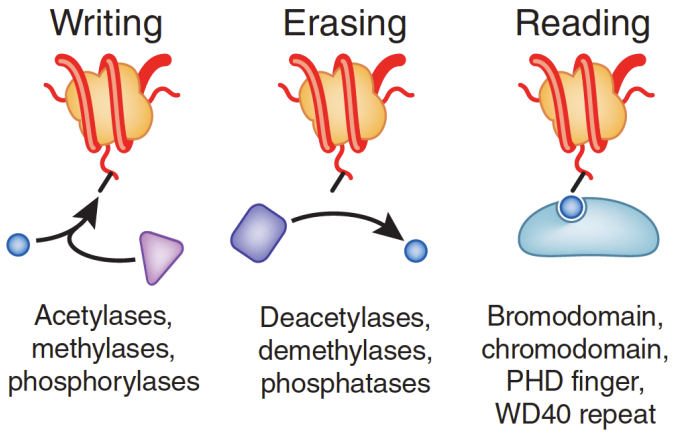

Figure 1: Components of epigenetic control represented in three classes: "writers ", "erasers" and "readers" each with distinct function. "Writers" establish modifications to histones, "erasers" remove modifications from histones and "readers" are responsible for recognizing specific modifications on histones. Modified from (Tarakhovsky 2010).

1.6.2 Histone Lysine Methylation

Histone lysine methyltransferases (HKMTs) catalyze the transfer of a methyl group from S-adenosylmethionine (SAM) to an amino group of a lysine residue (Bannister & Kouzarides 2011). HKMTs' catalytic activities are specific for defined histone lysine residues and for certain degrees of methylation: mono, di- or tri-. This specificity depends mainly on the structure of the catalytic site and its ability to accommodate pre-methylated groups at the catalytic core (Xing Zhang et al.

2003; Couture et al. 2008; Wu et al. 2010). All HKMTs contain a SET domain which was initially discovered as a common structure in the *Drosophila* proteins Su (var) (Suppressor of variegation), E (z) (Enhancer of zeste) and TRX (Trithorax) to be responsible for the enzymatic activity (Y Zhang & Reinberg 2001). However, two HKMTs, DOT1 in yeast and DOT1L in humans which methylate H3K79 within the histone globular domain, do not have the SET domain in their structure (Feng et al. 2002). SET domain proteins can be part of the Polycomb group (PcG) complex functioning in silencing of chromatin, or in Trithorax group (TrxG) families activating transcription. Remarkably, the expressions of HOX (homeobox) genes, which determine the pattern of body segments, are regulated by the interplay of these Pc and Trx groups during embryonic development (Ringrose & Paro 2004; Völkel & Angrand 2006). Although the SET domain is conserved between animals and plants, proteins with SET domains can have different functions, due to the differences in the rest of the structure and possible interactions with other proteins.

Arabidopsis encodes 32 SET domain-containing proteins grouped into four evolutionary conserved families based on homology to Drosophila SET domains proteins: E (z), TRX, ASH1 (Absent, small or homeotic disks), and SU (VAR) 3-9 and a fifth small group which is only found in yeast and plants (Baumbusch et al. 2001; Springer et al. 2003) (Table 2). The first two SET domain proteins identified in *Arabidopsis* were CLF (curly leaf) and MEA/FIS1 (Medea/Fertilization Independent Seed Formation) both of which are related to Drosophila E(z) and function in silencing chromatin as part of PcG via their H3K27 methyltransferase activity. Mutations in CLF cause morphological changes such as curly leaves and homeotic changes in flower development. The mutants of MEA, which functions in gametophyte-specific gene imprinting, develop endosperm in the absence of fertilization. (Goodrich et al. 1997; Grossniklaus et al. 1998).

ATX1 and ATX2 *Arabidopsis* TrxG members regulate or activate floral homeotic changes (Alvarez-Venegas & Avramova 2001). Kryptonite / SUVH4 (Su (var) 3-9 Homolog 4) acts synergistically with CMT3 to maintain transcriptional repression. CMT3 methylates DNA in CpHpG context while Kryptonite/SUVH4 is required for mono- and di-methylation of H3K9 which is a crucial step for initiation of heterochromatin formation by recruitment of heterochromatin binding proteins (HP1) (Jackson et al. 2002).

SET Domain Class	HKMT	Methylation Target
E(z)	MEA	H3K27me/me2/me3
	CLF	H3K27me/me2/me3
	SWN	H3K27me/me2/me3
ASH1	ASHH1	H3; H4
	ASHH2/EFS	H3K4me3; H3K36me2/me3
	ASHR3	H3K4me2; H3K36me2
TRX	ATX1	H3K4me3
	ATX2	H3K4me2
	ATXR3	H3K4me/me2/me3
	ATXR7	H3K4me/me2/me3
SU-(VAR) 3-9	SUVH2	H3K9me/me2; H4K20me; H3K27me2
	SUVH4/KYP	H3K9me/me2
	SUVH5	H3K9me/me2
	SUVH6	H3K9me/me2
	SUVR4	H3K9me2/me3
	SUVR5	H3K9me2, H3K27me2

Table 2: Histone lysine methyltransferases (HKMTs) with identified targets (HKMTs with non-identified targets are excluded) in *Arabidopsis* classified according to SET domain class (modified from (Thorstensen et al. 2011))

1.6.3 Histone Lysine Demethylation

Histone lysine demethylases (HKDMs) are a class of proteins that can remove methyl groups from methylated histones. Although several chemical reactions that can remove methyl groups were proposed (Bannister et al. 2002), histone lysine methylation was considered for many years as a stable, irreversible modification that cannot be erased by active mechanisms. The first class of HKDMs was found after the discovery of the lysine-specific demethylase 1 (LSD1) in humans. This enzyme requires FAD as a co-factor in an amine oxidation reaction and is able to remove methyl groups from H3K4me/me2 but not H3K4me3 (Shi et al. 2003). In *Arabidopsis*, there are four homologs of LSD1: LSD1-LIKE-1 (LDL1), LDL2, LDL3 and FLOWERING LOCUS D (FLD). Three of these, LDL1, LDL2 and FLD, were shown to demethylate H3K4me/me2 (Jiang et al. 2007; Prakash et al. 2014).

The second class of HKDMs was named "Jumonji C domain (JmjC)-containing histone demethylases". The name of the group comes from the domain found in a gene called *Jumonji*

(*Jmj*), which was named after the abnormal phenotype observed in mutant mice: during development, the neural tube resembles a cross shape or cruciform which is called "jumonji" in Japanese. Moreover, homozygous *Jmj* mutations in mice are embryonically lethal at day 15.5 (Takeuchi et al. 1995). Analyzing the protein structure of the Jumonji protein, it was found to have a DNA binding domain, JmjN, JmjC and an AT-rich interaction domain (ARID). Further comparative analysis proved that these domains are conserved among species (Takeuchi et al. 2006). Although additional domains could be found, proteins are grouped according to the presence of one or both of the JmjC or JmjN domains (Balciunas & Ronne 1999). Moreover, correlated evolutionary analysis of protein sequences highlights family-determining residues that can classify JmjC-containing proteins into five groups (Slama 2016). Jumonji proteins also have been shown to be involved in the control of cardiogenesis, acting as transcriptional repressor of cyclin D1 expression whose overexpression leads to cardiomyopathy in mice (Toyoda et al. 2002). In 2006, based on the oxidative demethylation reaction observed during DNA demethylation by AlkB family proteins, biochemical assays aimed to test if protein(s) utilize the same mechanism for histone demethylation in HeLa cells. A previously uncharacterized protein called FBXL11 (F box and leucine-rich repeat protein 11), which has domains of JmjC, Zinc finger, PHD, F-box and leucine rich repeats, were identified in purified samples and shown to be responsible for H3K36me2 demethylation. Moreover, the enzymatic activity was found to depend on the JmjC domain. Since it was not characterized before, and as it is the first proteins with a Jmj domain to be involved in histone demethylation, the name was changed to JmjC domain-containing histone demethylase 1A (JHMD1A) (Tsukada et al. 2006). Further studies identified several other members of the Jumonji protein family also as histone demethylases. Catalytic activity depending on a JmjC domain thus created a new class of histone demethylases, in addition to LSD1. Unlike the amine oxidation reaction employed by LSD1 using FAD as co-factor, enzymes of this class use Fe (II) and α-ketoglutarate (2-oxoglutarate) as co-factors in catalyzing the hydroxylation reaction that removes the methyl groups (Tsukada et al. 2006). Several members of the family remove methylation at mono-, di-, and tri- levels. In *Arabidopsis*, 21 JmjC domain-containing histone demethylases are found and so far, only a few have been functionally characterized. In general, they are essential components of transcriptional control in developmental pathways (Prakash et al. 2014). JMJ11/ELF6 and JMJ12/REF6, which are H3K27 demethylases, regulate flowering time and brassinosteroid response. Another H3K27 demethylase, JMJ30, acts in regulation of the circadian clock (Gan et al. 2015). Some JmjC-containing histone demethylases are involved in control of DNA methylation. JMJ25/IBM1 is required to remove H3K9me2 and prevents CHG methylation in actively transcribed gene bodies (Saze et al. 2008; Miura et al. 2009). A putative H3K9

demethylase, JMJ24, promotes basal transcription of endogenous silenced loci and interacts with RDR2 to initiate RNA-directed DNA methylation (RdDM) (S. Deng et al. 2015). A H3K4 demethylase, JMJ14, is also required to maintain non CG-methylation at RdDM target loci, in addition to regulating floral development (Deleris et al. 2010) .

1.7 Arabidopsis Pollen as A Model

The *Arabidopsis* pollen has a simple lineage with a haploid genome, which consists of three nuclei in a unique cell-within-a-cell structure (Figure 2). Two distinct developmental processes lead to the formation of mature pollen in anthers. The first one is called microsporogenesis, and the subsequent process is called microgametogenesis. Microsporogenesis consists of one meiosis event starting with a diploid sporogenous cell producing a tetrad of haploid microspores, which are released as single cells, or uninuclear pollen (Figure 2). The uninuclear pollen starts to polarize due to vacuolization, positioning the nucleus on the periphery of the pollen wall, followed by two subsequent mitosis events. The first one, mitosis I, ends with an asymmetric division generating two nuclei with opposing characteristics: one having a highly-condensed chromatin and one more open chromatin. Moreover, instead of a complete cytokinesis forming two separate daughter cells, the "vegetative cell" with the nucleus that has decondensed chromatin engulfs the smaller "sperm cell", creating the bicellular pollen (Figure 2). The two daughter cells differ in size and shape and are destined for distinct fates. The sperm cell undergoes another mitosis, mitosis II, giving rise to two identical sperm cells with highly condensed chromatin. Inside the mature tricellular pollen (Figure 2), the sperm cells conserve and transmit the genetic and epigenetic blueprint to the offspring, whereas the vegetative cell drives the pollen tube elongation over a tremendous distance, to deliver the sperm cells to the female gametophyte, and it degenerates before fertilization.

The difference between the chromatin in vegetative and sperm nuclei is generated only at the end of the first mitosis, which suggests that there might be active mechanisms responsible for decondensation of chromatin. As previously mentioned, several changes in nucleosome structure are required to organize the genome into heterochromatin and euchromatin. Epigenetic modifications at both DNA and histone level are required for transitions between the two states and their maintenance. Although the mechanism of heterochromatin condensation is well studied, the knowledge about the heterochromatin decondensation is limited. Therefore, *Arabidopsis* pollen represents an interesting and suitable model to explore novel genetic/epigenetic factors involved in differential chromatin fates, particularly factors required for heterochromatin decondensation.

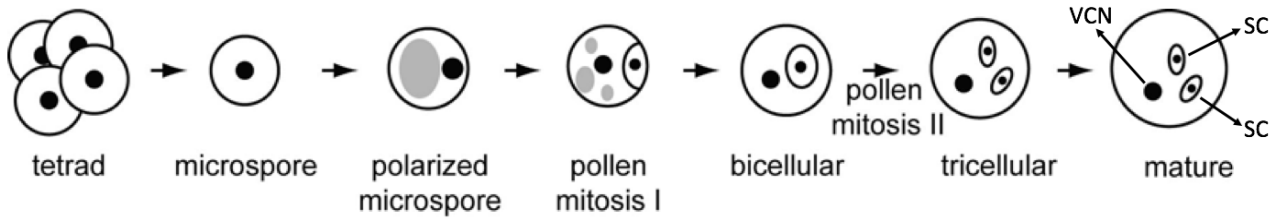

Figure 2: Microgametogenesis process of *Arabidopsis* pollen development. (VCN: vegetative cell nucleus, SC: sperm cell) (Modified from https://people.emich.edu/sbackues/Images/pollen-dev-fig.gif (accessed on 01/09/17))

1.8 Epigenetic Profile of Arabidopsis Pollen Nuclei

The differential condensation levels of vegetative and sperm nuclei are clearly visible with cytological methods. The heterochromatic nature of the sperm cells' nuclei and the euchromatic nature of the vegetative nucleus is evident from staining with DNA binding dyes (Figure 3A). The differential DAPI staining of the nuclei is in accordance with the well-defined epigenetic markers of heterochromatin and euchromatin in pollen nuclei (Schoft et al. 2009; Chumak 2012). The diffuse chromatin of the vegetative nucleus denotes a complete decondensation of constitutive heterochromatin. Chromocenters were studied by using probes for centromeric 180bp repeats (180CEN) in FISH experiments on sorted pollen nuclei. In the vegetative nucleus, the centromeric heterochromatin is dispersed, whereas intense signals corresponding to chromocenters are observed in sperm nuclei (Figure 3B). Chromocenters are also characterized by the concentration of the centromere-specific histone 3 variant, CenH3 (HTR12), which is essential for chromosome integrity. In contrast with canonical histone 3 variants, which exist in both sperm and vegetative nuclei, CenH3 is lost or barely visible in vegetative nuclei, whereas strong and concentrated signals indicative of chromocenters are detected in sperm nuclei (Figure 3C-D). Loss of visibility of these two constitutive heterochromatin regions, 180CEN and CenH3, while retaining the canonical histone 3 profile, suggests that the vegetative nucleus has undergone centromeric heterochromatin decondensation. Furthermore, it has likely lost its capacity of further cell divisions since centromeres can no longer be utilized during mitosis.

Regions of constitutive heterochromatin are marked with a well-known epigenetic modification: H3K9me2. Consistent with the loss of CenH3 and dissociation of centromeric 180bp repeats, immunostaining using an H3K9me2 antibody reveals the absence or great reduction of H3K9me2 in the vegetative nucleus, while sperm nuclei retain strong signals (Figure 3D). However, the loss of H3K9me2 marks does not lead to removal of global DNA methylation: immunostaining using antibodies against 5-methylcytosine (5meC) reveals DNA methylation distribution similar to the chromatin distribution in vegetative and sperm nuclei (Chumak 2012). In depth analysis of DNA methylation via bisulfite sequencing using sorted pollen nuclei showed the

different amounts of methylation at CG, CHG and CHH context. The vegetative nucleus has more CHH methylation than the sperm nuclei and nuclei from seedlings, while CG and CHG methylation are on comparable levels between the three samples. *de novo* DNA methylation at CHH sites originates from RdDM mechanism upon decondensation of constitutive heterochromatin (Schoft et al. 2009).

Besides H3K9me2, H3K27 monomethylation is another epigenetic modification on the same histone associated with repressed chromatin, especially at pericentromeric regions (H3K27me) (Jacob et al. 2009). Inspecting this methylation variant via immunostaining in vegetative and sperm nuclei showed two different phenotypes: four distinct signals can be spotted in sperm nuclei, whereas only one spot is observed in vegetative nuclei. Interestingly, while constitutive heterochromatin with H3K9me2 is largely decondensed in vegetative nuclei, some spots are still stained with the H3K27me1 antibody (Figure 3E). Further analysis identified the preserved regions to be 45SrDNA loci, known to form facultative heterochromatin, as FISH signals with 45SrDNA probes co-localized with H3K27me1 immunostainings in vegetative nuclei (Figure 3F).

Previous studies also showed via immunostaining that the active chromatin mark H3K4me2 is conserved in both sperm and vegetative nuclei, in patterns similar to the DNA counterstaining (Chumak 2012). This finding indicates chromatin integrity and active gene expression in vegetative nuclei on a large scale.

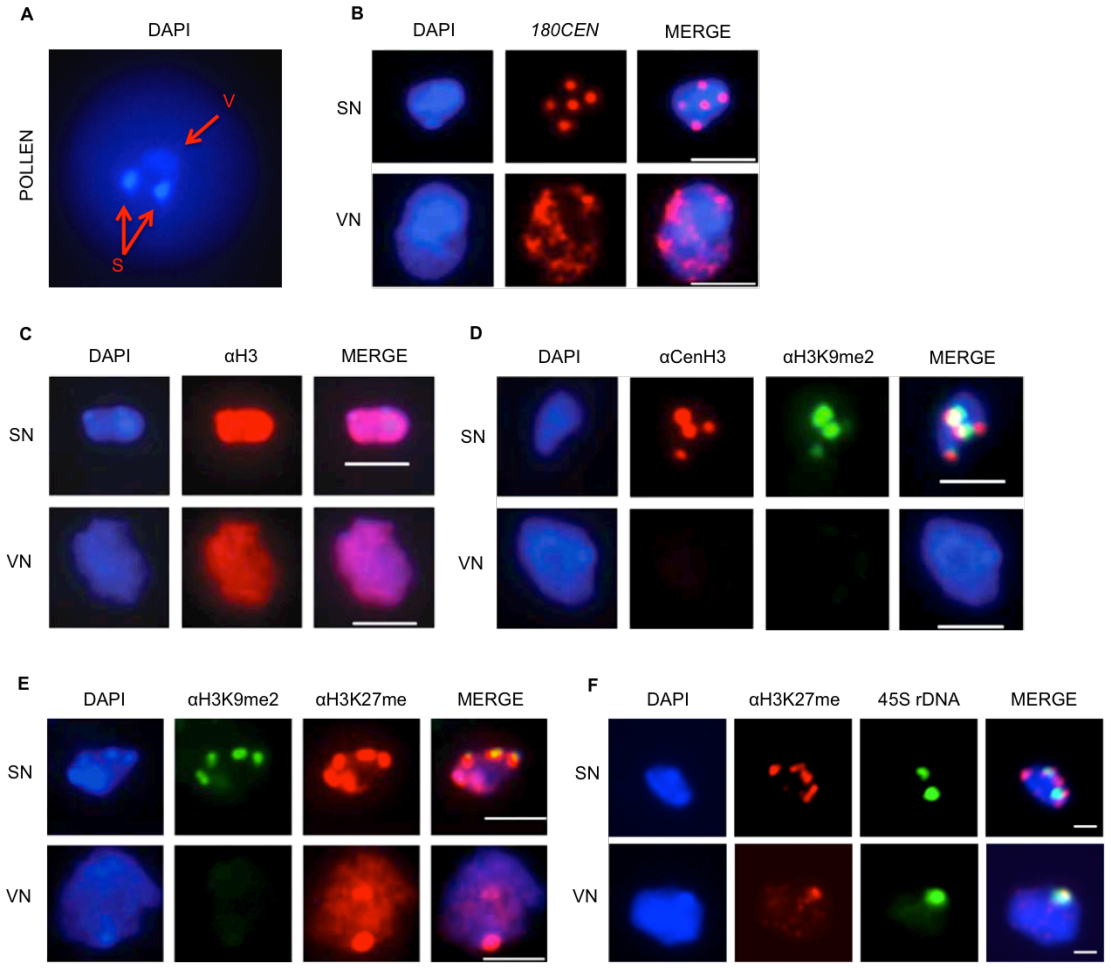

Figure 3: Epigenetic profile of wild type (Col-0) mature pollen analyzed by cytology. A) DAPI-stained mature pollen, S: sperm nuclei, V: vegetative nucleus. B) 180CEN repeats in pollen nuclei detected by FISH. Immunostaining of C) bulk H3, D) CenH3 (HTR12) and H3K9me2, E) H3K9me2 and H3K27me. F) Immuno-FISH image of H3K27me and 45S rDNA in pollen nuclei. (B-F) DAPI was used as DNA counterstain. Scale bars: (B-E) 3 µm, F) 1 µm. (Modified from (Schoft et al. 2009; Chumak 2012)

1.9 Role of H3K9me2 in Heterochromatin Decondensation of the Vegetative Nucleus

Epigenetic profiling of pollen nuclei suggested that removal of H3K9me2 could be the critical step in decondensation of constitutive heterochromatin in vegetative nuclei. In animals, a family of histone lysine demethylase proteins exist to actively erase methylation at specific lysine residues, although until recently this modification was thought to be irreversible (see chapter 1.6.3). A genome-wide screen for JmjC domain-containing proteins has revealed 21 proteins of this family in *Arabidopsis.* The comparison to human JmjC domain-containing proteins strongly indicated that these *Arabidopsis* homologs could have histone lysine demethylation activity (Lu et al. 2008). According to their JmjC domain sequences, the phylogenetic analysis of the *Arabidopsis* members revealed several clusters within the family. Potential enzymatic activities for each cluster were

inferred by comparison to the groups of the human histone lysine demethylases. Among the clusters, KDM3/JHDM2 group members have been predicted to be functional H3K9me2 demethylases (Lu et al. 2008) (Figure 4 & Figure 5). Utilizing the advantage of the haploid genome of pollen (see chapter 1.7), a reverse genetic approach was followed to analyze whether one or more members of the JmjC domain-containing protein family actively demethylate H3K9me2 and trigger heterochromatin decondensation in the vegetative nucleus (Chumak 2012). The KDM3/JHDM2 group consists of six members: JMJ24, JMJ25, JMJ26, JMJ27, JMJ28, JMJ29 (Figure 4), and a closer look on the domain structures of corresponding proteins, in the JmjC domain, the co-factor (Fe (II) and α-ketoglutarate (2-oxoglutarate)-binding sites revealed that these are conserved in only four of the six proteins: JMJ25, JMJ26, JMJ27 and JMJ29. This makes these genes strong candidates as active H3K9 demethylases (Lu et al. 2008). T-DNA insertion lines of all JmjC domain-containing proteins, including these four, were tested for their H3K9me2 profile of pollen nuclei by immunostainings. No difference was observed between mutants and wild type Col-0 ecotype for sperm nuclei. However, in vegetative nuclei of one line that has an insertion in *JMJ27* (SALK_092672), a cluster of smaller local signals of H3K9me2 is apparent (Figure 6). This phenotype is referred to as "*jmj27-1* phenotype" throughout the study. As the signal does not cover large areas, it is fair to speculate that a limited rather than a global region is affected. This is further supported by the same results for H3K9me2 immunolocalization with the two other T-DNA lines of JMJ27 *(*SALK_020986 (*jmj27-2*), SALK_044594 (*jmj27-3*) (not shown). Analysis of combined mutants in *JMJ27* and its close homologs *JMJ26* and *JMJ29,* in double *(jmj27/jmj26*, *jmj27/jmj29, jmj26/jmj29*) and triple mutants (*jmj26/jmj27/jmj29*), via immunostainings of pollen nuclei revealed that there is no functional redundancy between these family members (Chumak 2012).

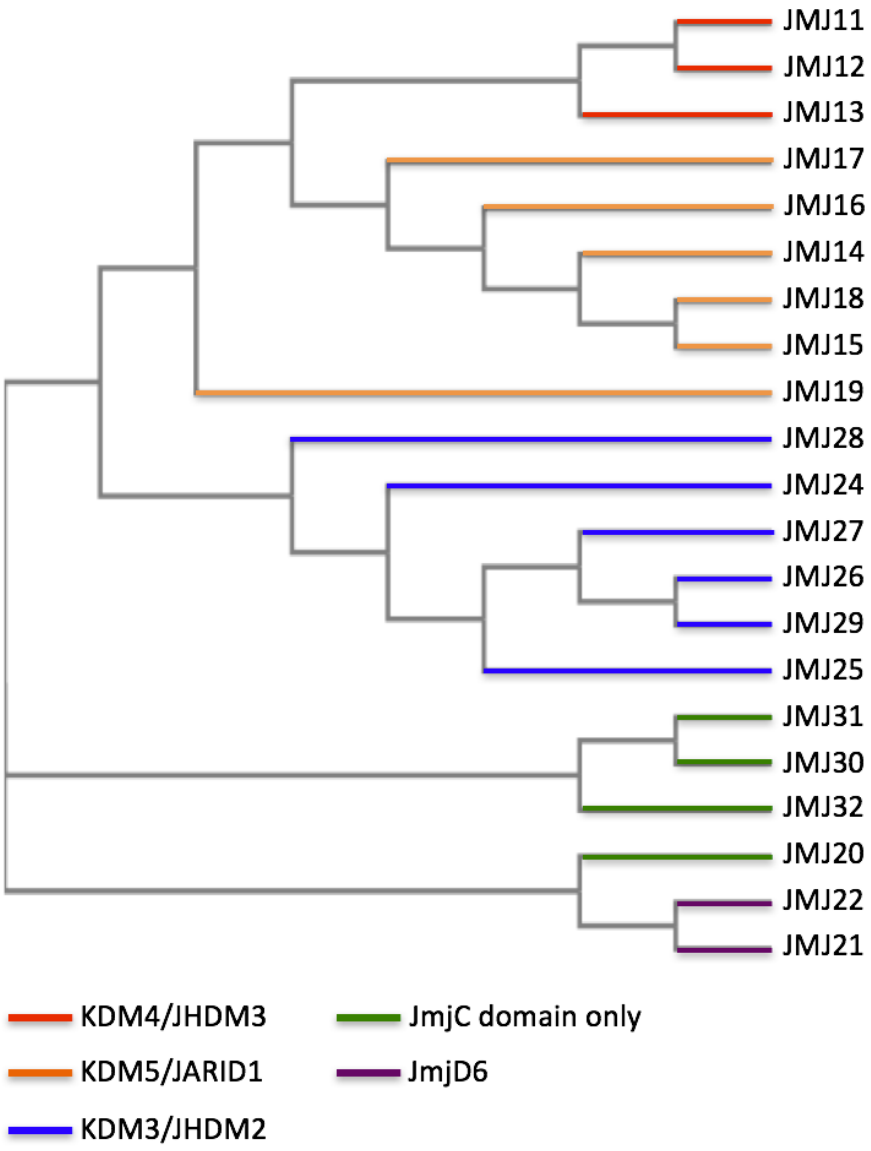

Figure 4: Phylogenetic analysis of JmjC domain-containing proteins in *Arabidopsis* (Clustal Omega & Clustal Phylogeny (http://www.ebi.ac.uk)). Proteins are grouped based on their comparison to human homologs (Lu et al. 2008).

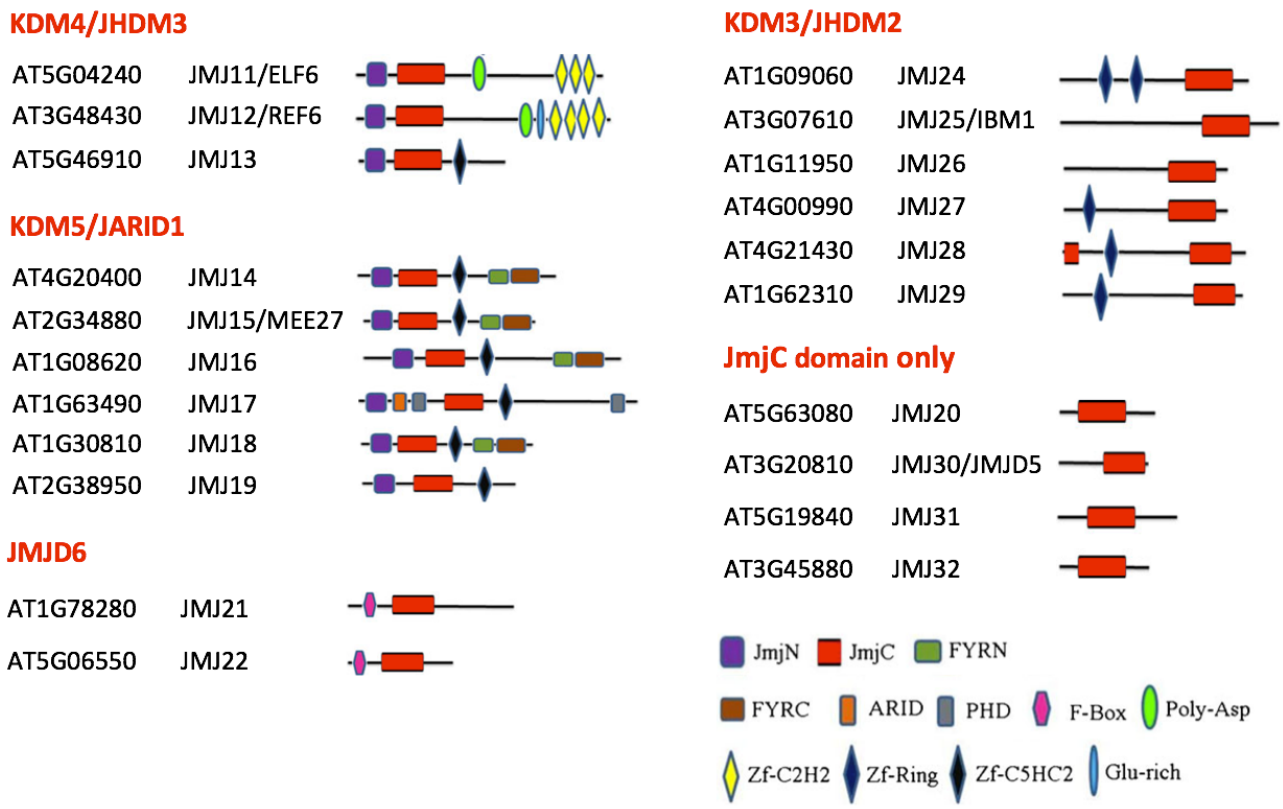

Figure 5: Domain architecture and functional categorization of *Arabidopsis* JmjC domain-containing proteins (modified from (Luo et al. 2013).

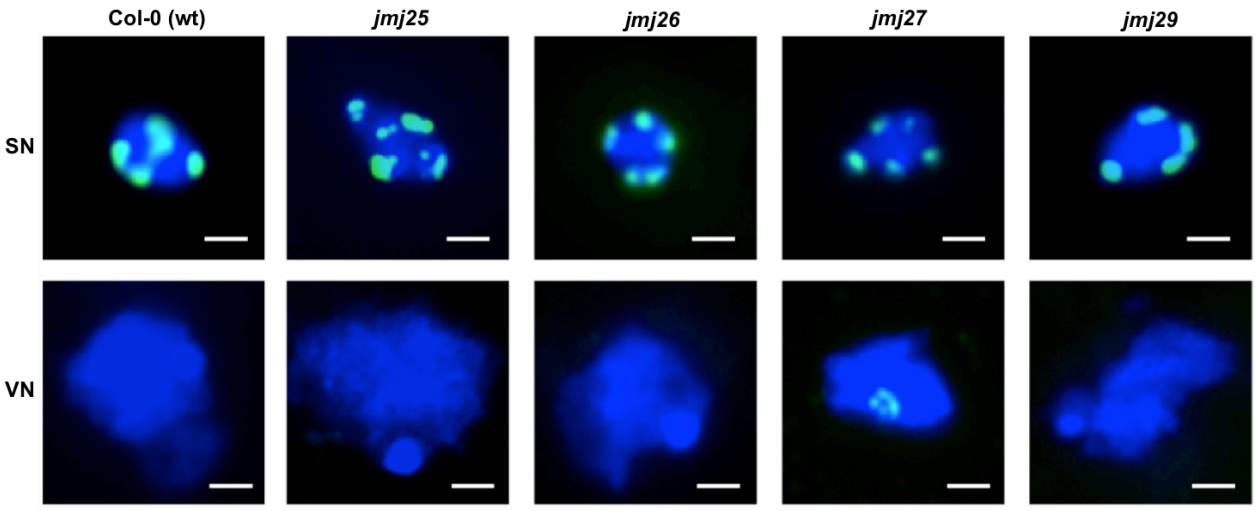

Figure 6: Immunostaining for H3K9me2 using H3K9me2 antibody (green) in pollen nuclei of Col-0 (wild type) and T-DNA insertion lines of KDM3/JHDM2 group of JmjC domain-containing proteins with putative H3K9 demethylase activity. H3K9me2 is preserved in *JMJ27* (SALK_092672) vegetative nuclei. SN: sperm nuclei, VN: vegetative nuclei, Scale bar: 1 µm. DAPI was used for counterstaining nuclei. (Modified from (Chumak 2012)

1.10 Profile of the jmj27-1 Phenotype

Plants homozygous for the JMJ27 mutation do not show morphological abnormalities. Moreover, although the mutation causes the epigenetically repressive mark H3K9me2 to be

observed in vegetative nuclei of pollen, no developmental and reproductive deficiencies were identified. Compared to wild type, pollen germination and pollen competition assays show no significant change in JMJ27 mutant background (Chumak 2012). As previously done for wild type pollen nuclei, several other epigenetic markers were tested in pollen nuclei of *jmj27-1* by double immunostaining or immuno-FISH, to further characterize the consequences of the lack of JMJ27. The epigenetic phenotype of chromocenters in pollen nuclei does not undergo a change in *jmj27-1* as revealed by FISH with the 180CEN probe (Figure 7-A). Similarly, immunostaining using CENH3 antibody shows no change in the chromocenters' identity, compared to wild type sperm and vegetative nuclei (Figure 7-B). The active chromatin mark, H3K4me2, also does not reveal any difference between wild type and *jmj27-1* sperm and vegetative nuclei (Figure 8-A). H3K27me, a repressive modification, is also equally distributed in *jmj27-1* compared to wild type sperm and vegetative nuclei. However, double immunostaining reveals that H3K9me2 and H3K27me signals co-localize in vegetative nuclei of *jmj27* mutant plants (Figure 8-B). Furthermore, an immuno-FISH experiment shows H3K9me2 signals colocalizing with 45S rDNA foci in *jmj27-1* vegetative nuclei (Figure 8-C). Indeed, the two signals display similar characteristics, such as two smaller foci cluster into one larger locus. In *Arabidopsis,* the two NORs (nucleolus organization region), NOR2 and NOR4, which contain 45S rDNA gene repeats, cluster into a single NOR locus in the wild type vegetative nucleus, and the signal in *jmj27-1* clearly forms a cluster of smaller signals, suggesting that the target of JMJ27-mediated H3K9 demethylation in the vegetative nucleus could be the 45S rDNA repeats.

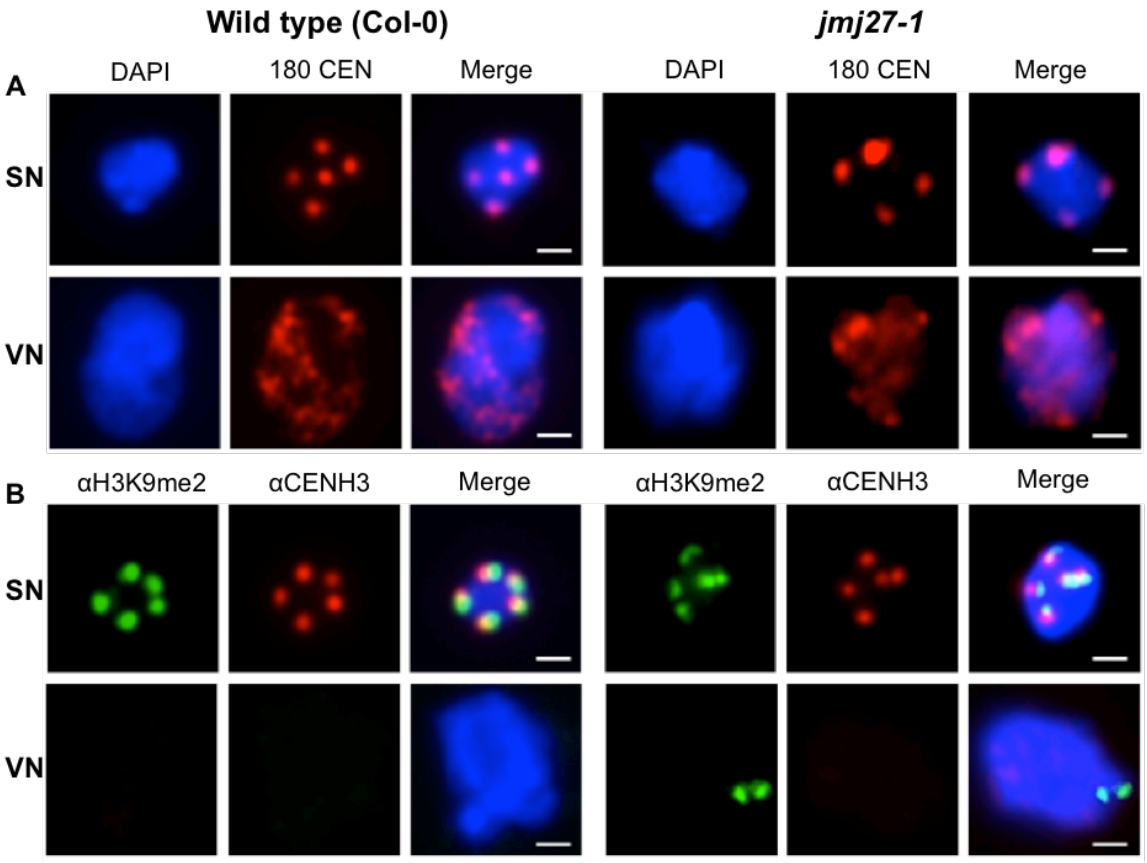

Figure 7: Characterization of centromeric heterochromatin in *jmj27-1* pollen nuclei. A) FISH using probes for 180CEN repeats shows similar dispersed patterns in both wild type and *jmj27-1* sperm and vegetative nuclei. B) Double immunostaining using antibodies against H3K9me2 and centromeric histone 3 variant (CENH3) indicates no change in chromocenters in *jmj27-1* sperm and vegetative nuclei. DAPI was used for counterstaining nuclei. (SN: sperm nuclei, VN: vegetative nuclei, Scale bar: 1 μm.) (Adapted from (Chumak 2012))

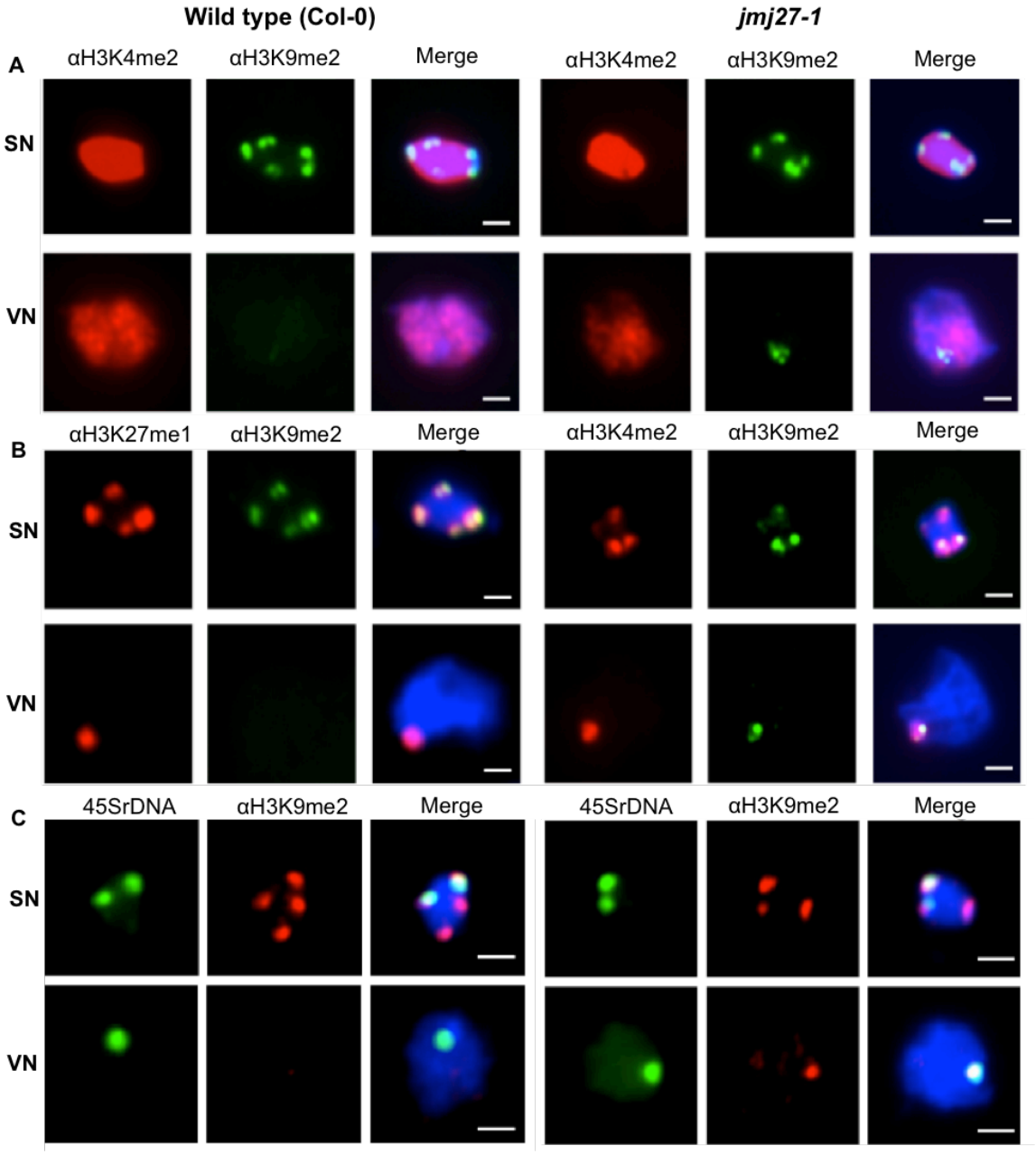

Figure 8: Analysis of chromatin in *jmj27-1* pollen nuclei for repressive and active histone marks via double immunostainings: A) antibodies against H3K4me2 and H3K9me2 reveal no difference for H3K4me2 signal in sperm and vegetative nuclei of *jmj27-1.* B) antibodies against H3K27me1 and H3K9me2 show colocalization of the two signals in vegetative nuclei of *jmj27-1* while there is no difference in sperm nuclei. C) Immuno-FISH using antibodies against H3K9me2 and probes for 45SrDNA reveal colocalization of the two signals in *jmj27-1* vegetative nuclei, while no difference is observed in sperm nuclei. (SN: sperm nuclei, VN: vegetative nuclei, Scale bar: 1 µm. DAPI was used for counterstaining nuclei) (Adapted from (Chumak 2012))

1.11 Increased H3K9me2 at 45S rDNA Promoters in jmj27-1 Vegetative Nucleus

The co-localization of signals observed by immuno-FISH for H3K9me2 and 45S rDNA experiments in *jmj27-1* vegetative nuclei hints at the possibility of an actual biological interaction. Using a FACS method (Schoft et al. 2015), sperm and vegetative nuclei from both wild type and

jmj27-1 plants were sorted. Chromatin immunoprecipitation (ChIP) assays were performed with H3K9me2 antibody, using both sorted nuclei samples and nuclei from seedlings. Following ChIP, qPCR was performed with a set of primers in different regions of the 45S rDNA genes, to check if any specific region would precipitate more in *jmj27-1* compared to wild type. Indeed, in *jmj27-1*, 45S rDNA promoter sequences were enriched in both nuclei types and in seedlings (Figure 9). The result showed that H3K9me2 is increased in promoter regions of 45S rDNA genes in *jmj27-1* in all tested nuclei types, supporting the hypothesis of a biological interaction between these H3K9me2 and JMJ27 at these repeats.

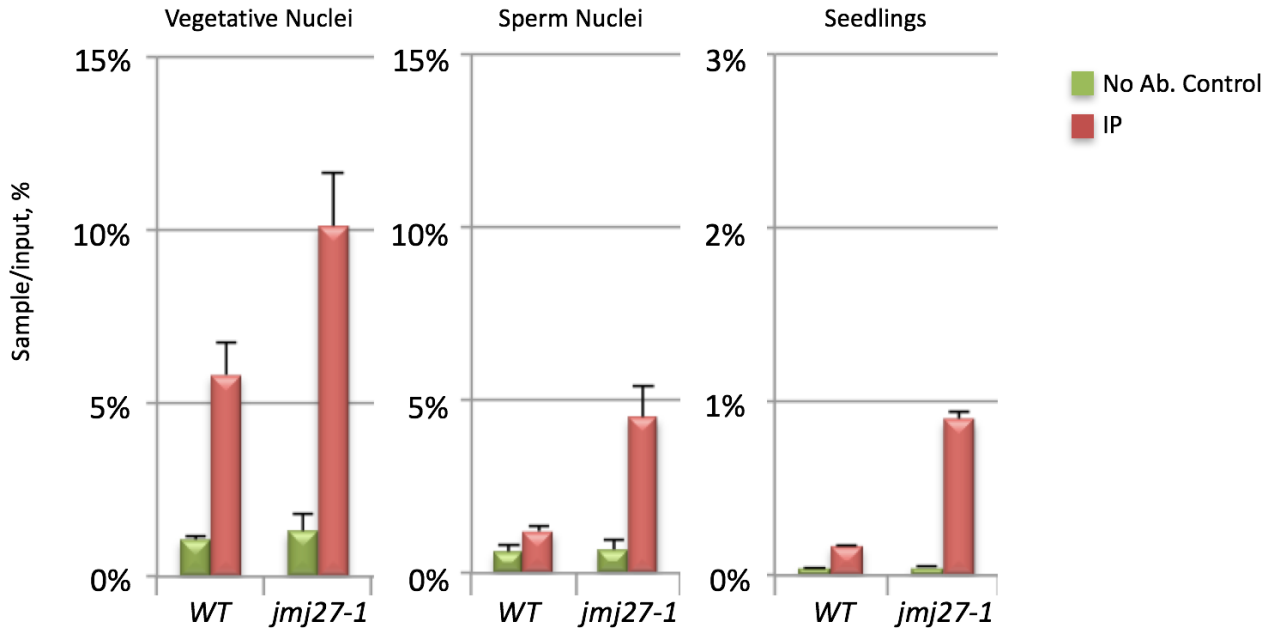

Figure 9: JMJ27 mediates demethylation of H3K9me2 at 45S rDNA promoters. Sorted sperm and vegetative nuclei and nuclei from seedling samples of wild type and *jmj27-1* plants were subjected to ChIP with H3K9me2 antibody, followed by qPCR using a set of primers in different regions of 45S rDNA. Compared to wild type samples, the promoter region was enriched in all nuclei types. Green bars: no antibody control, Red Bars: IP by H3K9me2 antibody. Enrichments are measured by the ratio of qPCR product of ChIP samples with or without antibody to qPCR product of input samples. Adapted from (Chumak 2012)

1.12 DNA Hypermethylation at 45S rDNA Promoters in jmj27-1 Vegetative Nucleus

Epigenetic regulation of chromatin involves interplay between histone modifications and DNA modifications that result in transcriptionally active or silent state (Cheng 2014). Therefore, increased amounts of repressive chromatin mark H3K9me2 at 45S rDNA promoters in *jmj27-1* suggest a possible alteration of DNA methylation as well. Bisulfite sequencing was performed to determine the methylation status of 45S rDNA promoters in sorted sperm and vegetative nuclei and seedling DNA in *jmj27-1* plants, in comparison to wild type (Chumak 2012). In all samples, and

considering the amount of total methylation in all three contexts (CG, CHG and CHH), the number of methylated promoter sequences was significantly higher in *jmj27-1* plants, compared to wild type (Figure 10). Furthermore, bisulfite sequencing analysis of the same promoter region in *jmj27-1* complemented via ectopic JMJ27 expression restored DNA methylation amounts to almost wild type levels (Chumak 2012), indicating that JMJ27 has a role in mediating DNA hypomethylation at 45S rDNA promoter regions.

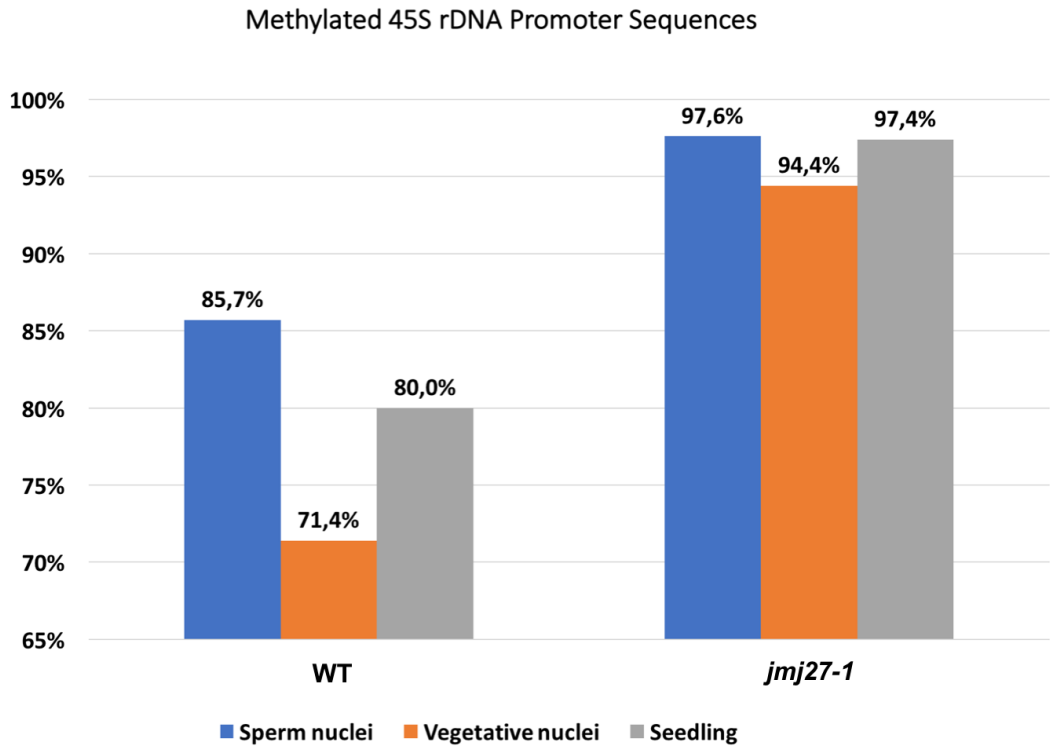

Figure 10: Sorted sperm and vegetative nuclei, and seedling DNA from wild type and *jmj27-1* were analyzed by bisulfite sequencing for the degree of DNA methylation at 45S rDNA promoters. The *JMJ27* mutation causes substantial hypermethylation in all samples, compared to their wild type counterparts. Bars represent the percentage of methylated 45S rDNA promoters found in all sequences analyzed for the given sample type. Modified from (Chumak 2012).

1.13 Gene and Protein Structure of JMJ27

JMJ27 (AT4G00990) is located on the plus strand of chromosome 4 short arm: 426,886 to 431,824. The full-length genomic region spans over 4878 bp with 13 exons and 12 introns, while the full-length cDNA is 2804 bp and the translation product is 840 aa (Figure 11A). The protein structure contains two conserved domains: a Zinc-finger RING (ZnF - RING) domain and a JmjC domain (Figure 11B). ZnF – RING is a specialized type of the ZnF domain with 40-60 residues and binds two Zinc ions. ZnF domains are found in proteins with a variety of functions including transcription, translation, mRNA trafficking, cell development and chromatin remodeling (Hall

2005; Freemont 1993). Recently, they were also shown to be required for demethylase activity (Yamane et al. 2006). The RING (Really Interesting New Gene) domain in the mammalian protein c-Cbl has an intrinsic E3 ubiquitin ligase activity, and it is speculated to be a general feature of this domain (Joazeiro et al. 1999). The finger-like protruding structure of this domain, with conserved cysteine and histidine residues at its core binding to Zinc ions, creates a firm pocket for binding to other molecules, thus facilitating protein-protein interaction (Gamsjaeger et al. 2007). The second domain, the JmjC domain, contains a conserved co-factor binding site for Fe (II) and α-ketoglutarate. Initially, JmjN and JmjC domains were considered functional partners, requiring the presence of each other for activity. However, this cannot be a general principle, as single domains are found separately in diverse proteins. The crystal structure of the JmjC domain revealed the existence of a barrel structure resembling the cupin superfamily proteins. Thus, the family were labeled as metalloenzymes, active upon compounding with metal ions as co-factors (Clissold & Ponting 2001; Balciunas & Ronne 1999). Three residues for Fe (II) and two residues for α-ketoglutarate were found to be essential for these coupling to take place (Klose et al. 2006). Beside their involvement in histone demethylase activity (Tsukada et al. 2006), a new function for JmjC domain-containing proteins as histone-modifying hydroxylases has been suggested (Trewick et al. 2005).

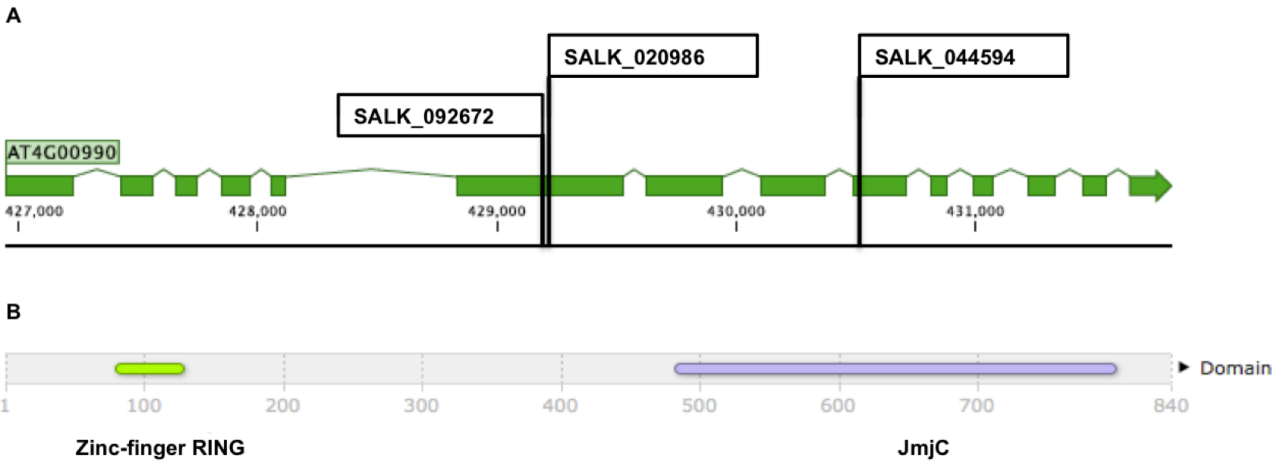

Figure 11: A) The gene structure of *JMJ27* (AT4G00990). Bars: exons; lines: introns. In addition, the insertion sites of three T-DNA lines: SALK_092672 (*jmj27-1*), SALK_020986 (*jmj27-2*) and SALK_044594 (*jmj27-3*) used for the reverse genetic screen are indicated (created by CLC Sequence Viewer 7, Qiagen). B) The graphical representation of the 840 aa long JMJ27 protein with two conserved protein domains, a Zinc-finger RING and a JmjC domain.

1.14 The jmj27-1 Phenotype is Complemented by Ectopic Expression of JMJ27

To assess whether the *jmj27-1* phenotype is essentially dependent on *JMJ27* expression, a complementation test was performed (Chumak 2012). I contributed to this experiment by

constructing the vector carrying JMJ27 under the native promoter fused to RFP at the C terminus (*pJMJ27: JMJ27: RFP*) (see chapter 3.4.1.1). This vector was transformed to *jmj27-1* plants, and the lines homozygous for the insert were selected. Free pollen nuclei were isolated from two independent lines (*JMJ27: RFP-1, JMJ27: RFP-2*). Immunocytochemistry with antibodies against H3K9me2 was performed to compare the phenotypes of vegetative and sperm nuclei from Col-0 wild type, *jmj27-1* and the two transgenic lines (Figure 12). A clear rescue of the H3K9me2 phenotype was observed in vegetative nuclei of *JMJ27: RFP-1* and *JMJ27-RFP-2*, which resembles the H3K9me2 profile of wild type Col-0 nuclei. This indicated that the fusion protein was functional and complemented the mutant phenotype, and it demonstrated that JMJ27 expression is needed for proper demethylation of H3K9me2 in vegetative nuclei of pollen (Chumak 2012).

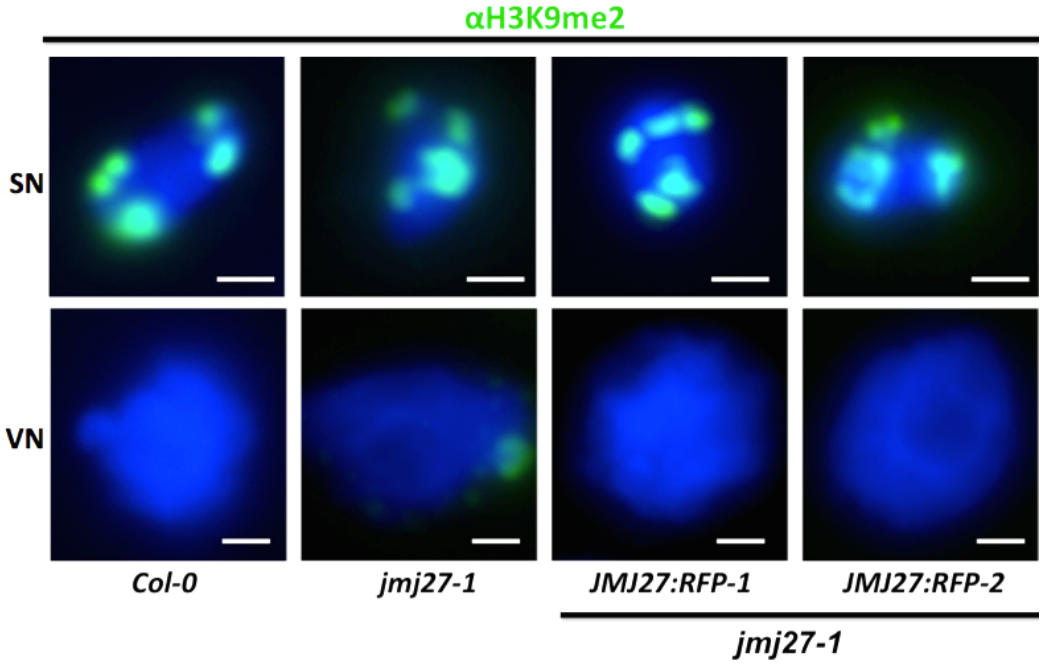

Figure 12: The *jmj27-1* phenotype is complemented by ectopic expression of JMJ27 in two independent lines. *JMJ27: RFP-1* and *JMJ27: RFP-2* homozygous for *pJMJ27: JMJ27: RFP* in *jmj27-1* background. Immunocytochemistry was performed with antibodies against H3K9me2 using free sperm and vegetative nuclei from wild type Col-0, *jmj27-1, JMJ27: RFP-1* and *JMJ27: RFP-2*. DAPI was used to stain the nuclei (modified from (Chumak 2012)). (Scale bars: 1 µm)

1.15 Expression Profile of JMJ27 in Arabidopsis

The expression pattern of JMJ27 in *Arabidopsis* homozygous for *pJMJ27: JMJ27: RFP* in *jmj27-1* background was analyzed (Chumak 2012). Also, these data were obtained with the lines containing my expression vectors (see chapter 3.4.1.1). JMJ27 was found primarily expressed in the vegetative nucleus of pollen compared to none or low expression observed in sperm nuclei (Figure 13). Inspecting somatic tissues of the same plants at different stages showed that JMJ27 is highly

expressed in rapidly dividing cells such as root tips. Moreover, during different stages of embryonic development, elevated expression of JMJ27 is observed (Figure 14).

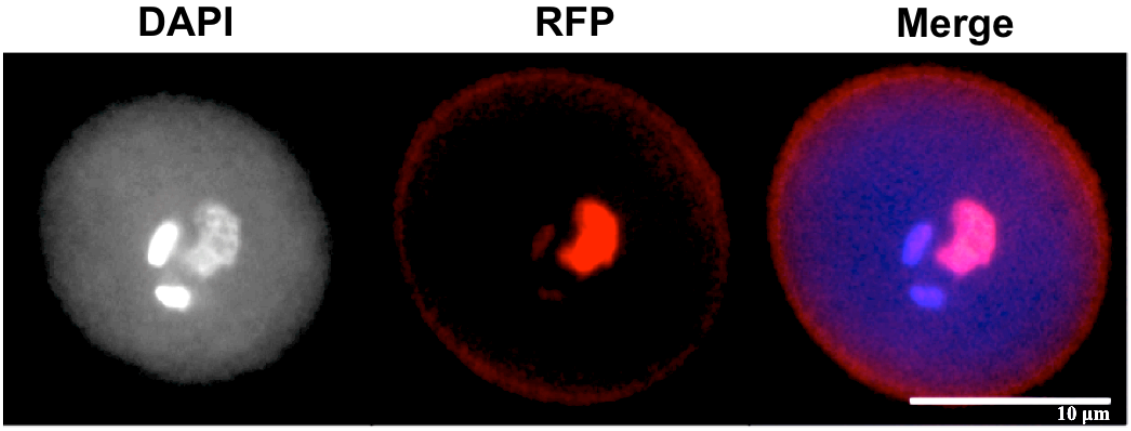

Figure 13: Expression profile of JMJ27 in *Arabidopsis* pollen. Pollen samples from *pJMJ27: JMJ27: RFP* transgenic line in *jmj27-1* background were stained with DAPI (left panel) and checked for RFP expression (mid panel). JMJ27-RFP expression was found primarily localized to the vegetative nucleus, while low levels of expression were observed in sperm nuclei (mid & right panel). (modified from (Chumak 2012))

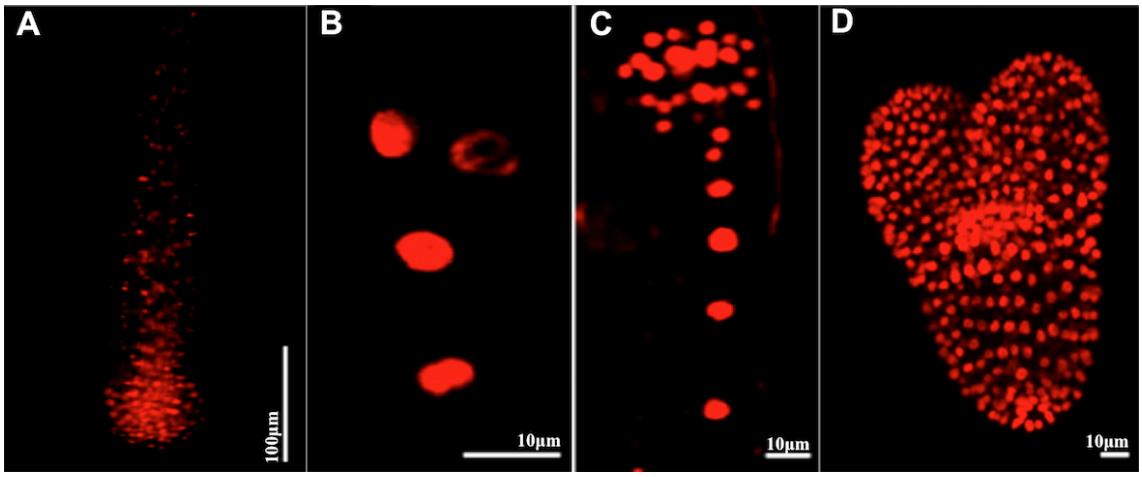

Figure 14: JMJ27 is highly expressed in rapidly dividing somatic cells. Somatic tissue samples from *pJMJ27: JMJ27: RFP* seedlings in *jmj27-1* mutant background are shown: (A) root tip of 10 day-old seedling, (B) – (D) expression profile during different stages of embryo development; (B) 4 cell stage, (C) globular stage, (D) torpedo stage. (modified from (Chumak 2012))

This expression profile suggests that, although JMJ27 might be expressed at basal level in all tissues, the elevated expression in the vegetative nucleus of pollen and rapidly proliferating cells indicate a distinct role in these cases (Chumak 2012). In a very recent study, a predominant and weak JMJ27 localization to nucleus and cytoplasm was shown, respectively. Moreover, *JMJ27* expression is induced in response to *Pseudomonas syringae* infection (Dutta et al. 2017).

2 Aim of the study

The overall aim of the study was to characterize the function of the putative H3K9me2 demethylase JMJ27 in *Arabidopsis thaliana.* Previously published data suggested a role for JMJ27 in H3K9me2 demethylation and DNA hypomethylation at 45S rDNA repeats. This and its possible action at additional target regions might be partially responsible for large-scale heterochromatin decondensation and epigenetic reconfiguration of the vegetative nucleus in pollen. However, the exact mechanism of how JMJ27 modulates these processes were not clear. To further investigate the role of JMJ27, I generated several transgenic lines. First, I modified the conserved catalytic JmjC domain and tested the effect on H3K9me2 methylation *in vivo*. For the second part, I generated an epitope-tagged JMJ27 expression construct. I searched for possible interacting protein partners of JMJ27 by co-immunoprecipitation followed by mass spectrometry analysis and generated a list of candidates.

3 Materials and Methods

3.1 Plant Material and Growth Conditions:

3.1.1 Growth of Plants on Soil

Seeds (Table 3) were sterilized with 2% sodium hypochlorite for 5 min followed by three washes with sterile water. Before sowing on soil, they are re-suspended with 0.1 % agarose at room temperature and spread on trays full of soil using a glass pipette. Following two days of stratification at 4 C°, trays were transferred into automated growth chambers at 22 C°, 60% humidity under daily 16 h light and 8 h dark cycles.

3.1.2 Growth of Plants on Murashige-Skoog Plates:

Seeds (Table 3) were sterilized as described in previous section 3.1.1. Murashige-Skoog plates (0.5X) with and without selection drug were used for the growth of seedlings in growth chambers under 22 C°, 60% humidity, under daily 16 h light and 8 h dark cycles.

Line ID	**Gene ID**
Columbia (Col-0)	Wild type
SALK_092672 (*jmj27-1*)	AT4G00990
N16157 (*emb1644 - 1*)	AT5G27720 *(EMB1644/LSM4)*
SALK_121177	AT5G26742 *(EMB1138)*
SAIL_103_A01	AT2G21660 *(CCR2/GRP7)*

Table 3: *Arabidopsis thaliana* lines used in this study

3.2 Pollen Isolation

Pollen was isolated from flowering *Arabidopsis thaliana* plants starting from four weeks by cutting and collecting inflorescences into a beaker. Sucrose solution (9% (w/v) was added 1:2 (v/v) and all material was immersed in the solution with a spatula. Pollen was released from flowers by continuous stirring for 1-2 min. The suspension was filtered through a 100 µm mesh filter into a clean beaker and transferred into appropriate centrifugation tubes. The remaining green material was kept for repetition of the procedure. The sample was centrifuged at 2800 rpm for 10 min. The supernatant was poured back into the beaker with the flowers to repeat the same stirring and filtering steps. After filtering, the sample was transferred into the same centrifugation tube to repeat the centrifugation step. The supernatant was disposed and the pellet was re-suspended with excess

Buffer A (1 M sorbitol, 7% Ficoll PM 400, 5 mM MgAc, 3 mM $CaCl_2$, 5 mM EGTA, 50 mM Tris-HCl pH 7.5, 20% glycerol, 2% Triton X-100) (1 - 5 ml). The suspension was filtered through a 40 µm mesh filter into a clean tube. The sample was centrifuged for 10 min at 2000 rpm. The supernatant was discarded and the pellet was re-suspended in 1 ml of Buffer A and transferred into an Eppendorf tube to centrifuge at 7400 rpm for 5 min. The supernatant was discarded and the pellet containing the isolated pollen was kept to either use freshly or was shock-frozen in liquid nitrogen and stored at – 80 C°.

3.3 Pollen Nuclei Isolation

Isolated pollen was re-suspended in 3 volumes of Buffer A (1 M sorbitol, 7% Ficoll PM 400, 5 mM MgAc, 3 mM $CaCl_2$, 5 mM EGTA, 50 mM Tris-HCl pH 7.5, 20% glycerol, 2% Triton X-100). Two-ml Eppendorf tubes were filled with approximately 1.8 ml volume of acid-washed glass beads (diameter 0.4-0.6 mm, BBI-8541701, Sartorius Stedim Biotech GmbH, Germany). Fifty µl - 100 µl of re-suspended pollen was pipetted on top of the beads and shaken at 15 Hz for 1.5 min (Mixer Mill MM400, Retsch, Germany). Using a fixed needle, the bottom of the tubes was punctured. The lid of a clean 2 ml Eppendorf tube was cut and placed into a 15 ml falcon tube or a glass tube. The lid of the sample tube was also cut and the tube was placed on top of a clean tube. The assembly was centrifuged for 10 min at 2000 rpm at 4 C° to collect the ground sample into the clean tube without beads. The supernatant was discarded and the pellet containing the free sperm and vegetative nuclei was kept. A small aliquot was used to confirm the nuclei in the pellet by DAPI staining and visualization under fluorescence microscope.

3.4 Transgenic Lines

Epitope-tagged and fluorescent-tagged expression vectors for JMJ27 were constructed by using conventional cloning methods and the Gateway cloning system (Invitrogen, Carlsbad, CA, USA) (Table 4).

Vector Name	**Experiment**	**Backbone**
pJMJ27: JMJ27: RFP	Expression and localization	pB7RWG2,0
pJMJ27: ΔJMJ27: RFP	*In vivo* histone demethylation	pB7RWG2,0
pJMJ27: JMJ27: HA	Immunoprecipitation	pEarleyGate 301
pJMJ27: JMJ27: FLAG	Immunoprecipitation	pEarleyGate 302
pJMJ27: JMJ27: cMyc	Immunoprecipitation	pEarleyGate 303

Table 4: Summary of transgenic lines constructed in this study

3.4.1 Fluorescent-Tagged Constructs

3.4.1.1 pJMJ27: JMJ27: RFP:

The pB7RWG2,0 (http://gateway.psb.ugent.be) (Figure 15) gateway destination vector was used as the backbone. The p35S promoter of pB7RWG2,0 was replaced with the promoter region of JMJ27 (approximately 1,5 kb upstream of the transcription start site) by conventional restriction cloning. *HindIII* and *SpeI* restriction sites flanking the p35S promoter were used to replace it with the *JMJ27* promoter fragment, which was amplified by PfuUltra II Fusion HS DNA Polymerase (#600670, Agilent, Santa Clara, CA, USA) with primers adding *HindIII* (promAT4G00990_Hind III _F:5'-GTTCGTTAAAGCTTATCAATGCTTAC-3') and *SpeI* (promAT4G00990_Spe I _R: 5'-GCATACACTAGTTCGGAGACAAAGAAGAGACCAC-3') cut sites. Following restriction by *HindIII* and *SpeI* enzymes (NEB, Ipswich, MA, USA), both vector and insert were purified using Wizard SV Gel and PCR Clean-Up kit (Promega, Wisconsin, USA) and ligated using T4 ligase (NEB, Ipswich, MA, USA) to create the pJMJ27: GW: RFP destination vector. Since the GW cassette contains the *ccdB* negative selection gene, OneShot ccdB Survival 2T1 *E. coli* strain (Invitrogen, Carlsbad, CA, USA) that is resistant to expression of the *ccdB* gene was used to grow cells following transformation. The *JMJ27* genomic region was amplified using attB1fw_AT4G00990: 5'-GGGGACAAGTTTGTACAAAAAAGCAGGCTTCATGGAGAAAAT GAGAGGGAAGCG-3' and attB2rev_AT4G00990: 5'-GGGGACCACTTTGTACAAGAAAGCT GGGTCGGTATCACTGCGTCGGGAGC-3' primers designed to add attB1 and attB2 sites, excluding the stop codon. The successive product is used in a BP reaction with pDONR221 donor vector (Invitrogen, Carlsbad, CA, USA), which includes attP1 and attP2 sites, using Gateway BP Clonase II Enzyme mix (#11789-020, Invitrogen, Carlsbad, CA, USA), following the manufacturers' protocol to generate the pENTRY-JMJ27 entry vector, which has *JMJ27*, flanked by attL1 and attL2 sites. pENTRY-JMJ27 and destination vector pJMJ27: GW: RFP with attR1 and attR2 sites were used in a LR reaction using Gateway LR Clonase II Enzyme mix (#11791-020, Invitrogen, Carlsbad, CA, USA), as instructed in the manufacturers' protocol to create the *pJMJ27: JMJ27: RFP* expression vector.

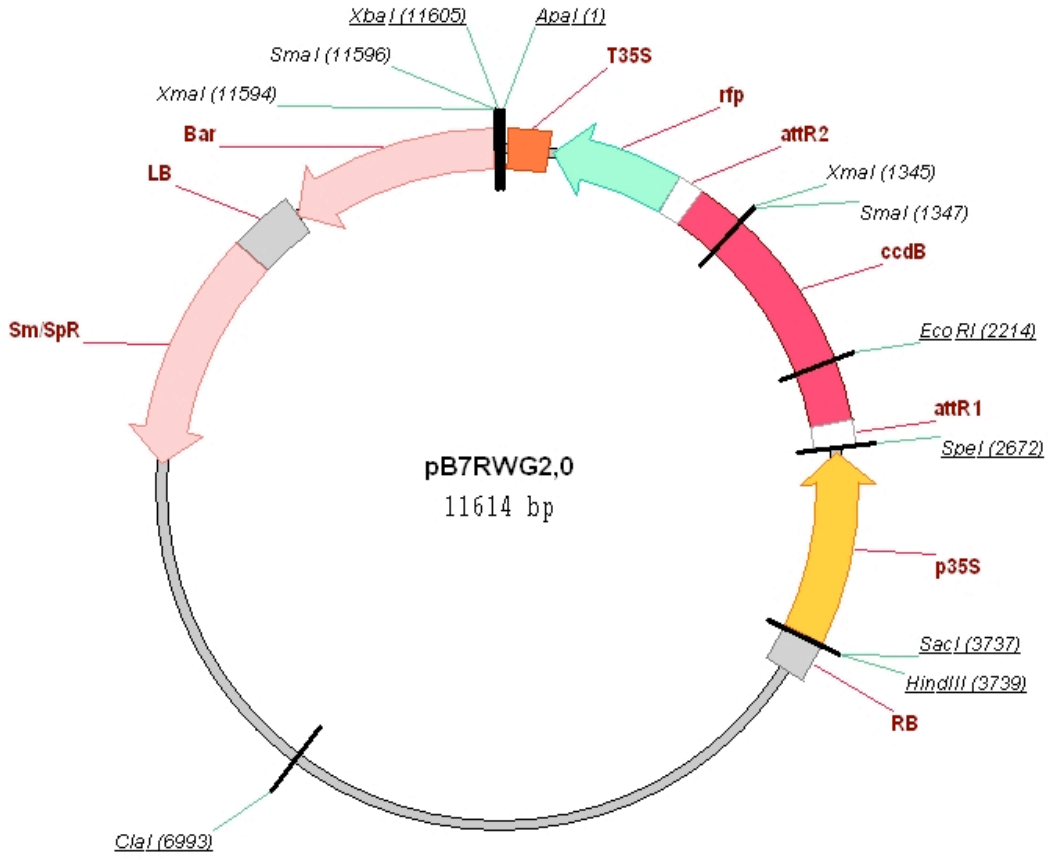

Figure 15: Schematic representation of pB7RWG2,0 destination vector (http://gateway.psb.ugent.be)

3.4.1.2 pJMJ27: ΔJMJ27: RFP

The pJMJ27: GW: RFP vector generated in the previous step was used as the backbone. A new entry vector for JMJ27, which has a mutation in the catalytic domain, was constructed. Based on previous data showing that the conserved cofactor Fe (II) iron binding site residues are essential for histone demethylase activity of JmjC domain-containing protein family members (Z. Chen et al. 2006; Klose et al. 2006; Lu et al. 2008), the QuikChange Lightning Site Directed Mutagenesis kit (Agilent, Santa Clara, CA, USA) was used to make HCD546_548AAA residue conversion by using primers At4G00990_SDM_F: 5'-CGGTGACAAAACTTGCTGCTGCCATTTCTGACGCGG-3' and At4G00990_SDM_R: 5'-CCGCGTCAGAAATGGCAGCAGCAAGTTTTGTCACCG-3'. The mutagenized *JMJ27* genomic fragment was amplified by using primers attB1fw_AT4G00990: 5'-GGGGACAAGTTTGTACAAAAAAGCAGGCTTCATGGAGAAAATGAGAGGGAAGCG-3' and attB2rev_AT4G00990: 5'-GGGGACCACTTTGTACAAGAAAGCTGGGTCGGTATCACTG CGTCG GGAGC-3', excluding the stop codon, to add attB sites. The product was used in a BP reaction with the pDONR221 donor vector, which included attP1 and attP2 sites, (Invitrogen, Carlsbad, CA, USA) using Gateway BP Clonase II Enzyme mix (#11789-020, Invitrogen, Carlsbad, CA, USA), following the manufacturers' protocol, to generate the pENTRY-mutJMJ27 entry

vector, which had mutagenized *JMJ27*, flanked by attL1 and attL2 sites. pENTRY- mutJMJ27 and destination vector pJMJ27: GW: RFP with attR1 and attR2 sites were used in a LR reaction using Gateway LR Clonase II Enzyme mix (#11791-020, Invitrogen, Carlsbad, CA, USA) as instructed in the manufacturers' protocol to create the *pJMJ27: ΔJMJ27: RFP* expression vector.

3.4.2 Epitope-Tagged Constructs

3.4.2.1 pJMJ27: JMJ27: HA

pEarleyGate 301 gateway vector (Earley et al. 2006) was used as the destination vector (Figure 16).

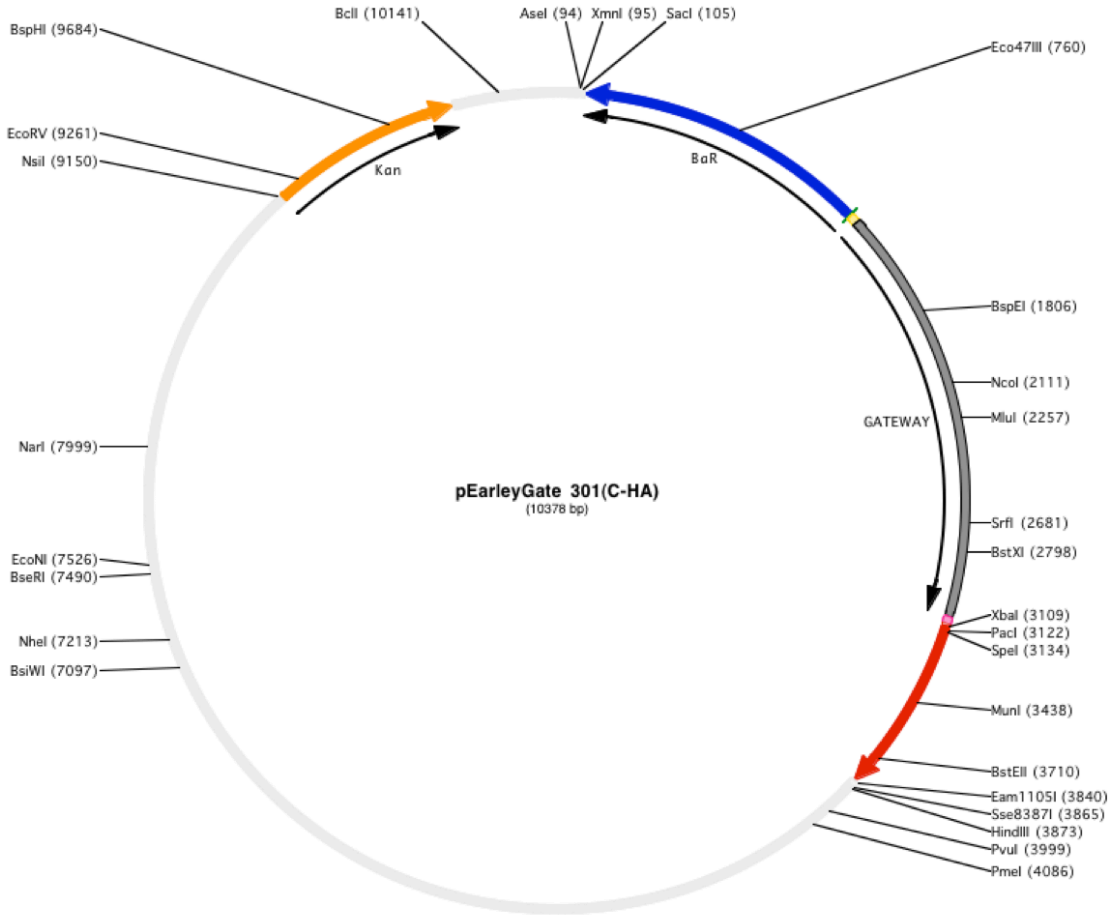

Figure 16: pEarleyGate 301 graphical vector map (Earley et al. 2006)

The *JMJ27* genomic region including 1.5 kb upstream of the transcription start site was amplified using primers: attB1_proJMJ27_Frw: 5'-GGGGACAAGTTTGTACAAAAAAGCAGGC TTCGTTCGTTAAAGCTTATCAATGCTTAC-3' and attB2rev_AT4G00990: 5'-GGGGACCACT

TTGTACAAGAAAGCTGGGTCGGTATCACTGCGTCGGGAGC-3' to produce a fragment flanked by attB1 and attB2 sites. pDONR221, which had attP sites, (Invitrogen, Carlsbad, CA, USA) was used as donor vector in a BP reaction using Gateway BP Clonase II Enzyme mix (#11789-020, Invitrogen, Carlsbad, CA, USA) to produce the entry vector pENTRY-pJMJ27: JMJ27. pEarleyGate 301 was used as destination vector in an LR reaction using Gateway LR Clonase II Enzyme mix (#11791-020, Invitrogen, Carlsbad, CA, USA) to produce pJMJ27: JMJ27: HA expression vector.

3.4.2.2 pJMJ27: JMJ27: FLAG

pEarleyGate 302 gateway vector (Earley et al. 2006) was used as the destination vector (Figure 17).

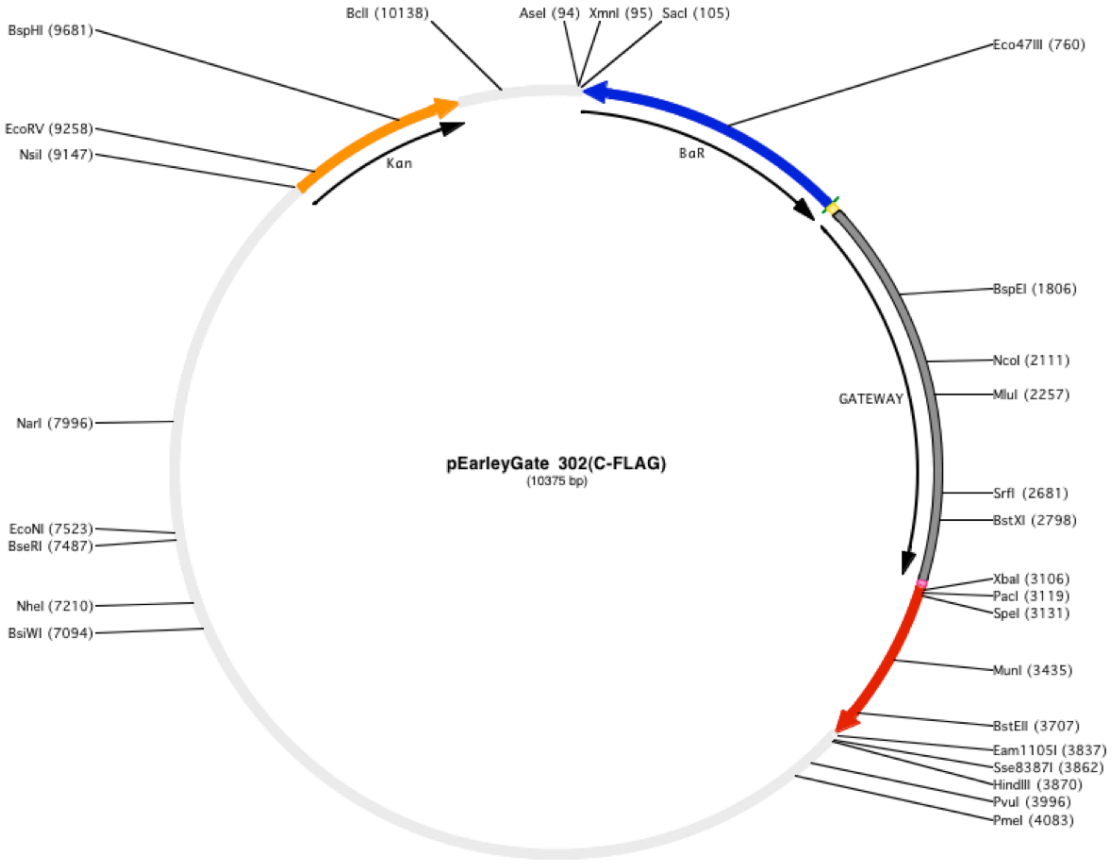

Figure 17: pEarleyGate 302 vector map graph (Earley et al. 2006)

pENTRY-pJMJ27:JMJ27 (see chapter 3.4.2.1) was used as entry vector in an LR reaction using Gateway LR Clonase II Enzyme mix (#11791-020, Invitrogen, Carlsbad, CA, USA) to produce the pJMJ27: JMJ27: FLAG expression vector.

3.4.2.3 pJMJ27: JMJ27: cMyc

pEarleyGate 303 gateway vector (Earley et al. 2006) was used as the destination vector (Figure 18).

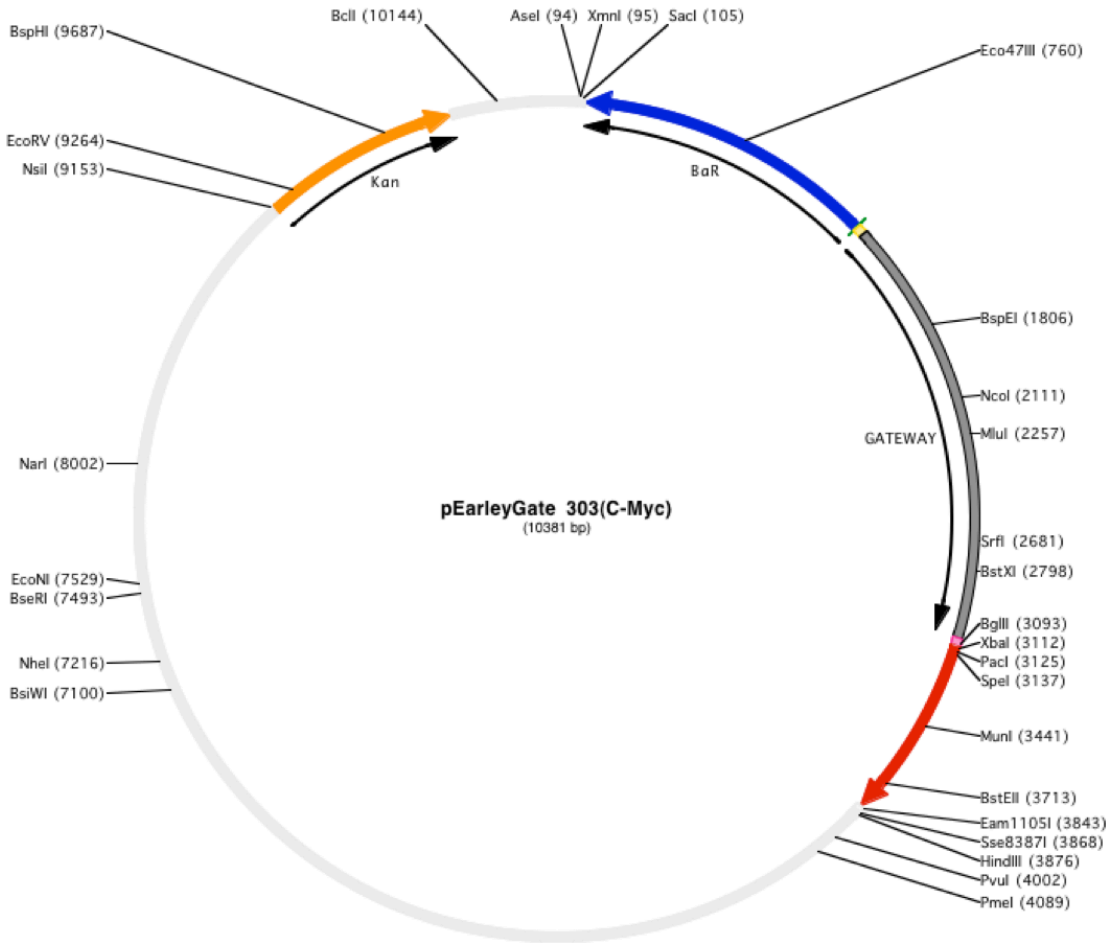

Figure 18: pEarleyGate 303 vector map graph (Earley et al. 2006)

pENTRY-pJMJ27:JMJ27 (see 3.4.2.1) was used as entry vector in an LR reaction using Gateway LR Clonase II Enzyme mix (#11791-020, Invitrogen, Carlsbad, CA, USA) to produce the pJMJ27: JMJ27: cMyc expression vector.

3.4.3 Transformation

The floral dip transformation method for *Arabidopsis thaliana* mediated by *Agrobacterium tumefaciens* strain GV3101 was used for all transformation experiments (Clough & Bent 1998). Fluorescent-tagged and epitope-tagged constructs were transformed to electro-competent *Agrobacterium* using pre-set protocol of Bio-Rad GenePulser XCell electroporator (Bio-Rad, California, USA) at 2400 volts, 25 µF, 200 Ω using 1 mm cuvettes. Selection media containing

rifampicin (100 µg/ml) (*Agrobacterium* selection) and gentamycin (50 µg/ml) (Ti-plasmid selection) was supplemented with antibiotics to which resistance was provided by the transformed expression vectors. For selecting successful transformants, spectinomycin at 75 µg/ml and kanamycin at 50 µg/ml were added to the media for pB7RWG2,0 and pEarleyGate originating transformants, respectively.

3.5 Protein Extraction

3.5.1 Western Blot Experiments:

Leaf tissue was collected from transgenic plants homozygous for pJMJ27: JMJ27: HA and Col-0 wt control plants into Eppendorf tubes. The samples were shock-frozen in liquid nitrogen and 2 volumes of 1x SDS-PAGE buffer was added, followed by grinding with a plastic micro pestle. The samples were vortexed twice for 5 seconds and incubated on a preheated block at 95 C° for 5 min. The samples were centrifuged at 13,000 rpm and supernatants were collected into new tubes and used for further procedures.

3.5.2 Immunoprecipitation Experiments:

Five g of 2-3 weeks-old transgenic or wt *Arabidopsis thaliana* seedlings were shock-frozen in liquid nitrogen in a ceramic mortar and ground with a ceramic pestle until a fine powder was obtained. Powdered seedlings were re-suspended in 5 ml of ice-cold grinding-sonication buffer (1 mM EDTA, 1 mM DTT, 0.05% SDS, 10% glycerol, 150 mM NaCl, 0.1% NP40/Triton X100, 1 mM PMSF, 50 mM Tris-HCl pH 7.5) supplied with protease inhibitor (#05892988001, Complete ULTRA Tablets, glass vial, Roche, Basel, Switzerland). The tubes were kept on ice for 15 min and vortexed every 5 min briefly. Samples were transferred into Eppendorf tubes and were incubated by gentle rotation at 4 C° for 15 min. The tubes were centrifuged at 13,000 rpm for 10 min at 4 C°. The supernatants were transferred to new tubes and centrifugation was repeated but for 5 min. Aliquots were kept from supernatants to measure protein concentration, and the remaining supernatants were transferred to new tubes and kept for further steps.

3.6 Western Blot

Protein samples were extracted as previously described (see chapter 3.5.1) and were boiled in SDS loading buffer (250 mM Tris-HCl pH 6.8, 8% (w/v) SDS, 40% glycerol, 0.08% bromophenol blue (w/v), 147 mM beta-mercaptoethanol) for 5 min at 95 C°. Pre-casted 7.5% Tris-Glycine gel (#456-1024S, Mini-Protean TGX Gel Bio-Rad, California, USA) was used for running samples at

200 V for 30 min using 1X Tris-Glycine-SDS running buffer (#161-0732, Bio-Rad, California, USA). Samples were transferred to nitrocellulose membrane (Hybond ECL, #RPN3032D, GE Healthcare, Little Chalfont, UK) for 1 hour at 90 V or overnight at 30 mA using a wet transfer chamber in the 4C° room. Blocking was done using non-fat milk (5%) in 1X PBS at room temperature for 1 hour on an orbital shaker (#SSL1, Stuart Equipment, Staffordshire, UK). Incubation with the primary antibody (Table 5) was done at room temperature for 1 hour or overnight at 4 C°. The membrane was washed 3 times for 5 min each using 1X PBS containing 0.1% Tween. The incubation with the secondary antibody (Table 5) was done for 1 hour at room temperature. The membrane was washed 3 times for 5 min each using 1X PBS containing 0.1% Tween. All incubations and washing steps were done on an orbital shaker. ECL Prime WB Detection Reagent (#RPN2232, GE Healthcare, Little Chalfont, UK) was used as instructed by the manufacturer. Amersham Hyperfilm ECL (#10607665, GE Healthcare, Little Chalfont, UK) was used to develop signals using an AGFA Cirox60 X-Ray developer (AGFA Healthcare, Belgium).

Antibody	Working concentration	Supplier
rabbit anti-H3K9me2 (#55)	1:200	Gift from Dr. Thomas Jenuwein (MPI, Freiburg, Germany) (#4677)
mouse anti-H3K9me2 (#59)	1:200	WAKO, Germany (#302-32369)
anti-rabbit IgG DyLight 547 (#36), goat	1:200	Pierce, IL, USA (#31020)
anti-mouse IgG FITC (#24), goat	1:200	Abcam, Cambridge, UK (#ab6785)

Table 5: Antibodies used throughout the study

3.7 Immunoprecipitation

Protein extraction from seedlings was done as previously described (see chapter 3.5.2). Samples were divided into two groups; one for sonication and the other group without. Sonication (Bioruptor Standard, Diagenode, Belgium) was done at high power with on and off cycles for 15 seconds each, for 5 min in total. Sonicated samples were centrifuged for 10 min at 13,000 rpm at 4 C°, and supernatants were collected into new tubes (MAXYMum Recovery Microtube, #MCT-175-L-C, Axygen Scientific, CA, USA). µMACS Anti-HA Starting Kit (#130-091-286, Miltenyi Biotech, Bergisch Gladbach, Germany) was used for pull-down experiments. All samples, with or without sonication, were incubated with anti-HA magnetic beads (the antibody produced in mouse) included in the kit for 1 hour at 4 C° with gentle rotation. Equipment supplied by the kit (separator,

multi-stand and columns) were used to purify protein complexes following the manufacturers' manual. The buffers supplied with the kit were used in all steps as instructed by the manufacturer. The protein complexes were eluted into new tubes (MAXYMum Recovery Microtube, #MCT-175-L-C, Axygen Scientific, CA, USA) at the last step.

3.8 Silver Staining & Mass Spectrometry

Pre-casted 7.5% Tris-Glycine gels (#456-1024S, Mini-Protean TGX Gel Bio-Rad, California, USA) were used for running samples and silver staining afterwards. The ProteoSilver Plus Silver Stain kit (#1001191713, ProtSIL2-1KT, Lot: SLBB0889V, Sigma Aldrich, MO, USA) was used for silver staining following the manufacturers' protocol. Fixing solution was prepared by adding 50 ml of ethanol and 10 ml of acetic acid to 40 ml of ultrapure water. Sensitizer solution was prepared by adding 1 ml of ProteoSilver sensitizer solution provided with the kit to 99 ml of ultrapure water. The solution was prepared freshly each time; it should be used within 2 hours. Silver solution was prepared freshly (should be used within 2 hours) by adding 1 ml of ProteoSilver solution provided with the kit to 99 ml of ultrapure water. Developer solution was prepared by adding the two solutions provided with the kit, 5 ml of ProteoSilver Developer 1 and 0.1 ml of ProteoSilver Developer 2, to 95 ml of ultrapure water. This solution should be prepared fresh as well and used within 20 min. All steps were carried out at room temperature on an orbital shaker at 60 rpm to 70 rpm. The gel was soaked in fixing solution for 40 min (alternatively overnight at 4C°). The fixing solution was decanted and the gel was washed for 10 min with 100 ml of 30% ethanol solution. The solution was decanted and washing was repeated with 200 ml of ultrapure water for 10 min. The gel was incubated with sensitization solution for 10 min and subsequently washed twice each time for 10 min with 200 ml of ultrapure water. The gel was equilibrated for 10 min with 100 ml of silver solution. The silver solution was decanted and the gel was washed for 1 min (washing more than 1,5 min will decrease sensitivity) with 200 ml of ultrapure water. The gel was incubated in developer solution until reaching the desired band intensity. Adding 5 ml of ProteoSilver Stop solution and incubating for 5 min stopped the development. The solution was decanted and the gel was stored 4C° in ultrapure water or 1% acetic acid. Bands which appeared specific for the samples pulled down together with the tag, as well as the corresponding gel fragments in the control counterparts were excised with a scalpel. In-gel trypsin digestion of slices to be followed by mass spectrometry analysis of peptides were performed by the IMP/IMBA/GMI Protein Chemistry Facility (Vienna, Austria). UltiMate 3000 HPLC Rapid Separation liquid chromatography nanosystem coupled to a Q Exactive mass spectrometer, equipped with a Proxeon nanospray source was utilized for the analysis (all from Thermo Fisher Scientific). Proteome Discoverer (version

1.4.0.288; Thermo Scientific) and Mascot 2.2.07 (Matrix Science) were used to identify the peptides by searching through the *A. thaliana* protein sequence database.

3.9 Genotyping T-DNA Insertion Lines

3.9.1 DNA Extraction

Young leaves or seedlings of *Arabidopsis thaliana* plants either grown on soil or on plates were used to extract DNA sufficiently clean for PCR analysis. Tissue samples from individual plants were collected into separate Eppendorf tubes (1,2 ml), which were loaded with 1-3 small metal beads beforehand. Four hundred µl of extraction buffer (200 mM Tris-HCl pH 7.5, 250 mM NaCl, 0.5% SDS, 25 mM EDTA) were added into each tube. The tubes were shaken for 4 min at 30 Hz in a bead beater (Mixer Mill MM400, Retsch, Germany). The tubes were centrifuged at 10,000 rpm for 10 min at room temperature. Following centrifugation, 200 µl of supernatant from each tube were transferred into new tubes containing 200 µl isopropanol and mixed gently by inverting several times. The tubes were incubated at room temperature for 10 min or kept at -20 C° overnight. Samples were centrifuged at room temperature for 10 min at 10,000 rpm. The supernatants were discarded and the pellets were washed with 500 µl ice-cold EtOH. The tubes were spun 5 min at 4000 rpm at room temperature and supernatants were discarded. The residual ethanol was carefully pipetted off as much as possible without disturbing the pellets. The tubes were air-dried or dried inside the hood to evaporate remaining ethanol. The pellets were resuspended in 100 µl of dH_20 or TE buffer (10 mM Tris-HCl pH 8, 1 mM EDTA) and stored at -20 C° or 4 C° (if in TE).

3.9.2 Genotyping

The genotypes of *Arabidopsis thaliana* T-DNA lines obtained from NASC (Nottingham *Arabidopsis* Stock Centre, University of Nottingham, UK) were analyzed by PCR with primers specific to genomic regions flanking the respective insertion sites and primers specific to border regions of the inserted sequence. The border primers are shared within the lines from common origin, e.g. all lines from SALK share the same left border sequence. The primers that I designed specific to flanking regions were named to contain the ID of the line followed by the L/LP or R/RP after an underscore. The primers that are closer to the 3' end of the insertion site (left border of insertion) were labeled as R or RP (right primer), and the primers on flanking regions closer to the 5' end of the insertion were labeled as L or LP (left primer) (Table 6). Left border primer (LB) and right primer on flanking region (RP) were used to confirm the presence of the insertion, whereas left primer (LP) and right primer (RP) on flanking regions were used to confirm the wild type

genotype. In case of lines that are homozygous for insertion, no bands were expected from LP and RP primers due to the long inserts, while LB and RP primers amplify a specific product. If both primer pairs produce bands, the lines were confirmed to be heterozygous for the insertion. The plants for which no bands for insertions (LB+RP) were produced but for which flanking regions (LP+RP) were amplified were genotyped as wild type.

All PCR amplifications were done using GoTaq DNA polymerase (#M3178, Promega, Wisconsin, USA) in a total reaction volume of 20 µl containing 1X of GoTaq Green buffer (supplied with the kit), 0,5 µM of primers (Table 6), 0.5 mM dNTP mix (#R0192, Fermentas, Canada), 2 µl of DNA (30-50 ng) and 1 U of polymerase. All reactions were run in a Mastercycler Thermal Cycler (#950000058, Eppendorf, Hamburg, Germany) using the conditions shown in Table 7.

Primers for Genotyping T-DNA lines (5'-3')		**Description & NASC IDs**	
SALKLBb1.3	ATTTTGCCGATTTCGGAAC	SALK lines left border primer	
SAILLB3	TAGCATCTGAATTTCATAACCAATCTCGATACAC	SAIL lines left border primers	
SAILLB1	GCCTTTTCAGAAATGGATAAATAGCCTTGCTTCC		
SAILRB1	ATTAGGCACCCCAGGCTTTACACTTTATG	SAIL lines right border primer	
N16157_LP	CACCATAGGATGCCCTTGAG	N16157	AT5G27720 (*EMB1644/LSM4*)
N16157_RP	TGCCAACGGCTACAAATACA		
SALK_121177_L	CATGTTTCAACCTAATTTGGTATGAC	N621177	AT5G26742 (*EMB1138*)
SALK_121177_R	TCAGCTTCAACGTTGTTGTTG		
SAIL_103_A01_L	TCAGCTCCTCTTGGAAGTGAG	N871121	AT2G21660 (*CCR2/GRP7*)
SAIL_103_A01_R	CCTTGATCTTCCAGTCTCACG		

Table 6: Primers for genotyping T-DNA lines

Initial denaturation		95 C°	3 min
Denaturation	33 X	95 C°	30 sec
Annealing		60 C°	30 sec
Extension		72 C°	1 min
Final extension		72 C°	5 min

Table 7: PCR conditions

3.10 Immunocytochemistry

3.10.1 Slide Preparation

Ten µl of pollen suspension was resuspended in 50 µl of Buffer A, and pollen nuclei were isolated as described previously in section 3.2. The pellets containing free nuclei were resuspended with 1 ml of Cytospin buffer (15 mM Tris-HCl pH 7.5, 2 mM EDTA, 0.5 mM spermin, 80 mM KCl, 20 mM NaCl, 15 mM beta-mercaptoethanol, 0.1% Triton X-100, 1X protease inhibitor (#05892988001, Complete ULTRA Tablets, glass vial, Roche, Basel, Switzerland)) and filtered through double-layered 10 µm mesh on a funnel into new tubes. The samples were fixed in 3.7% (final conc.) formaldehyde for strictly 20 min incubation on ice. Following fixation, samples were neutralized with 125 µM (final conc.) glycine. The Cytospin apparatus was assembled for each sample in a way that each slide ID oriented away from collection tubes to prevent that leaking solution would erase the IDs. Samples were centrifuged for 7 min at 2500 rpm (750 rcf) in the Cytospin centrifuge (#MPW223C, MPW Instruments, Warsaw, Poland). Slides were post-fixated in ice-cold 96% EtOH for 5 min in a glass chamber. The slides were transferred into a new chamber filled with ice-cold 1X PBS and washed for 1 min. Slides were stored in 50% glycerol in PBS for longer periods at -20 C°, or they were used immediately as described in the following.

3.10.2 Immunocytochemistry

In case of storage at -20 C°, the slides were taken out of the freezer and washed 3 times with 1X PBS for 5 min each. Epitope demasking was done in the next step by boiling slides in a glass chamber filled with 1X DAKO (#S1699, DAKO, Denmark) for 15 min at 95 C° in a microwave. Slides were rinsed with dH_20 to dispose of remaining DAKO solution and washed 3 times with 1X PBS for 5 min each. Slides were blocked with 3% BSA in 1X PBS with 0.1% Tween 20 for 30 min at room temperature inside a humid chamber. Parafilm cover slips were used to cover slides during the incubation.

The slides were rinsed with 1X PBS to remove parafilm cover slips, before the primary antibody (#55 or #59, Table 5) was diluted 1:200 in 1X PBS with 0,1% Tween 20) and applied on each slide. The slides were covered with parafilm cover slips and incubated at 37 C° for 2 h or overnight at 4 C° inside the humid chamber. After incubation, the slides were washed 3 times with 1X PBS for 5 min each. The secondary antibody (#24 or #36, Table 5) was diluted 1:200 in 1X PBS with 0.1% Tween 20 and applied. The slides were covered with parafilm cover slips and were incubated for 1 h at 37 C° or overnight at 4 C° inside the humid chamber. Afterwards, the slides were washed 3 times with 1X PBS with 0.1% Tween 20 in the dark. Vectashield mounting medium

(H-1000, Vector laboratories, CA, USA) supplemented with DAPI was used to prepare slides for microscopy. Axio Imager M1 (HBO 100) (Zeiss, Oberkochen, Germany) equipped with a Spot RT – KE Slider 7.4 cooled-CCD camera was used to analyze immunostainings and Spot Advanced software (SPOT Imaging Solutions, MI, USA) for capturing images.

3.10.3 Immunocytochemistry-FISH

Probes for FISH were prepared beforehand by using the Nick-Translation kit (#1745808, Roche, Basel, Switzerland) following the manufacturers' protocol. For fluorescent labeling, Cy3-dUTP (#PA53022, GE Healthcare, Little Chalfont, UK) or Spectrum Green-dUTP (#30-803200, Vysis, Abbott Molecular, IL, USA) was used. Slides were prepared as described in section 3.10.1. Immunocytochemistry was performed as explained in previous chapter 3.10.2. In parallel, a fresh 4% (w/v) paraformaldehyde solution in PBS was prepared by dissolving paraformaldehyde powder in PBS by slowly mixing at 60 C° and adding drops of 1 M NaOH solution until it became clear. Then, the pH of the solution was adjusted to pH 7.0-7.2 by adding drops of 3 N HCl. The slides were fixed in paraformaldehyde solution cooled down to room temperature for 30 min (over-fixation should be avoided), in the dark. The slides were washed 3 times for 5 min each with 1X PBS, in the dark. RNAse A was diluted 1:200 in 2X SSC (1X SSC buffer: 3 M NaCl and 300 mM trisodium citrate (adjusted to pH 7.0 with HCl). Twenty µl were applied to each slide to degrade RNA by incubating for 30 min at 37 C° in the dark in a humid chamber. Formamide solution (70% formamide, 2X SSC) was prepared and pre-warmed in a water bath at 75 C°. The hybridization solution (for one slide: 1 µl of probe, 2 µl of 50% dextran sulphate (high viscosity, prepared freshly beforehand as it requires some time to dissolve), 5 µl formamide, 1 µl 20X SSC, 1 µl dH_2O) was prepared by denaturing for 10 min at 75 C° and immediately cooling down on ice. Following RNAse A digestion, the slides were washed 3 times with 1.5X SSC for 5 min each. Dehydration of the slides was achieved by brief ethanol washes, first with 70% and then with absolute ethanol. The slides were dried on a block for slides fitted into a PCR machine at 75 C° for a few seconds (over-drying should be avoided). Formamide solution pre-warmed to 75 C° was used to incubate slides for 2 min in the dark. Immediately afterwards slides were transferred to a new glass chamber for a series of quick ethanol washes at room temperature: first with 70% EtOH, then 90% EtOH and finally with absolute ethanol. The slides were air-dried on the bench for a few seconds. Ten µl of the hybridization solution, which was already denatured, was applied on each slide and covered using parafilm cover slips. The slides were incubated at 37 C° for 3 hours in the dark inside a humid chamber, followed by 3 times washing with first 1.5X SSC for 5 min, afterwards with 1.5X SSC with 0.1% Tween 20 for 5 min and finally with 1.5X SSC for 5 min. All washing steps were done in

the dark. Vectashield mounting medium (H-1000, Vector laboratories, CA, USA) supplemented with DAPI was used to prepare slides for microscopy. An Axio Imager M1 (HBO 100) (Zeiss, Oberkochen, Germany) equipped with Spot RT – KE Slider 7.4 cooled-CCD camera was used for analyzing immunostainings and Spot Advanced software (SPOT Imaging Solutions, MI, USA) for capturing images.

4 Results

4.1 Requirement of JmjC Domain for Histone Demethylase Activity of JMJ27 in vivo

Although experimental evidence *in vivo* strongly suggests that JMJ27 functions as a histone demethylase, previous efforts *in vitro*, using purified recombinant JMJ27 and calf bulk histones, did not reveal any significant demethylation activity, neither with mono-, di-, or tri-methylation levels of H3K9 (Chumak 2012). Previously identified histone demethylases from the family of JmjC domain-containing proteins in both mammals and plants denote the requirement of the JmjC domain for functional activity. Moreover, phylogenetic analysis of amino acid sequences revealed that cofactor binding sites, Fe (II) (iron) and alpha-keto-glutarate (αKG), are conserved and essential for histone demethylase activity (Lu et al. 2008; Z. Chen et al. 2006; Klose et al. 2006; Slama 2016). A conserved HCD motif in the Fe (II) (iron) binding site of JMJ27 was mutated into AAA sequence by site-directed mutagenesis, and a mutated JMJ27 construct driven by the native promoter and fused to RFP at the C terminus was generated to conduct an *in vivo* histone demethylation activity assay. Constructs were transformed to *jmj27-1* plants, and pollen nuclei were tested with immunostaining for H3K9me2 signal in selected lines with the inserted gene. The vegetative nucleus was indeed found to be defective in demethylation of H3K9me2 in the transgenic lines expressing *pJMJ27: Δjmj27: RFP* in *jmj27-1* background (Figure 19). This proves that the HCD motif is necessary for demethylation of H3K9me2 catalyzed by JMJ27, and the activity depends on the conserved Fe (II) iron-binding site of the protein, which is well conserved in JmjC domain-containing histone demethylase family members.

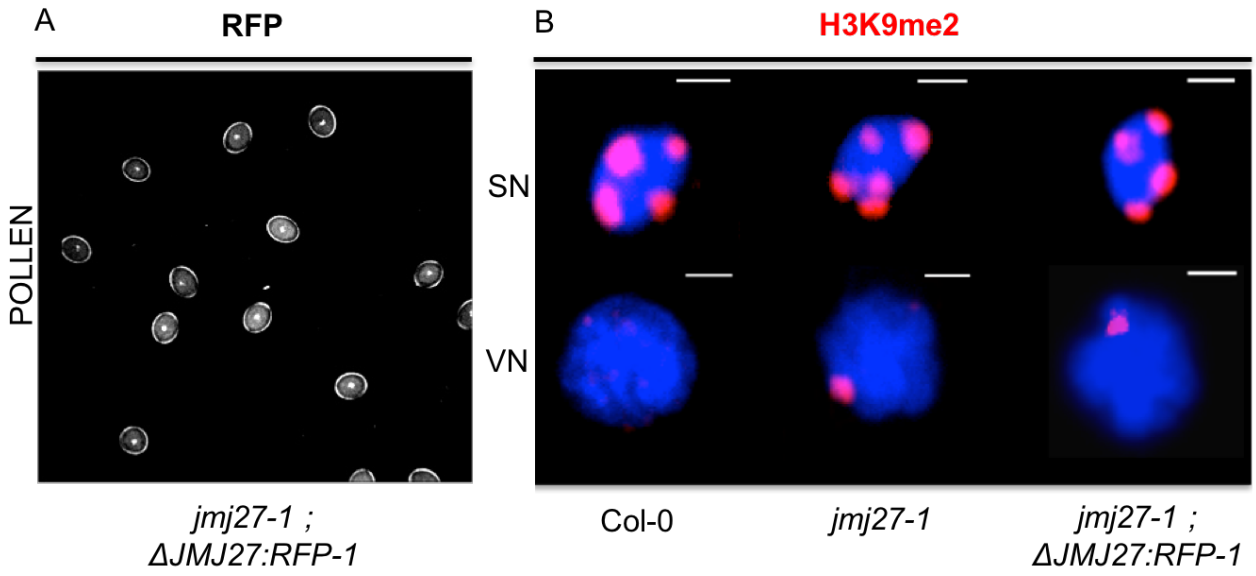

Figure 19 : The JmjC domain of JMJ27 is essential for *in vivo* histone demethylase activity. A) *pJMJ27: ΔJMJ27: RFP* is expressed in vegetative nucleus of mature pollen; B) immunocytochemistry was performed on free sperm (SN) and vegetative (VN) nuclei of pollen from wild type Col-0, *jmj27-1* and transgenic plants homozygous for *pJMJ27: ΔJMJ27: RFP* in *jmj27-1* background (*jmj27-1*; Δ*JMJ27: RFP-1*) using antibodies against H3K9me2 (red). No complementation is observed in *jmj27-1*; Δ*JMJ27: RFP-1* line, and the vegetative nucleus retains H3K9me2 methylation. DAPI (blue) is used to stain nuclei. (Scale bars: 1 µm)

4.2 *JMJ27 Interacting Proteins were Co-immunoprecipitated and Selected for Analysis by Mass Spectrometry*

Different epitope tags (HA, cMyc and FLAG) were fused to native JMJ27 at its C terminus and constructs transformed to Col-0 wild type and *jmj27-1* plants. Homozygous lines were obtained and were tested for successful expression of epitope-tagged JMJ27. The first line tested and detected to express a tagged JMJ27 was *pJMJ27: JMJ27: HA*. Consequently, through the rest of the study, this line was used for further experiments. Western blots using antibodies against the HA tag could detect JMJ27-HA-tagged protein in leaf tissue, with a molecular weight around 120 kDa, which is higher than the expected 98 kDa (Figure 20). Furthermore, in pollen nuclei, expression was identified via immunocytochemistry using antibodies against HA tag (Figure 21). This confirmed strong expression in the vegetative nucleus. In contrast to the exclusive expression of JMJ27 in the vegetative nucleus previously shown (Figure 13), some epitope-tagged JMJ27 was detectable also in sperm nuclei in these lines. This could be due to integration of multiple copies of the transgene, insertion into highly expressed regions within the genome, lack of endogenous regulatory sequences or disruptions in post-transcriptional gene silencing (PTGS) (Butaye et al. 2004).

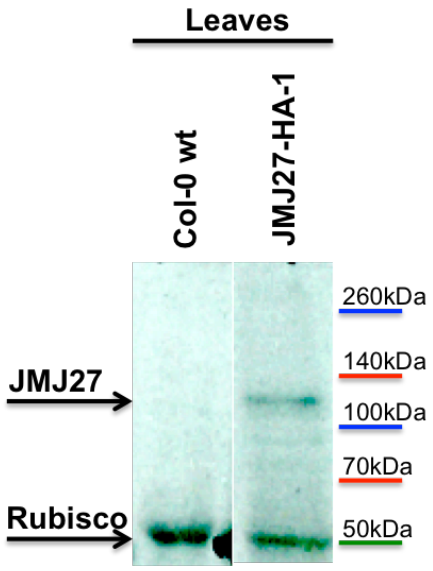

Figure 20: Western blot analysis of JMJ27 expression in pJMJ27: JMJ27: HA transgenic line (JMJ27-HA-1). Leaf material was used to detect the expression of JMJ27 tagged with the HA epitope using antibodies against the HA tag. Protein size was determined with a mix of proteins of known size (ladder at the right).

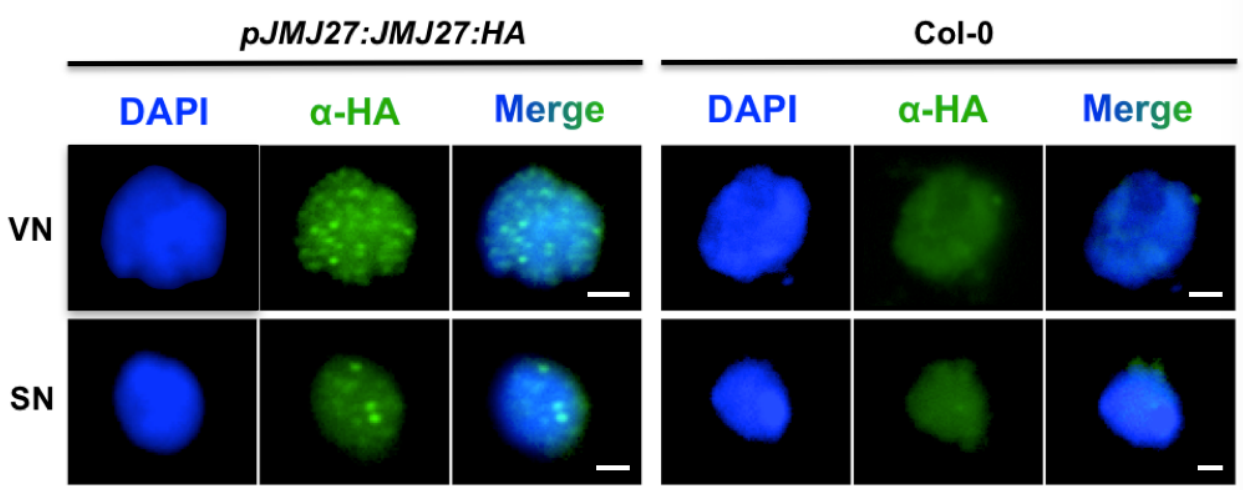

Figure 21: JMJ27-HA expression in free pollen nuclei of plants homozygous for *pJMJ27: JMJ27: HA* detected by immunocytochemistry using antibodies against the HA epitope tag. (Scale bars: 1 µm)

As the next step, I extracted total protein from whole seedlings and performed a Co-IP. I used sonication for extracting nuclear proteins, however, the method might disrupt weak protein-protein interactions. Therefore, in parallel, an additional Co-IP without sonication was performed. The Co-IP step was followed by a mass spectrometry analysis. For this, immediately after separating the proteins eluted together with the tagged JMJ27 in polyacrylamide gels, I applied a silver staining protocol and developed the bands until adequate visualization was achieved (Figure 22). The gel was inspected for bands which seemed specifically pulled down from JMJ27-HA seedlings and were not detectable in control lanes. In total, 16 slices were excised that way: samples S1 to S6 from lanes with sonicated JMJ27-HA IP and samples S7 and S8 from lanes with non-

sonicated JMJ27-HA IP. In addition, I cut slices at the same height of the specific bands from the corresponding control lanes (Figure 22). The slices were in gel trypsin-digested and analyzed by a mass spectrometry procedure.

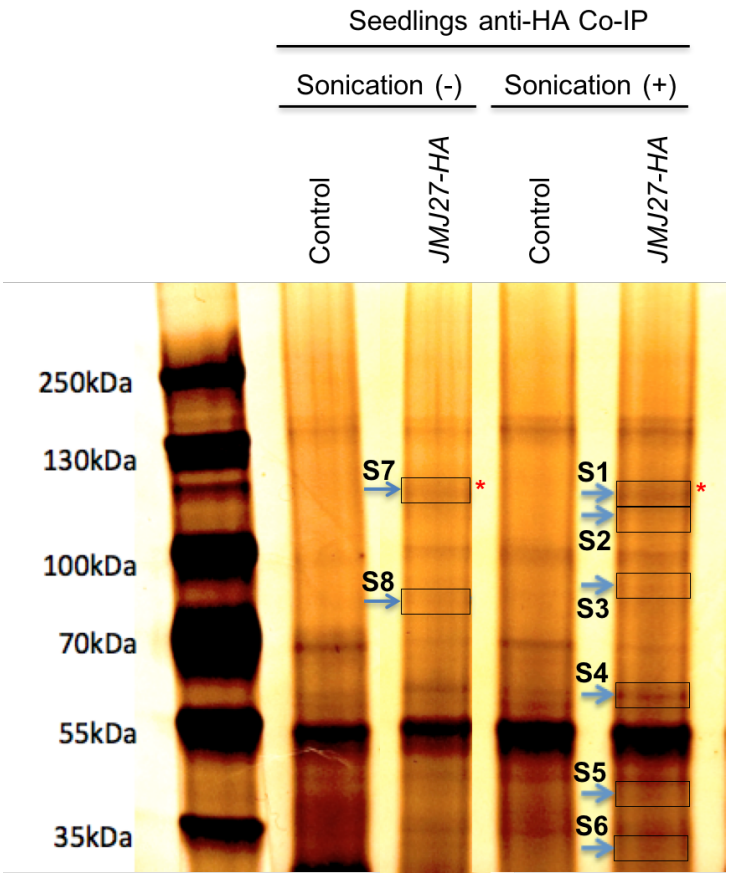

Figure 22: Silver-stained polyacrylamide gel of co-immunoprecipitated proteins by anti-HA from non-sonicated and sonicated protein extracts of seedlings with (*JMJ27-HA*) or without (Control) the transgene pJMJ27: JMJ27: HA. Gel excisions for samples S1-S8 were performed at areas within the boxes. Slices at the same positions from the corresponding control samples (C1-C8 (not outlined)) were excised in parallel. The position of JMJ27-HA protein is indicated with asterisks.

4.3 A Subset of Nine Proteins Potentially Interacting with JMJ27 Was Identified by MS Analysis

Mass spectrometry analysis generated a list of 116 proteins identified in both, sample and control groups, in total (Appendix table 1). As expected, the list also included JMJ27, and no JMJ27 peptides were discovered in control groups C1-C8. The highest JMJ27 peptide contents were found in slices S1 and S7, which belong to the position of the expected protein size of JMJ27 (Appendix table 2). The initial list produced by Proteome Discoverer (v1.4.0.288, Thermo Scientific) and Mascot (v2.2.07, Matrix Science, London, UK) was reviewed to eliminate proteins which were detected in both sample and control groups, as they cannot represent unique proteins specifically

eluted together with the JMJ27 complex. Among the 116 proteins, 30 of them including JMJ27 were classified as such unique proteins found only in sample groups (Table 8, Appendix table 3).

Accession	Description
AT5G27720.1	EMB1644/LSM4
AT4G00990.1	**JMJ27**
AT3G20250.1	PUM5
AT5G63560.1	HXXXD-type acyl-transferase family protein
AT3G01540.1	DRH1
AT5G20950.1	Glycosyl hydrolase family protein
AT1G15690.2	AVP1
AT5G03170.1	FLA11
AT3G45140.1	LOX2
AT5G50920.1	CLPC
AT5G49910.1	CPHSC70-2
AT4G24280.1	Heat shock 70kDa protein-6 (HSP70-6)
AT3G60750.2	Transketolase
AT5G42020.1	BIP2
AT5G26742.3	EMB1138/DEAD box RNA helicase (RH3)
AT1G09080.2	BIP3
AT5G26630.1	MADS-box transcription factor family protein
AT4G37930.1	SHM1
AT1G48030.1	mtLPD1
AT2G21660.2	ATGRP7/CCR2
AT1G56190.2	Phosphoglycerate kinase family protein
AT1G03630.2	POR C
AT4G25050.1	ACP4
AT2G01210.1	LRR-RLK family protein/ZAR1
AT2G25140.1	HSP98.7
AT4G13940.4	HOG1/SAHH1
AT3G52960.1	Thioredoxin superfamily protein
AT5G17920.1	ATCIMS
AT2G37270.1	RPS5B
AT2G04842.1	EMB2761/threonyl-tRNA synthetase, putative / threonine--tRNA ligase, putative

Table 8: Sample group (S1-S8)-specific interacting protein candidates obtained by filtering out proteins detected also in control group (C1-C8).

These proteins were further analyzed using online tool "DAVID (v6.8) Functional Annotation Clustering" (Huang, Sherman & Lempicki 2009b; Huang, Sherman & Lempicki 2009a) to identify the proteins most functionally relevant to JMJ27. The algorithm creates clusters based on several criteria such as cellular location, biological process and molecular function data, which are gathered from numerous proteomics and genomics sources. The analysis showed enrichment of nine genes together with JMJ27 in relevant categories (Table 9). The rest of the input genes were mostly clustered in categories of cytosol, chloroplast, mitochondria, or metabolic processes. However,

among the nine genes, several were also found in these clusters (data not shown). Therefore, among all proteins identified by mass spectrometry, these nine proteins appear as the most promising candidates for interactors of JMJ27, but validation studies must be conducted.

Annotation Cluster 1	
Category	**Genes**
RNA-binding	AT2G21660, AT3G01540, AT5G26742, AT5G27720
Nucleus	AT5G42020, AT5G26630, AT1G09080, AT2G21660, AT4G24280 AT3G01540, AT4G37930, **AT4G00990**, AT5G26742, AT5G27720
Annotation Cluster 2	
Category	**Genes**
Nucleus	AT5G42020, AT5G26630, AT1G09080, AT2G21660, AT3G01540, AT5G27720
Regulation of transcription	AT5G42020, AT5G26630, AT1G09080, **AT4G00990**
Accession	**Description**
AT1G09080	Heat shock protein 70 (Hsp 70) family protein (BIP3)
AT2G21660	Cold, circadian rhythm, and RNA binding 2 (CCR2/GRP7)
AT3G01540	DEAD box RNA helicase 1 (DRH1)
AT4G24280	Heat shock 70kDa protein-6 (HSP70-6)
AT4G37930	Serine transhydroxymethyltransferase 1 (SHM1)
AT5G26630	MADS-box transcription factor family protein
AT5G26742	DEAD box RNA helicase (RH3) (EMB1138)
AT5G27720	Small nuclear ribonucleoprotein family protein (EMB1644/LSM4)
AT5G42020	Heat shock protein 70 (Hsp 70) family protein (BIP2)

Table 9: Genes encoding sample group-specific proteins were analyzed by "DAVID (v6.8) Functional Annotation Clustering Tool" with default settings and medium stringency selected (Huang, Sherman & Lempicki 2009a; Huang, Sherman & Lempicki 2009b). Among 30 genes analyzed, 9 genes group together with *JMJ27* (AT4G00990) in two related clusters (modified DAVID (v6.8) output table).

4.4 Preliminary Test Reveals jmj27-1 alike Phenotype in Vegetative Nuclei from emb1644/lsm4, emb1138 and ccr2/grp7 Mutant Lines

Three proteins in the first annotation cluster (RNA binding and nucleus) (Table 9), were tested for a possible connection with JMJ27. T-DNA insertion lines (Table 3) for these three candidates: EMB1644/LSM4, EMB1138 and CCR2/GRP7 were used to assess by cytology if a hypermethylation phenotype like in *jmj27-1* would occur in pollen vegetative nuclei. First, the H3K9me2 mark was checked in *emb1644/lsm4*, *emb1138* and *ccr2/grp7* by immunocytochemistry. An altered H3K9me2 signal comparable to *jmj27-1* was displayed in a few nuclei from each tested

line (Figure 23A). Then, among these lines, the *emb1644/lsm4* mutant, which seemed to produce a stronger signal, was tested further by immuno-FISH to investigate whether any association between H3K9me2 and 45S rDNA exists as in *jmj27-1*. A co-localization of the two signals could be observed (Figure 23B). All three mutant lines tested were heterozygous; thus, half of the pollen would be expected to display the mutant phenotype. However, only a few nuclei were found to present such *jmj27-1* phenotype in all experiments (statistical analysis not available). The results were not conclusive, but the cytological methods represent a good starting point. It is necessary to repeat and conduct additional validation tests, by characterizing more T-DNA lines and more individual nuclei and by using other methods, such as Bimolecular Fluorescence Complementation (BiFC).

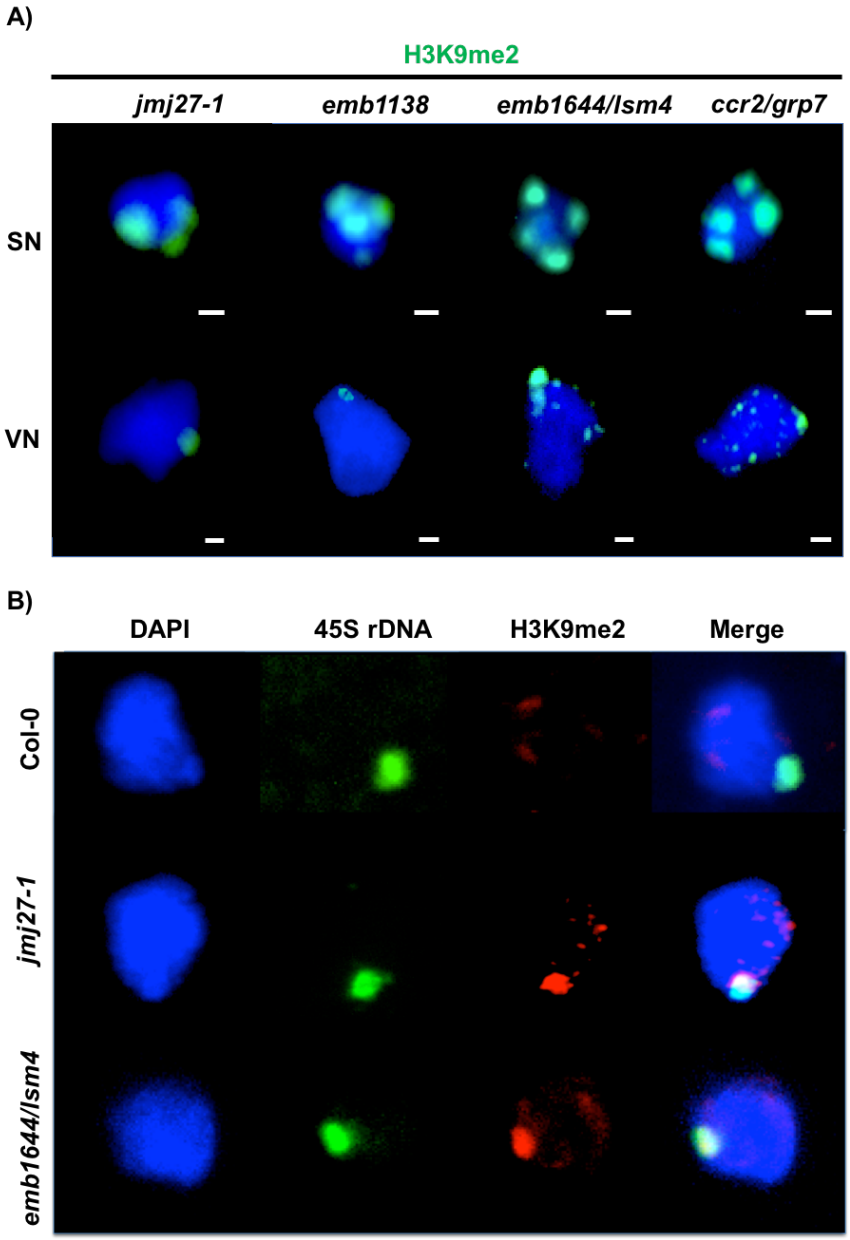

Figure 23: T-DNA insertion mutants of JMJ27 interaction candidates: *emb1644/lsm4* (N16157), *emb1138* (N621177), *ccr2/grp7* (N871121) were compared to *jmj27-1* phenotype in pollen nuclei A) Presence of H3K9me2

mark in a few vegetative nuclei from each three candidates were observed by immunocytochemistry B) Immuno-FISH analysis for H3K9me2 and 45S rDNA shows that the two signals are co-localized in *emb1644/lsm4* vegetative nucleus. (Scale bars: 1 µm)

4.5 Additional Experiments

In addition to the results described in the previous sections, I worked on some side projects of the lab during my PhD. Due to circumstances out of my responsibility, these projects were not finished. However, I will briefly explain the aim of these experiments and the approaches followed in each case.

4.5.1 Forward Genetic Screen of Ethyl Methanesulfonate (EMS) Mutagenized Arabidopsis

The vegetative nucleus of pollen undergoes active decondensation of centromeric heterochromatin, while losing H3K9me2 and centromeric histone 3 variant CenH3 (Schoft et al. 2009). The haploid genome of pollen facilitates mutant screens. I conducted a forward genetic screen in *Arabidopsis* searching for mutant pollen that would retain CenH3 in their vegetative nucleus. In case of candidates, it was planned to map the gene causing the mutant phenotype by whole-genome sequencing. A previously generated transgenic *Arabidopsis* line homozygous for *pCenH3:CenH3:GFP pLAT52:H2B:RFP* in Col-0 background (Schoft et al. 2009) was used for the mutant screen setup. Pollen collected from this line expresses GFP-tagged CenH3 and RFP-tagged Histone 2B (H2B). The CenH3 expression is under the control of its endogenous promoter and the signal is detected in sperm nuclei but not in the vegetative nucleus since it is lost during centromeric heterochromatin decondensation. The H2B expression is controlled by the pLAT52 promoter specifically active in the vegetative nucleus. Therefore, the mutant candidate pollen would be identified by showing five CenH3-GFP centromeric foci within the vegetative nucleus expressing H2B-RFP. I started the mutant screen in a collection of M1 plants of this line previously mutagenized with EMS (0.2%) (Chumak 2012). Later, I continued the screen by mutagenizing a new batch of seeds from the same line, with a higher concentration of EMS (0.3%). The flow of the experiment was pooling pollen grains from five individual M1 plants and mounting them onto a microscope slide. DNA was counterstained with DAPI. Afterwards, a Zeiss M1 inverted microscope supplied with a spinning disc unit (Ultraview Vox; Perkin Elmer) was used to scan the whole slide. For each scanning region, three channels (GFP, RFP and DAPI) were activated sequentially and 40 Z-stacks each were obtained. The images were saved and analyzed in batches with Definiens Image Analysis Software (Munich, Germany). Possible candidates were analyzed individually for confirmation. However, despite the time- and labor-consuming efforts, I could not

identify a single candidate with the expected phenotype, neither in the 0.2% nor 0.3% EMS-mutagenized plant pools.

4.5.2 Analysis of DME Expression in Arabidopsis Pollen by Western Blot

In this project, my aim was to detect DME expression in pollen to support the results produced in our group. Previously, DME was shown to be expressed in the central cell of the female gametophyte and required for gene imprinting and maternal allele expression of imprinted genes in endosperm (Choi et al. 2002). However, its function in pollen was less known. Our group showed that DME is also functional in the male gametophyte and essential for normal pollen germination in certain ecotypes (Schoft et al. 2011). Moreover, it demethylates the small euchromatic transposable elements (TEs) in the vegetative nucleus and reinforces methylation of homologous TEs in sperm cells (Ibarra et al. 2012). JMJ27 was also shown to act on TEs similarly in pollen (Chumak 2012). Therefore, in addition to detecting DME expression in pollen, a long-term aim was to reveal any interaction between DME and JMJ27 by Co-IP.

I used a DME antibody (gift from Prof. Teresa Roldan-Arjona (University of Cordoba, Spain)) to detect DME expression in wild type (Col-0) mature pollen by western blot. However, the attempts were not successful with this approach. This found an explanation in a recent study, which showed that DME expression is restricted to pollen vegetative nuclei specifically at the late bicellular stage of pollen development (Park et al. 2017). The expression rapidly decreases in the tricellular stage as pollen matures, and it is not expressed in sperm cells or any other stage. This is likely the reason why I was not able to detect DME expression via western blot, since I used mature pollen in my experiments.

4.5.3 JMJ27 Expression in Sperm Nuclei

In *jmj27* mutants, a H3K9me2 signal at the 45S rDNA region is preserved in the vegetative nucleus (Figure 8). JMJ27 is highly expressed in vegetative nucleus in contrast to sperm nuclei where no significant level of expression is detected (Figure 13). I constructed an expression vector of RFP-tagged JMJ27 driven by the sperm cell-specific promoter DUO (*pDUO: JMJ27: RFP)*. The aim was to observe if JMJ27 expression in sperm cells would cause any reduction in H3K9me2 signals in sperm nuclei. However, no difference was observed in sperm nuclei of homozygous *pDUO: JMJ27: RFP* lines compared to wild type by immunostaining for H3K9me2. This indicates that JMJ27 has a vegetative cell-specific role and perhaps needs interaction partners, which are not present in sperm cells.

4.5.4 JMJ27 Overexpression

JMJ27 expression is specifically higher in the vegetative nuclei of pollen and rapidly dividing sporophytic tissues (Figure 13, Figure 14). The *jmj27* plants do not display any evident morphological abnormalities (Chumak 2012). I constructed an expression vector for YFP-tagged JMJ27 driven by the constitutively active 35S promoter (*p35S: JMJ27: YFP*). The aim was to observe whether overexpression may result in any morphological abnormalities which could give more information on the function of JMJ27. Before generating stable transformants, I tested the construct by transient transformation into young *Arabidopsis* leaves using FAST technique (J.-F. Li et al. 2009). The construct was functional, and YFP-tagged JMJ27 could be detected in transformed leaves, therefore I proceeded to stable transformation to Col-0 plants. However, none of the transgenic plants displayed any morphological difference compared to wild type. Pollen collected from transgenic lines expressed YFP-tagged JMJ27 in vegetative nucleus but not in sperm nuclei. In one interesting line, the YFP positive vegetative nucleus was similarly condensed as sperm nuclei in DAPI-counterstained pollen. However, this line did not produce viable seeds and could not be propagated for further investigation.

5 Discussion:

Chromatin dynamics play an essential role for the regulation of transcription by altering the accessibility of DNA to the transcription machinery at different levels. The basic site of such control is at nucleosomes where chemical modifications on both, DNA and histone proteins, in addition to non-coding RNAs and DNA-binding proteins cooperate in fine tuning of chromatin structure. In general, decondensed or open chromatin is necessary to initiate and maintain a transcriptionally accessible euchromatin state, while a condensed structure is required to form a heterochromatic region that represses the transcription. Therefore, heterochromatic regions are usually considered as the “dead” zone of the genome in terms of gene expression. However, they have a fundamental role during cell division for proper segregation of daughter cells via centromeric heterochromatin and protecting chromosome ends via telomeres (Peters et al. 2001; Pidoux & Allshire 2005; Schoeftner & Blasco 2009). Moreover, heterochromatin formation is critical for keeping genome integrity, by silencing sequences that contain mobile genetic elements which are also potentially detrimental for offspring genomes (Slotkin & Martienssen 2007). Genome-wide epigenetic reprogramming of chromatin during gametogenesis is vital to prevent such mobilization over generations in plants. A primary difference between gametogenesis of

animals and flowering plants is that gametes are the direct products of meiosis in animals, whereas gametes are generated by post-meiotic mitotic divisions in flowering plants (Figure 2).

Pollen, the *A. thaliana* male gametophyte, is an attractive model to investigate such germ line epigenetic reprogramming, since it has a unique structure where a larger vegetative cell engulfs two smaller sperm cells, and the two cell types differ from each other by an asymmetric cell division at the end of the first post-meiotic mitosis event. In terms of chromatin state, major differences were observed upon epigenetic profiling via cytology, consistent with the apparent change in chromatin condensation levels where the vegetative cell undergoes a large-scale heterochromatin decondensation, while sperm cells form a compact dense heterochromatin. Since the two cell types are set apart by only one mitosis event, the mechanisms leading to distinct chromatin states must be rapid and active processes. Although the initiation and function of heterochromatin formation is a well-documented phenomenon, is not very well understood how heterochromatin decondensation is achieved and what is the biological significance of it. As this process in *Arabidopsis* pollen occurs in the haploid life phase, which allows easy mutant screens, this is an attractive model to investigate mechanisms and significance of active heterochromatin decondensation. The vegetative cell was earlier considered as a less interesting component of the male gametophyte compared to sperm cells, since it is a terminally differentiated cell destined to degenerate at the end of fertilization and does not contribute any genetic material to the next generation. However, it is required for rapid germination and successful delivery of sperm cells to ovules by driving pollen tube growth over long distances. Moreover, an increasing number of recent studies suggest new roles of the vegetative nucleus in pollen physiology and reinforcement of genomic integrity in sperm cells, thereby indirectly contributing to correct transfer of genetic material to next generations (Creasey & Martienssen 2010; Slotkin et al. 2009; Gehring et al. 2009).Therefore, the characterization of mechanisms that actively remodel the vegetative cell nucleus has a greater implication than previously imagined.

5.1 Local Heterochromatin Decondensation and DNA Demethylation in Vegetative Nucleus Mediated by Putative H3K9 Demethylase JMJ27

In a previous study conducted by Nina Chumak, a reverse genetic screen had identified JMJ27 (AT4G00990) to be responsible for local heterochromatin decondensation, evident by a H3K9me2 signal in vegetative nuclei of the mutant plants. This mark is lost completely in wild type (Chumak 2012). Moreover, the modification was found to be co-localized with the 45S rDNA FISH signal. ChIP and bisulfite-sequencing analyses indeed showed that H3K9me2 is increased at 45S rDNA promoter sequences, accompanied with DNA hypermethylation. Therefore, JMJ27 seems to

be involved in modulation of H3K9me2 demethylation and DNA demethylation at 45S rDNA promoters in pollen vegetative nucleus. Here, in this thesis, I have taken the next steps for functional analysis of JMJ27 with the aim to explain how it modulates the described events. I generated several transgenic lines to test for complementation of the mutant JMJ27 phenotype by ectopic expression of the functional protein, to identify the JMJ27 expression pattern, to demonstrate JMJ27 has a functional JmjC domain required for histone demethylation activity *in vivo* and to identify any possible interacting partners which might be required for its functional activity.

Introducing the wt JMJ27 gene to mutant *jmj27* plants resulted in removal of H3K9me2 in vegetative nuclei, as in Col-0 wt where no signals can be detected for this modification (Figure 12). Therefore, JMJ27 expression is indeed responsible for disappearance of the H3K9me2 signal that co-localizes with 45S rDNA. As a putative H3K9 demethylase, it is likely that JMJ27 demethylates H3K9me2 at 45S rDNA promoters during the chromatin remodeling step in the vegetative nucleus. It would be of interest for further studies to investigate pollen from different developmental stages for the exact time frame of JMJ27 activity removing H3K9me2 marks from chromatin.

JMJ27 was shown to be highly expressed in gametophytes, remarkably at the vegetative nucleus of pollen, with little or no expression observed in sperm nuclei (Figure 13). In sporophytic tissues, its expression was found to be associated with regions of high cell proliferation such as root tip, the embryo proper and suspensor cells (Figure 14). Considering such high expression in both gametophytic and sporophytic tissues, and the involvement in H3K9 demethylation and DNA demethylation at 45S rDNA loci, one would expect several growth abnormalities in mutant plants. However, no morphological defects were observed, pollen germination and fertility are not affected by the mutation (Chumak 2012). One reason for that could be functional redundancy, although tests with double and triple mutants lacking also the closest homologs have shown that only JMJ27 is responsible for the H3K9me2 phenotype observed (Chumak 2012). Thus, ruling out redundancy, another reason could be a conditional requirement which would bring out phenotypical defects only under specific circumstances, if chromatin reorganization is induced upon conditions like heat, drought, pathogen stress etc. (Probst & Mittelsten Scheid 2015). This might depend on which copies of rDNA genes are repressed in mutants and whether a compensation by active rDNA genes takes place under normal conditions, not possible under suboptimal conditions. Using the transgenic reporter line generated in this study could reveal how JMJ27 expression changes under different stress conditions in sporophytic tissues and in pollen and could elaborate whether such conditional phenotypic defects are present.

JMJ27 belongs to the *Arabidopsis* JHDM2/KDM3 family of proteins and thus has been considered a putative H3K9 demethylase. JmjC domain-containing proteins were shown to cause demethylation by a hydroxylation reaction (Klose et al. 2006), but we still do not know the mechanism of histone demethylation catalyzed by JMJ27, as previous *in vitro* assays were not positive (Chumak 2012). As stated already by the author of the cited thesis, the optimal conditions might not have been achieved *in vitro,* or the reaction would require interacting partners that were not included. Here, in my study, a transgenic line expressing fluorescence-tagged JMJ27 that has a catalytic JmjC domain mutation (*pJMJ27: ΔJMJ27: RFP*) was tested whether histone demethylation could still be achieved *in vivo* (Figure 19). The rationale of the experiment was to modify the functional JmjC domain of JMJ27 since that domain was shown to be responsible for demethylase activity in other family members and is conserved among JmjC domain histone demethylases. In contrast to the wt *JMJ27* that could complement the *jmj27* mutant phenotype, ΔJMJ27 did not complement the phenotype and did not remove H3K9me2 marks in the vegetative nucleus (Figure 19). This strongly suggests that the JmjC domain is essential for the histone demethylase activity and JMJ27 is indeed an active histone demethylase. However, its specificity must be further investigated, as it is highly possible that it has affinity also for mono- and tri-methylated states, and eventually for other substrates. In a very recent article, the only study on the function of JMJ27 so far, confirmed the histone demethylase activity of JMJ27 *in vitro* and *in vivo* (Dutta et al. 2017). The study identifies JMJ27 as a histone demethylase specific to H3K9me1, H3K9me2, and H3K9me3. However, H3K9me3 marks were removed at a much slower rate (16 hours) compared to H3K9me1 and H3K9me2 (5 hours each). These two marks were also shown to be more abundant in *jmj27* mutants compared to WT plants (Dutta et al. 2017).

5.2 Mass Spectrometry-Based Detection of Interacting Partners of JMJ27

The primary aim was to find interacting partners of JMJ27 required for mediating the demethylation of H3K9me2 and DNA in 45S rDNA promoter in pollen VN. However, the amount of protein that could be extracted from pollen was not optimal for co-immunoprecipitation. As substantial JMJ27 expression was also shown in vegetative tissue, and as *jmj27* seedlings had increased H3K9me2 and DNA hypermethylation in 45S rDNA promoter like the VN in pollen (Figure 9, Figure 10, Figure 14), I first performed a Co-IP from whole seedlings, since it was easier to collect enough material. The subsequent MS experiment was intended to be an initial test, and replicates were planned to see if the same proteins are detected again. In parallel, using T-DNA insertion mutants in genes encoding the identified candidate proteins, I screened pollen by cytology to check if a similar H3K9me2 signal localized to 45S rDNA as in *jmj27* would be found.

Accordingly, this initial Co-IP from seedlings and subsequent MS identified indeed several candidates for JMJ27-interacting proteins that were missing in the control sample. Out of 116 initial proteins identified, I obtained by functional annotation clustering 9 proteins as most likely interactors. These proteins seemed to have a higher chance of interaction since they were found under the same annotation clusters as JMJ27 (Table 8, Table 9). LRR-RLK/ZAR1 (AT2G01210) was detected as the candidate with the highest relative intensity by peak area measurements of the mass spectra (Appendix table 1). However, LRR-RLKs are transmembrane proteins with intracellular kinase activity, and this specific family member was found to be essential for the first asymmetric division of the zygote, hence the name ZAR1: ZYGOTIC ARREST 1, and homozygous mutants are embryo-lethal (Yu et al. 2016). JMJ27 is a nuclear protein and was observed to be expressed in nuclei (Figure 13, Figure 14). Its interacting proteins are more likely to be associated with it at that location. Therefore, LRR-RLK/ZAR1 (AT2G01210) was ruled out as a potential interactor of JMJ27, and indeed it was not found in any annotation cluster together with JMJ27. Most likely, as total protein from seedlings was used for Co-IP, it is possible that interactions with non-nuclear proteins occurred non-specifically during the assay.

As explained, a reverse genetic approach was followed next to compare the phenotype in the pollen VN of mutant lines lacking the potential interactors by immunocytochemistry using the H3K9me2 antibody. Since the main phenotype observed in vegetative nuclei of *jmj27* pollen was methylation of H3K9me2, I asked whether a similar presence of H3K9me2 could be observed also in pollen from mutant lines of these interactors, assuming they co-operate with JMJ27. T-DNA lines for the three genes in the first annotation cluster (RNA and Nucleus) (Table 9), *emb1644/lsm4*, *emb1138*, *ccr2/grp* were chosen for this preliminary test. Some clear H3K9me2 signals could be observed in several VNs in each line tested. Moreover, in the *emb1644/lsm4* mutant line, colocalization to 45S rDNA foci was observed by immune-FISH experiments, as in *jmj27* pollen. The T-DNA insertion lines tested (Figure 24) were heterozygous for the insertions. As in the case of *emb1644/lsm4*, also for *emb1138* only heterozygous mutants were available since homozygous mutants are embryonic lethal.

A. *EMB1644/LSM4*

B. *EMB1138*

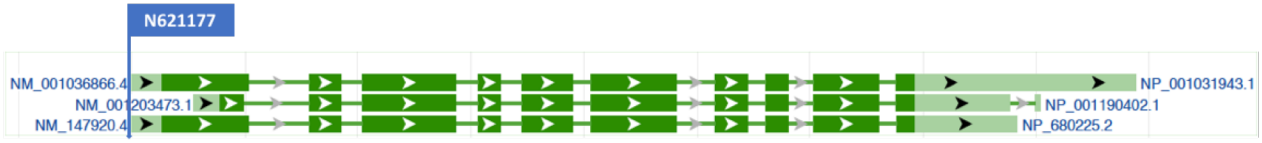

C. *CCR7/GRP7*

Figure 24: T-DNA lines and insertion sites for A) *EMB1644/LSM4* (N16157), B) *EMB1138* (N621177), C) *CCR2/GRP7* (N871121) (Light green bars: 5' UTR, 3'UTR; Dark green bars: Exons; Green lines: Introns)

However, increased H3K9me2 was observed in less than half of the pollen, in contrast to the expectation for a heterozygous population. Unfortunately, due to time constraints the experiments could not be reproduced with larger samples and a statistical analysis. Since these were not conducted it is not possible to make a clear statement about the role of these genes for the H3K9me2 demethylation process at 45s rDNA, based on pollen cytology. For an assessment, repeating the experiment with greater numbers of plants and a statistical analysis remains. Some of the mutants have the T-DNA insertion in the 5' regulatory region and might not be loss-of-function mutants. Other lines with different insertion sites should be included in further experiments. The T-DNA lines used so far should be tested for residual expression of the genes: it might be possible that the genes were not or not completely dysfunctional. This could be one reason why the H3K9me2 phenotype was not prominent in half of the nuclei as expected if indeed a functional connection with JMJ27 would exist. Also, it might be that the interactions occur only at certain developmental stages or depend on environmental conditions. They might be as well interactions of JMJ27 specific for sporophytic tissues. Previously, it was suggested that JMJ27 may have a role at constitutive heterochromatic regions, besides at facultative heterochromatin such as 45S rDNA. A ChIP-Seq experiment using H3K9me2 antibody showed that, in addition to 45S rDNA, several transposable elements were also detected with hypermetyhlated DNA in *jmj27* pollen (Chumak 2012). However, in sporophytic tissues, demethylation of transposable elements would be detrimental, and it might be possible that instead of targeting TEs, JMJ27 may have a different role in these tissues. Alternatively, isoforms of the candidate proteins could be the actual interacting partners since isoforms of some proteins were detected in the MS identification (Appendix table 1).

The expression of these isoforms should be checked in the T-DNA lines as well. However, these experiments would at best provide indirect evidence, and other experiments such as true interaction assays as BiFc should be considered to validate the connection at the molecular level.

The 45S rDNA methylation status should be also checked in mutants lacking these interactor proteins for resemblance with *jmj27*. The three proteins are implicated for RNA binding and RNA processing activities; therefore, it may be possible that their absence does not affect the H3K9 demethylase activity of JMJ27, but other coupled processes. It is possible that their absence may still affect the stability of a multi-protein complex and causes defective H3K9 demethylation on some occasions. The results from MS do not provide information by which domain or conformation the proteins are interacting with each other *in vivo*. Further experiments are therefore required to know more about the type and nature of interaction and which region or domains are more critical and required for making a functionally active complex. The RNA binding nature of these proteins and JMJ27's localization at 45S rDNA might suggest also a role in pre-rRNA processing. In fact, a previous literature search reveals that such connection is possible (Kufel, Allmang, Petfalski, et al. 2003). No expression of EMB1644/LSM4 (Like-Sm) ribonucleoprotein, a protein with 129aa length, was reported in pollen, however, since mature pollen is mostly transcriptionally quiescent, it is possible that its expression at earlier stages was missed. For the rest of the tissues, the expression level is very high (Figure 25).

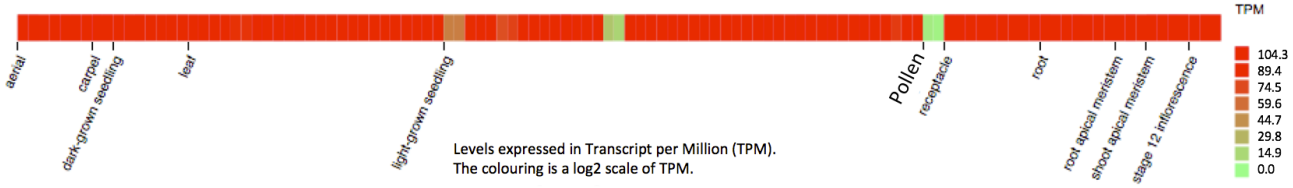

Figure 25: EMB1644/LSM4 expression levels in *Arabidopsis*. Although no expression was detected in mature pollen, it is expressed at very high amounts in most tissues (Krishnakumar et al. 2015; Krishnakumar et al. 2017).

EMB1644/LSM4 is one of the eight LSM (Like-Sm) proteins which are conserved in eukaryotes and have roles in RNA biogenesis and turn-over (He & Parker 2000). Two different heteroheptameric LSM complexes are formed: LSM1-7 which is cytoplasmic and functions in mRNA decapping and decay pathways, and LSM2-8 which is nuclear and functions in pre-mRNA splicing by stabilizing U6 snRNA. However, the LSM2-8 complex was suggested to also have a role in 5'–3' degradation of mRNA in nucleus (Golisz et al. 2013). EMB1644/LSM4, beside LSM6 and LSM7, was found to directly interact with U6 snRNA in the spliceosome complex, and *emb1644/lsm4* and *lsm7* homozygous mutants were shown to be lethal (He & Parker 2000; Zhaoliang Zhang et al. 2011; Golisz et al. 2013). In recent years, several studies in yeast suggested that the complex has a function also for several other RNA species, such as rRNA, tRNA and U3

snoRNA, in addition to pre-mRNA (Kufel et al. 2002; Kufel, Allmang, Petfalski, et al. 2003; Kufel, Allmang, Verdone, et al. 2003). Remarkably, yeast homologs of LSM2-8 were shown to be essential for the proper pre-rRNA processing and are required for the stability of both pre-rRNA and mature rRNA (Kufel, Allmang, Petfalski, et al. 2003). Depletion of LSM proteins cause aberrant pre-rRNA splicing and accumulation of degradation intermediates in yeast. Interestingly, degradation of mature rRNAs, pre-tRNA and mature tRNAs is also activated in these mutant strains. In general, yeast Lsm proteins were shown to be required for proper organization of rRNA processing steps, and a direct association between Lsm3p, but not Lsm1p, with pre-rRNAs was shown by IP followed by Northern blots (Kufel, Allmang, Petfalski, et al. 2003). Previous studies provide further proof of their function in ribosome biogenesis as they showed interactions between ribosome subunit proteins and LSM proteins (Neubauer et al. 1998; Uetz et al. 2000). An MS-based characterization of the spliceosome complex in human cells identified a 40S ribosomal protein, Rps4X, to interact with the spliceosome complex (Mann et al. 1998) where in a wide-scale yeast two hybrid screen, Lsm4 as well as Lsm2 and Lsm8 were found to interact with the 40S ribosomal protein S28, Rps28 (Uetz et al. 2000). In fact, revisiting the JMJ27 interactor candidate list, an *Arabidopsis* 40S ribosomal protein, Rps5B was identified in the sample-specific group (Table 8, Appendix table 3). However, during functional annotation clustering, this protein was not clustered with JMJ27, since the nucleus was not defined in its annotation category. This could be a false negative result due to insufficiency of annotation data. Reconsidering this protein in the validation list would be worthwhile since intriguing information are noticed by available interactome data (Chatr-aryamontri et al. 2017). Interestingly, the Rps5B protein was shown to directly interact with several proteins, and one protein, ROS4/IDM1 (increased DNA methylation 1), is notable and provides a potential link to chromatin features. ROS4/IDM1 (AT3G14980) is a histone H3 acetyltransferase that can recognize methylated DNA through its MBD domain and unmethylated H3K4 through its PHD domain (Q. Li et al. 2015). Remarkably, this protein itself was shown to interact with CCR2/GRP7, and though not the same HSP70 family proteins as in my list, there are two other members of the HSP70 family, HSC70-1 (AT5G02500) and Hsp70-2 (AT5G02490) (Q. Li et al. 2015). ROS4/IDM1 functions by relaxing chromatin structure via H3 acetylation which favors the recruitment of active DNA demethylases and in turn prevents silencing of the DNA (Qian et al. 2012). Moreover, it was shown that it is preferentially active at regions containing homologous multi-copy genes and repetitive sequences, which are normally targeted by 5-methylcytosine DNA glycosylases (ROS1, DME, DML2 and DML3). While H3K4 di- or trimethylation inhibit the activity, H3K9 di- or tri methylation has no effect (Qian et al. 2012). Compared to wild type, in *ros4/idm1* plants DNA hypermethylation is observed in all sequence

context, but non-CG methylation could be suppressed by mutants lacking RNA polymerase IV (*nrpd1-3)*, suggesting that the RdDM pathway is responsible for these methylations. The *idm1* mutation did not cause any DNA methylation changes at 5S and 45S ribosomal DNA at CG and CHG context, as shown by Southern blot (Qian et al. 2012). However, the probes used to test it correspond to 18S and 25S rDNA coding sequences. In the previous study identifying the JMJ27 mutant phenotype (Chumak 2012), a 45S rDNA promoter probe was used to reveal DNA hypermethylation in *jmj27* (Figure 10). Through bisulfite sequencing, the total amount of methylation could be evaluated only over the total 45S rDNA promoters since it was not possible to distinguish individual promoters among the highly similar copies. Therefore, it would be still necessary to check methylation levels at specific 45S rDNA promoter sequences in *ros4/idm1*, asking whether ROS4/IDM1 is cooperating with JMJ27 in demethylation of H3K9me2 and DNA at 45S rDNA promoter via an interaction, which could be mediated by Rps5B. However, it is possible that different control mechanisms of rDNA demethylation are active in seedlings and pollen, since all four rRNA variants were found to be transcribed in wt pollen whereas wt seedlings do not express the longest variant VAR1 (Mérai et al. 2014). It might be possible that only a subset is controlled by JMJ27.

In addition to its involvement in processing of diverse pre-RNA species, a connection between EMB1644/LSM4 and stress response-mediated chromatin modification was shown previously (Zhaoliang Zhang et al. 2011). SK1B, a protein arginine methyltransferase is bound to chromatin and responsible for H4R2 symmetric dimethylation (H4R3sme2), under normal conditions. Upon salt stress, it detaches from chromatin, causing reduced H4R2 methylation levels and increased transcription of stress-responsive genes. Moreover, it methylates EMB1644/LSM4 which induces pre-mRNA splicing and alternative splicing variants of several stress-responsive genes. Both *sk1b* and *emb1644/lsm4* mutants were found to display splicing defects and hypersensitivity to salt (X. Deng et al. 2010; Zhaoliang Zhang et al. 2011). Interplay between alternative splicing, the transcriptional machinery and histone modifications has already been described (Luco et al. 2010). A close association between siRNA-mediated transcriptional silencing and alternative splicing was also shown, as repressive histone marks were used to regulate splicing site preference (Alló et al. 2009). Therefore, in plants, alternative splicing might be associated with more diverse events regulated by chromatin modifications and extrinsic stimuli such as stress conditions. Production of splicing isoforms and increased processing capacity of pre-mRNA and most likely pre-rRNA and pre-tRNA, too, could be advantageous for survival. This might be a reason why LSM proteins as part of the spliceosome complex is integrated in different networks involving RNA processing, and specificity could be provided through interactor partners. In this

case, JMJ27 and other proteins in the complex might mediate 45S rDNA expression and consequently pre-rRNA maturation into ribosomes, and this activity could be further altered by stress conditions. This principle can be crucial in case of pollen since this is a fragile plant tissue sensitive to environmental stress, and it requires protective mechanisms to complete its development and successfully deliver genetic material to the next generation (Chaturvedi et al. 2016; Müller & Rieu 2016; Fragkostefanakis et al. 2016; Y. Chen et al. 2015) . Moreover, upon unfavorable conditions, these mechanisms would be needed immediately, and this could be the reason why a subset of 45S rDNA chromatin is kept in a stand-by state, H3K9me2 demethylation regulated by JMJ27 under normal conditions. Upon stress, proteins such as EMB1644/LSM4, EMB1138, CCR2/GRP7 could be integrating stress signaling pathways with JMJ27 and induce transcription and maturation of additional rRNA. A recent finding that JMJ27 is required for defense against *Pseudomonas syringae* and modulation of flowering time, supports such model (Dutta et al. 2017). The *jmj27* mutation causes increased disease susceptibility upon infection (~7 fold higher) compared to WT. Moreover, under short day conditions, the mutant plants flower significantly earlier (10 d – 16 d) than WT. The authors also note that, except early flowering, no differences in morphology is apparent in the mutants. In general, JMJ27 seems to play a role in a multiprotein complex to integrate environmental conditions to physiological responses. In pollen, this role may also include the control of TEs (Chumak 2012). Under unfavorable conditions, its expression may be induced to provide increased fitness to the plant.

Involvement of the nucleolus, the site of rDNA transcription and processing, in stress sensing and responses as well as cell cycle control and DNA damage, were previously suggested in addition to its role in ribosome biogenesis (Boisvert et al. 2007; Shaw & Brown 2012; Lam & Trinkle-Mulcahy 2015). In humans, an HSP family protein, NKRF, was identified to monitor such stress conditions in nucleoli and to regulate rRNA processing via interacting with the spliceosome machinery under stress conditions (Coccia et al. 2017). The three HSP70 family proteins identified by MS in this study, BIP2, BIP3 and HSP70-6 (Table 9) may have a similar function in *Arabidopsis*, likewise they could be acting as a scaffold for the multi-protein complex involving JMJ27 and required for its stability. Increasing amount of evidence suggests that, beside LSM proteins and RNA processing enzymes, several other members of snoRNPs, RNA helicases, GTPases, AAA-ATPases and Gly-rich RNA binding protein families are predicted to function in rRNA maturation and ribosome biogenesis (Tanner & Linder 2001; Fatica & Tollervey 2002; Kufel, Allmang, Petfalski, et al. 2003; Raab & Hoth 2007; Lorkovic 2009). Therefore, it is likely that the spliceosome complex is associated with other networks through participation of diverse proteins that serve in multiple cellular events in plants. Interestingly, animal pre-mRNAs cannot be

spliced in plants, and this suggests that the splicing mechanism in plants involves plant-specific components that can have different functions.

The spliceosome complex is a dynamic structure requiring multiple remodeling steps during its function. DEAD-box RNA helicase proteins are known to be part of this complex, providing ATP or hydrolysis-dependent conformational changes particularly in the assembly phase (Cordin et al. 2012). Some members of the family also have an additional activity in ribosome biogenesis, e.g. in yeast, where 19 putative mostly DEAD-box family RNA helicases are required in ribosome biogenesis (Linder 2006; Bohnsack et al. 2009). One such protein, Prp43, which was originally identified for its intron removal function in pre-mRNA splicing, was shown to bind pre-rRNA and to regulate ribosome synthesis, suggesting that it possibly coordinates between these two processes (Leeds et al. 2006). EMB1138 and DRH1, which are two DEAD-box RNA helicases, are among the interaction partner candidates of JMJ27 (Table 9). Furthermore, in a preliminary test, the vegetative nucleus of pollen from *emb1138* mutants was found to resemble the *jmj27* H3K9me2 phenotype in several cases (Figure 23). In fact, a similar dual role like Prp43 has been shown for EMB1138 in chloroplast where it is required for intron splicing and ribosome biogenesis. Furthermore, a link to stress response was shown, as it is required for accurate splicing under cold and salt stress (Asakura et al. 2012; Gu et al. 2014). EMB1138 may also have a function as RNA chaperone, and it is essential for seedling growth, as homozygous mutants are embryonic lethal (Gu et al. 2014).Thus, in addition to interaction validation, it remains to be tested whether EMB1138 has the same activity in the nucleus. If similar results were also found with DRH1, this could add two new members to RNA helicases with dual functions, such as Prp43 in yeast.

The third interactor which was tested in pollen and for which the mutant produced a similar *jmj27* H3K9me2 phenotype was CCR2/GRP7 (Cold circadian rhythm and RNA binding 2/Glycine rich RNA binding protein 7) (Figure 23). CCR2/GRP7 is one of the eight glycine rich RNA binding proteins encoded in *Arabidopsis*, and its expression is highly increased during cold stress. It affects seedling growth and provides freezing tolerance under cold conditions (Kim et al. 2008; Kwak et al. 2011). As an RNA binding protein, GRP7 influences the alternative splicing process by binding to pre-mRNAs and affecting the choice of alternative 5' splice sites (Streitner et al. 2012). Moreover, it has been suggested that it acts as RNA chaperone and thus is required for increasing the stability of pre-mRNAs which are expressed throughout the stress response (Kwak et al. 2011). Interestingly, CCR2/GRP7 also negatively auto-regulates its own circadian clock-regulated transcription by causing alternatively spliced forms of its pre-mRNA that are targeted to NMD (Staiger et al. 2003; Schöning et al. 2008; Schmal et al. 2013). A role in innate immunity has been discovered in several cases. Infiltration with *Pseudomonas syringae* prevents its interaction with mRNAs of pattern

recognition receptors which results in their decreased protein levels (Jeong et al. 2011; Nicaise et al. 2013). Beside *Pseudomonas syringae*, a role in plant defense against several other pathogens was shown (Lee et al. 2012). Site directed mutation studies identified a conserved arginine-49 residue in its RNA recognition motif (RRM) domain that is crucial for the activity of CCR2/GRP7 in alternative splicing, circadian oscillation-mediated autoregulation and innate immunity (Schoening et al. 2007; Jeong et al. 2011; Streitner et al. 2012). CCR2/GRP7 also functions in floral development through the autonomous pathway by regulating the expression of FLC (Streitner et al. 2008) Remarkably, SKB1, which is an arginine methyltransferase, also acts in the same pathway by suppressing FLC expression via catalyzing H4R3sme2 on its promoter (X. Wang et al. 2007). Additionally, SKB1 methylates the Arg-141 residue of CCR2/GRP7 among other non-histone target proteins such as LSM4, and mutants display extensive splicing defects (X. Deng et al. 2010). Therefore, via arginine methylation of histone and non-histone proteins, SKB1 is part of a process in which alternative splicing regulated by circadian rhythm exists (Sanchez et al. 2010). In recent years, some of the LSM genes were also found to be involved in circadian rhythm networks in plants and mammals. Further, an *emb1644/lsm4* mutation was also shown to cause elongation of the circadian period in *Arabidopsis*, and alternative (but not constitutive) splicing was affected in mutant lines (Perez-Santángelo et al. 2014). A role of environmental conditions in this network can also be considered, since EMB1644/LSM4 and CCR2/GRP7 are both associated with stress conditions (Kim et al. 2008; Zhaoliang Zhang et al. 2011). Finally, a connection with DNA demethylation is possible since CCR2/GRP7 is a direct interactor of ROS4/IDM1 (Q. Li et al. 2015). In humans, the SKB1 homolog PRMT5 was shown to recruit DNMT3A, the *Arabidopsis* DRM1 human homolog, by H4R3 methylation (Zhao et al. 2009). In mice, 45S rDNA transcription and ribosome biogenesis was shown to be events coordinated by the circadian rhythm (Jouffe et al. 2013). Overall, a connection between these interactors seems possible. Further work to validate and specify the interaction of JMJ27 with the proteins described here should be designed and performed, to substantiate the role of JMJ27 in such networks.

The remaining two other proteins in the putative interactor list, the MADS-box protein (AT5G26630) and SHM1 (AT4G37930) (Table 9) could be also participating in JMJ27 multi-protein complexes. MADS-box family proteins are known as transcription factors regulating diverse events, coordinating many developmental activities including male and female gametophyte development and flowering time (Gramzow & Theissen 2010). They could be required for transcriptional assembly at 45S rDNA promoters. Their binding to these sequences could be tested by ChIP experiments. SHM1, the serine hydroxymethyltransferase 1, is a nucleus-encoded photorespiratory pathway protein, with a prominent function in mitochondria. However, several

research papers suggest also connections to other biological processes and functions, such as the circadian rhythm (McClung et al. 2000), cold and salt stress (Goulas et al. 2006; Zhou et al. 2012) and poly(U) RNA binding (Xu et al. 2007). Experimental validation is required to evaluate if it participates also in similar networks in the nucleus or is required for the stability of the complex via its poly(U) RNA binding function. Nevertheless, further validation tests must be conducted with all candidates described in this study to demonstrate and confirm interaction, prior to speculations about how the proteins, together with JMJ27, might be involved in demethylation of H3K9me2 and cytosine residues in the 45S rDNA promoter.

6 References

Ahmad, K. & Henikoff, S., 2002. Epigenetic consequences of nucleosome dynamics. *Cell*, 111(3), pp.281–284.

Alló, M. et al., 2009. Control of alternative splicing through siRNA-mediated transcriptional gene silencing. *Nature Structural & Molecular Biology*, 16(7), pp.717–724.

Alvarez-Venegas, R. & Avramova, Z., 2001. Two Arabidopsis homologs of the animal trithorax genes: a new structural domain is a signature feature of the trithorax gene family. *Gene*, 271(2), pp.215–221.

Asakura, Y. et al., 2012. Chloroplast RH3 DEAD box RNA helicases in maize and Arabidopsis function in splicing of specific group II introns and affect chloroplast ribosome biogenesis. *Plant Physiology*, 159(3), pp.961–974.

Balciunas, D. & Ronne, H., 1999. Evidence of domain swapping within the jumonji family of transcription factors. *Trends in Biochemical Sciences*, 25(6), pp.274–276.

Bannister, A.J. & Kouzarides, T., 2011. Regulation of chromatin by histone modifications. *Cell Research*, 21(3), pp.381–395.

Bannister, A.J. & Kouzarides, T., 2005. Reversing histone methylation. *Nature*, 436(7054), pp.1103–1106.

Bannister, A.J., Schneider, R. & Kouzarides, T., 2002. Histone methylation: dynamic or static? *Cell*, 109(7), pp.801–806.

Bartee, L., Malagnac, F. & Bender, J., 2001. Arabidopsis cmt3 chromomethylase mutations block non-CG methylation and silencing of an endogenous gene. *Genes & Development*, 15(14), pp.1753–1758.

Baumbusch, L.O. et al., 2001. The Arabidopsis thaliana genome contains at least 29 active genes encoding SET domain proteins that can be assigned to four evolutionarily conserved classes. *Nucleic Acids Research*, 29(21), pp.4319–4333.

Benoit, M. et al., 2013. Heterochromatin dynamics during developmental transitions inArabidopsis— a focus on ribosomal DNA loci. *Gene*, 526(1), pp.39–45.

Berger, S.L., 2007. The complex language of chromatin regulation during transcription. *Nature*, 447(7143), pp.407–412.

Bohnsack, M.T. et al., 2009. Prp43 bound at different sites on the pre-rRNA performs distinct functions in ribosome synthesis. *Molecular Cell*, 36(4), pp.583–592.

Boisvert, F.-M. et al., 2007. The multifunctional nucleolus. *Nature Reviews Molecular Cell Biology*, 8(7), pp.574–585.

Bostick, M. et al., 2007. UHRF1 Plays a Role in Maintaining DNA Methylation in Mammalian Cells. *Science*, 317(5845), pp.1760–1764.

Bourc'his, D., 2001. Dnmt3L and the Establishment of Maternal Genomic Imprints. *Science*, 294(5551), pp.2536–2539.

Butaye, K.M.J. et al., 2004. Stable high-level transgene expression in Arabidopsis thaliana using gene silencing mutants and matrix attachment regions. *Plant Journal*, 39(3), pp.440–449.

Cao, X.F. & Jacobsen, S.E., 2002. Role of the Arabidopsis DRM methyltransferases in de novo DNA methylation and gene silencing. *CURBIO*, 12(13), pp.1138–1144.

Chatraryamontri, A. et al., 2017. The BioGRID interaction database: 2017 update. *Nucleic Acids Research*, 45(D1), pp.D369–D379.

Chaturvedi, P., Ghatak, A. & Weckwerth, W., 2016. Pollen proteomics: from stress physiology to developmental priming. *Plant reproduction*, 29(1), pp.119–132.

Chen, Y. et al., 2015. Epigenetic events in plant male germ cell heat stress responses. *Plant reproduction*, 29(1), pp.21–29.

Chen, Z. et al., 2006. Structural Insights into Histone Demethylation by JMJD2 Family Members. *Cell*, 125(4), pp.691–702.

Cheng, X., 2014. Structural and functional coordination of DNA and histone methylation. *Cold Spring Harbor Perspectives in Biology*, 6(8), pp.a018747–a018747.

Choi, Y. et al., 2002. DEMETER, a DNA Glycosylase Domain Protein, Is Required for Endosperm Gene Imprinting and Seed Viability in Arabidopsis. *Cell*, 110(1), pp.33–42.

Chumak, N., 2012. *Control and function of epigenetic reconfiguration in the Arabidopsis thaliana male gametophyte*.

Clissold, P.M. & Ponting, C.P., 2001. JmjC: cupin metalloenzyme-like domains in jumonji, hairless and phospholipase A2beta. *Trends in Biochemical Sciences*, 26(1), pp.7–9.

Clough, S.J. & Bent, A.F., 1998. Floral dip: a simplified method for Agrobacterium-mediated transformation of Arabidopsis thaliana. *The Plant Journal*, 16(6), pp.735–743.

Coccia, M. et al., 2017. Human NF-kappa B repressing factor acts as a stress-regulated switch for ribosomal RNA processing and nucleolar homeostasis surveillance. *Proceedings of the National Academy of Sciences*, 114(5), pp.1045–1050.

Coleman-Derr, D. & Zilberman, D., 2013. DNA Methylation, H2A.Z, and the Regulation of Constitutive Expression. *Cold Spring Harbor Symposia on Quantitative Biology*, 77(0), pp.147–154.

Cordin, O., Hahn, D. & Beggs, J.D., 2012. Structure, function and regulation of spliceosomal RNA helicases. *Current Opinion in Cell Biology*, 24(3), pp.431–438.

Couture, J.-F. et al., 2008. Structural origins for the product specificity of SET domain protein methyltransferases. *PNAS*, 105(52), pp.20659–20664.

Creasey, K.M. & Martienssen, R.A., 2010. Germline reprogramming of heterochromatin in plants. *Cold Spring Harbor Symposia on Quantitative Biology*, 75(0), pp.269–274.

Del Prete, S. et al., 2014. Nuclear Architecture and Chromatin Dynamics in Interphase Nuclei of Arabidopsis thaliana. *Cytogenetic and Genome Research*, 143(1-3), pp.28–50.

Deleris, A. et al., 2010. Involvement of a Jumonji-C domain-containing histone demethylase in DRM2-mediated maintenance of DNA methylation. *EMBO reports*, 11(12), pp.950–955.

Deng, S. et al., 2015. JMJ24 binds to RDR2 and is required for the basal level transcription of silenced loci in Arabidopsis. *The Plant Journal*, 83(5), pp.770–782.

Deng, X. et al., 2010. Arginine methylation mediated by the Arabidopsis homolog of PRMT5 is essential for proper pre-mRNA splicing. *Proceedings of the National Academy of Sciences*, 107(44), pp.19114–19119.

Dimitri, P. et al., 2009. Constitutive heterochromatin: a surprising variety of expressed sequences. *Chromosoma*, 118(4), pp.419–435.

Dutta, A. et al., 2017. JMJ27, an Arabidopsis H3K9 histone demethylase, modulates defense against Pseudomonas syringae and flowering time. *The Plant Journal*, 22, p.1425.

Earley, K. et al., 2006. Gateway-compatible vectors for plant functional genomics and proteomics. *The Plant Journal*.

Eymery, A., Callanan, M. & Vourc'h, C., 2009. The secret message of heterochromatin: new insights into the mechanisms and function of centromeric and pericentric repeat sequence transcription. *The International Journal of Developmental Biology*, 53(2-3), pp.259–268.

Fatica, A. & Tollervey, D., 2002. Making ribosomes. *Current Opinion in Cell Biology*, 14(3), pp.313–318.

Fedoroff, N.V., 2012. Presidential address. Transposable elements, epigenetics, and genome evolution., 338(6108), pp.758–767.

Feng, Q. et al., 2002. Methylation of H3-lysine 79 is mediated by a new family of HMTases without a SET domain. *CURBIO*, 12(12), pp.1052–1058.

Fragkostefanakis, S. et al., 2016. Unfolded protein response in pollen development and heat stress tolerance. *Plant reproduction*, 29(1), pp.81–91.

Freemont, P.S., 1993. The RING finger. A novel protein sequence motif related to the zinc finger. *Annals of the New York Academy of Sciences*, 684, pp.174–192.

Fuchs, J. et al., 2006. Chromosomal histone modification patterns – from conservation to diversity. *Trends in Plant Science*, 11(4), pp.199–208.

Furner, I.J. & Matzke, M., 2011. Methylation and demethylation of the Arabidopsis genome. *Current Opinion in Plant Biology*, 14(2), pp.5–5.

Gamsjaeger, R. et al., 2007. Sticky fingers: zinc-fingers as protein-recognition motifs. *Trends in Biochemical Sciences*, 32(2), pp.63–70.

Gan, E.-S., Xu, Y. & Ito, T., 2015. Dynamics of H3K27me3 methylation and demethylation in plant development. *Plant Signaling & Behavior*, 10(9), pp.e1027851–8.

Gehring, M., Bubb, K.L. & Henikoff, S., 2009. Extensive Demethylation of Repetitive Elements During Seed Development Underlies Gene Imprinting. *Science*, 324(5933), pp.1447–1451.

Golisz, A. et al., 2013. Arabidopsis thaliana LSM proteins function in mRNA splicing and degradation. *Nucleic Acids Research*, 41(12), pp.6232–6249.

Goll, M.G., 2006. Methylation of tRNAAsp by the DNA methyltransferase homolog Dnmt2. *Science*, 311(5759), pp.395–398.

Goodrich, J. et al., 1997. A polycomb-group gene regulates homeotic gene expression in Arabidopsis. *Nature*, 386(6620), pp.44–51.

Goulas, E. et al., 2006. The chloroplast lumen and stromal proteomes of Arabidopsis thaliana show differential sensitivity to short- and long-term exposure to low temperature. *Plant Journal*, 47(5), pp.720–734.

Gramzow, L. & Theissen, G., 2010. A hitchhiker's guide to the MADS world of plants. *Genome biology*, 11(6), p.214.

Grewal, S.I.S. & Jia, S., 2007. Heterochromatin revisited. *Nature Reviews Genetics*, 8(1), pp.35–46.

Grossniklaus, U. et al., 1998. Maternal control of embryogenesis by MEDEA, a polycomb group gene in Arabidopsis. *Science*, 280(5362), pp.446–450.

Gu, L. et al., 2014. A chloroplast-localized DEAD-box RNA helicaseAtRH3 is essential for intron splicing and plays an important role in the growth and stress response in Arabidopsis thaliana. *Plant physiology and biochemistry : PPB*, 82, pp.309–318.

Hall, L.E., Mitchell, S.E. & O'Neill, R.J., 2012. Pericentric and centromeric transcription: a perfect balance required. *Chromosome research : an international journal on the molecular, supramolecular and evolutionary aspects of chromosome biology*, 20(5), pp.535–546.

Hall, T.M.T., 2005. Multiple modes of RNA recognition by zinc finger proteins. *Current Opinion in Structural Biology*, 15(3), pp.367–373.

Hata, K. et al., 2002. Dnmt3L cooperates with the Dnmt3 family of de novo DNA methyltransferases to establish maternal imprints in mice., 129(8), pp.1983–1993.

He, W. & Parker, R., 2000. Functions of Lsm proteins in mRNA degradation and splicing. *Current Opinion in Cell Biology*, 12(3), pp.346–350.

Heitz, E., 1928. Das Heterochromatin der Moose. I. Jahrb Wiss Bot, 69:762-818.

Holliday, R., 2006. Epigenetics: a historical overview. *Epigenetics*, 1(2), pp.76–80.

Hsieh, T.-F. et al., 2011. Regulation of imprinted gene expression in Arabidopsis endosperm. *PNAS*, 108(5), pp.1755–1762.

Hsieh, T.F. et al., 2009. Genome-Wide Demethylation of Arabidopsis Endosperm. *Science*, 324(5933), pp.1451–1454.

Huang, D.W., Sherman, B.T. & Lempicki, R.A., 2009a. Bioinformatics enrichment tools: paths toward the comprehensive functional analysis of large gene lists. *Nucleic Acids Research*, 37(1), pp.1–13.

Huang, D.W., Sherman, B.T. & Lempicki, R.A., 2009b. Systematic and integrative analysis of large

gene lists using DAVID bioinformatics resources. *Nature Protocols*, 4(1), pp.44–57.

Huisinga, K.L., Brower-Toland, B. & Elgin, S., 2006. The contradictory definitions of heterochromatin: transcription and silencing. *Chromosoma*, 115(2), pp.110–122.

Ibarra, C.A. et al., 2012. Active DNA Demethylation in Plant Companion Cells Reinforces Transposon Methylation in Gametes. *Science*, 337(6100), pp.1360–1364.

Jackson, J.P. et al., 2002. Control of CpNpG DNA methylation by the KRYPTONITE histone H3 methyltransferase. *Nature*, 416(6880), pp.556–560.

Jacob, Y. et al., 2009. ATXR5 and ATXR6 are H3K27 monomethyltransferases required for chromatin structure and gene silencing. *Nature Structural & Molecular Biology*, 16(7), pp.763–768.

Jenuwein, T., 2001. Translating the histone code. *Science*, 293(5532), pp.1074–1080.

Jeong, B.-R. et al., 2011. Structure function analysis of an ADP-ribosyltransferase type III effector and its RNA-binding target in plant immunity. *Journal of Biological Chemistry*, 286(50), pp.43272–43281.

Jiang, D. et al., 2007. Arabidopsis relatives of the human lysine-specific Demethylase1 repress the expression of FWA and FLOWERING LOCUS C and thus promote the floral transition. *THE Plant Cell Online*, 19(10), pp.2975–2987.

Joazeiro, C.A. et al., 1999. The tyrosine kinase negative regulator c-Cbl as a RING-type, E2-dependent ubiquitin-protein ligase. *Science*, 286(5438), pp.309–312.

Jouffe, C. et al., 2013. The circadian clock coordinates ribosome biogenesis. P. E. Hardin, ed. *PLoS Biology*, 11(1), p.e1001455.

Kim, J.S. et al., 2008. Glycine-rich RNA-binding protein 7 affects abiotic stress responses by regulating stomata opening and closing in Arabidopsis thaliana. *The Plant Journal*, 55(3), pp.455–466.

Klose, R.J., Kallin, E.M. & Zhang, Y., 2006. JmjC-domain-containing proteins and histone demethylation. *Nature Reviews Genetics*, 7(9), pp.715–727.

Kornberg, R.D. & Lorch, Y., 1999. Twenty-Five Years of the Nucleosome, Fundamental Particle of the Eukaryote Chromosome. *Cell*, 98(3), pp.285–294.

Krishnakumar, V. et al., 2015. Araport: the Arabidopsis Information Portal. *Nucleic Acids Research*, 43(D1), pp.D1003–D1009.

Krishnakumar, V. et al., 2017. ThaleMine: A Warehouse for Arabidopsis Data Integration and Discovery. *Plant and Cell Physiology*, 58(1).

Kufel, J. et al., 2002. Lsm proteins are required for normal processing of pre-tRNAs and their efficient association with La-homologous protein Lhp1p. *Molecular and Cellular Biology*, 22(14), pp.5248–5256.

Kufel, J., Allmang, C., Petfalski, E., et al., 2003. Lsm Proteins are required for normal processing and stability of ribosomal RNAs. *Journal of Biological Chemistry*, 278(4), pp.2147–2156.

Kufel, J., Allmang, C., Verdone, L., et al., 2003. A complex pathway for 3' processing of the yeast U3 snoRNA. *Nucleic Acids Research*, 31(23), pp.6788–6797.

Kunert, N., 2003. A Dnmt2-like protein mediates DNA methylation in Drosophila. 130(21), pp.5083–5090.

Kwak, K.J. et al., 2011. Structural determinants crucial to the RNA chaperone activity of glycine-rich RNA-binding proteins 4 and 7 in Arabidopsis thaliana during the cold adaptation process. *Journal of Experimental Botany*, 62(11), pp.4003–4011.

Kwon, S.H. & Workman, J.L., 2011. The changing faces of HP1: From heterochromatin formation and gene silencing to euchromatic gene expression. *BioEssays*, 33(4), pp.280–289.

Lam, Y.W. & Trinkle-Mulcahy, L., 2015. New insights into nucleolar structure and function. *F1000prime reports*, 7(48), p.48.

Law, J.A. & Jacobsen, S.E., 2010. Establishing, maintaining and modifying DNA methylation patterns in plants and animals. *Nature Reviews Genetics*, 11(3), pp.204–220.

Lee, H.J. et al., 2012. Different roles of glycine-rich RNA-binding protein7 in plant defense against Pectobacterium carotovorum, Botrytis cinerea, and tobacco mosaic viruses. *Plant physiology and biochemistry : PPB*, 60, pp.46–52.

Leeds, N.B. et al., 2006. The splicing factor Prp43p, a DEAH box ATPase, functions in ribosome biogenesis. *Molecular and Cellular Biology*, 26(2), pp.513–522.

Li, C.F. et al., 2006. An ARGONAUTE4-Containing Nuclear Processing Center Colocalized with Cajal Bodies in Arabidopsis thaliana. *Cell*, 126(1), pp.93–106.

Li, J.-F. et al., 2009. The FAST technique: a simplified Agrobacterium-based transformation method for transient gene expression analysis in seedlings of Arabidopsis and other plant species. *Plant Methods*, 5(1), p.6.

Li, Q. et al., 2015. Regulation of Active DNA Demethylation by a Methyl-CpG-Binding Domain Protein in Arabidopsis thaliana C. S. Pikaard, ed. *PLoS Genetics*, 11(5).

Linder, P., 2006. Dead-box proteins: a family affair--active and passive players in RNP-remodeling. *Nucleic Acids Research*, 34(15), pp.4168–4180.

Lindroth, A.M., 2001. Requirement of CHROMOMETHYLASE3 for Maintenance of CpXpG Methylation. *Science*, 292(5524), pp.2077–2080.

Lorkovic, Z.J., 2009. Role of plant RNA-binding proteins in development, stress response and genome organization. *Trends in Plant Science*, 14(4), pp.229–236.

Lu, F. et al., 2008. Comparative analysis of JmjC domain-containing proteins reveals the potential histone demethylases in Arabidopsis and rice. *Journal of Integrative Plant Biology*, 50(7), pp.886–896.

Luco, R.F. et al., 2010. Regulation of alternative splicing by histone modifications. *Science*, 327(5968), pp.996–1000.

Luger, K. et al., 1997. Crystal structure of the nucleosome core particle at 2.8|[thinsp]||[Aring]|

resolution. *Nature*, 389(6648), pp.251–260.

Luo, M. et al., 2013. Histone Lysine Demethylases and Their Functions in Plants. *Plant Molecular Biology Reporter*, 32(2), pp.558–565.

Mann, M. et al., 1998. Mass spectrometry and EST-database searching allows characterization of the multi-protein spliceosome complex. *Nature Genetics*, 20(1), pp.46–50.

Matzke, M.A. & Mosher, R.A., 2014. RNA-directed DNA methylation: an epigenetic pathway of increasing complexity. *Nature Reviews Genetics*, 15(6), pp.394–408.

McClung, C.R. et al., 2000. Integrated temporal regulation of the photorespiratory pathway. Circadian regulation of two Arabidopsis genes encoding serine hydroxymethyltransferase. *PLANT PHYSIOLOGY*, 123(1), pp.381–392.

Mérai, Z. et al., 2014. The AAA-ATPase molecular chaperone Cdc48/p97 disassembles sumoylated centromeres, decondenses heterochromatin, and activates ribosomal RNA genes. *PNAS*, 111(45), pp.16166–16171.

Millanes-Romero, A. et al., 2013. Regulation of Heterochromatin Transcription by Snail1/LOXL2 during Epithelial-to-Mesenchymal Transition. *Molecular Cell*, 52(5), pp.746–757.

Miura, A. et al., 2009. An Arabidopsis jmjC domain protein protects transcribed genes from DNA methylation at CHG sites. *EMBO Journal*, 28(8), pp.1078–1086.

Murray, N.E., 2002. Immigration control of DNA in bacteria: self versus non-self. *Microbiology-Sgm*, 148(Pt 1), pp.3–20.

Müller, F. & Rieu, I., 2016. Acclimation to high temperature during pollen development. *Plant reproduction*, 29(1), pp.107–118.

Neubauer, G. et al., 1998. Mass spectrometry and EST-database searching allows characterization of the multi-protein spliceosome complex. *Nature Genetics*, 20(1), pp.46–50.

Nicaise, V. et al., 2013. Pseudomonas HopU1 modulates plant immune receptor levels by blocking the interaction of their mRNAs with GRP7. *EMBO Journal*, 32(5), pp.701–712.

Ooi, S.K.T.S. et al., 2007. DNMT3L connects unmethylated lysine 4 of histone H3 to de novo methylation of DNA. *Nature*, 448(7154), pp.714–717.

Otani, J. et al., 2009. Structural basis for recognition of H3K4 methylation status by the DNA methyltransferase 3A ATRX–DNMT3–DNMT3L domain. *EMBO reports*, 10(11), pp.1235–1241.

Park, J.-S. et al., 2017. Control of DEMETER DNA demethylase gene transcription in male and female gamete companion cells in Arabidopsis thaliana. *Proceedings of the National Academy of Sciences*, 114(8), pp.2078–2083.

Penterman, J., Uzawa, R. & Fischer, R.L., 2007. Genetic Interactions between DNA Demethylation and Methylation in Arabidopsis. *Plant Physiology*, 145(4), pp.1549–1557.

Penterman, J., Zilberman, D., et al., 2007. DNA demethylation in the Arabidopsis genome. *PNAS*, 104(16), pp.6752–6757.

Perez-Santángelo, S. et al., 2014. Role for LSM genes in the regulation of circadian rhythms. *PNAS*, 111(42), pp.15166–15171.

Peters, A.H.F.M. et al., 2001. Loss of the Suv39h Histone Methyltransferases Impairs Mammalian Heterochromatin and Genome Stability. *Cell*, 107(3), pp.323–337.

Pfluger, J. & Wagner, D., 2007. Histone modifications and dynamic regulation of genome accessibility in plants. *Current Opinion in Plant Biology*, 10(6), pp.645–652.

Pidoux, A.L. & Allshire, R.C., 2005. The role of heterochromatin in centromere function. *Philosophical transactions of the Royal Society of London. Series B, Biological sciences*, 360(1455), pp.569–579.

Pikaard, C.S. & Mittelsten Scheid, O., 2014. Epigenetic Regulation in Plants. *Cold Spring Harbor Perspectives in Biology*, 6(12), pp.a019315–a019315.

Ponferrada-Marín, M.I., Roldán-Arjona, T. & Ariza, R.R., 2012. Demethylation initiated by ROS1 glycosylase involves random sliding along DNA. *Nucleic Acids Research*, 40(22), pp.11554–11562.

Prakash, S., Singh, R. & Lodhi, N., 2014. Histone demethylases and control of gene expression in plants. *Cellular and molecular biology (Noisy-le-Grand, France)*, 60(5), pp.97–105.

Probst, A.V. & Mittelsten Scheid, O., 2015. ScienceDirect Stress-induced structural changes in plant chromatin. *Current Opinion in Plant Biology*, 27, pp.8–16.

Qian, W. et al., 2012. A Histone Acetyltransferase Regulates Active DNA Demethylation in Arabidopsis. *Science*, 336(6087), pp.1445–1448.

Raab, S. & Hoth, S., 2007. A mutation in the AtPRP4 splicing factor gene suppresses seed development in Arabidopsis. *Plant biology (Stuttgart, Germany)*, 9(3), pp.447–452.

Ramsahoye, B.H. et al., 2000. Non-CpG methylation is prevalent in embryonic stem cells and may be mediated by DNA methyltransferase 3a. *PNAS*, 97(10), pp.5237–5242.

Ringrose, L. & Paro, R., 2004. Epigenetic Regulation of Cellular Memory by the Polycomb and Trithorax Group Proteins. *dx.doi.org*, 38(1), pp.413–443.

Roldán-Arjona, T. & Ariza, R.R., 2009. DNA demethylation. *DNA and RNA modification Enzymes: Comparative Structure, Mechanism, Functions, Cellular Interactions and Evolution. Landes Bioscience, Austin, TX*, pp.149–161.

Rothbart, S.B. & Strahl, B.D., 2014. Interpreting the language of histone and DNA modifications. *BBA - Gene Regulatory Mechanisms*, pp.1–17.

Saksouk, N., Simboeck, E. & Déjardin, J., 2015. Constitutive heterochromatin formation and transcription in mammals. *Epigenetics & Chromatin*, 8(1), p.3.

Sanchez, S.E. et al., 2010. A methyl transferase links the circadian clock to the regulation of alternative splicing. *Nature*, 468(7320), pp.112–.

Saze, H. et al., 2008. Control of Genic DNA Methylation by a jmjC Domain-Containing Protein in Arabidopsis thaliana. *Science*, 319(5862), pp.462–465.

Schmal, C., Reimann, P. & Staiger, D., 2013. A circadian clock-regulated toggle switch explains AtGRP7 and AtGRP8 oscillations in Arabidopsis thaliana. C. V. Rao, ed. *PLoS computational biology*, 9(3), p.e1002986.

Schoeftner, S. & Blasco, M.A., 2009. A "higher order" of telomere regulation: telomere heterochromatin and telomeric RNAs. *EMBO Journal*, 28(16), pp.2323–2336.

Schoening, J.C. et al., 2007. Auto-regulation of the circadian slave oscillator component AtGRP7 and regulation of its targets is impaired by a single RNA recognition motif point mutation. *Plant Journal*, 52(6), pp.1119–1130.

Schoft, V.K. et al., 2011. Function of the DEMETER DNA glycosylase in the Arabidopsis thaliana male gametophyte. *PNAS*, 108(19), pp.8042–8047.

Schoft, V.K. et al., 2009. Induction of RNA-directed DNA methylation upon decondensation of constitutive heterochromatin. *EMBO reports*, 10(9), pp.1015–1021.

Schoft, V.K. et al., 2015. SYBR Green-activated sorting of Arabidopsis pollen nuclei based on different DNA/RNA content. *Plant reproduction*, 28(1), pp.61–72.

Schöning, J.C. et al., 2008. Reciprocal regulation of glycine-rich RNA-binding proteins via an interlocked feedback loop coupling alternative splicing to nonsense-mediated decay in Arabidopsis. *Nucleic Acids Research*, 36(22), pp.6977–6987.

Sharif, J. et al., 2007. The SRA protein Np95 mediates epigenetic inheritance by recruiting Dnmt1 to methylated DNA. *Nature*, 450(7171), pp.908–912.

Shaw, P. & Brown, J., 2012. Nucleoli: Composition, Function, and Dynamics. *PLANT PHYSIOLOGY*, 158(1), pp.44–51.

Shi, Y. et al., 2003. Histone Demethylation Mediated by the Nuclear Amine Oxidase Homolog LSD1. *Cell*, 119(7), pp.941–953.

Slama, P., 2016. Identification of family determining residues in Jumonji-C lysine demethylases: A sequence-based, family wide classification. *Proteins: Structure, Function, and Bioinformatics*, 84(3), pp.397–407.

Slotkin, R.K. & Martienssen, R., 2007. Transposable elements and the epigenetic regulation of the genome. *Nature Reviews Genetics*, 8(4), pp.272–285.

Slotkin, R.K. et al., 2009. Epigenetic Reprogramming and Small RNA Silencing of Transposable Elements in Pollen. *Cell*, 136(3), pp.461–472.

Springer, N.M. et al., 2003. Comparative analysis of SET domain proteins in maize and Arabidopsis reveals multiple duplications preceding the divergence of monocots and dicots. *Plant Physiology*, 132(2), pp.907–925.

Staiger, D. et al., 2003. The circadian clock regulated RNA-binding protein AtGRP7 autoregulates its expression by influencing alternative splicing of its own pre-mRNA. *Plant Journal*, 33(2), pp.361–371.

Strahl, B.D. & Allis, C.D., 2000. The language of covalent histone modifications. *Nature*, 403(6765), pp.41–45.

Strålfors, A. & Ekwall, K., 2011. *Heterochromatin and Euchromatin—Organization, Boundaries, and Gene Regulation*, Weinheim, Germany: Wiley-VCH Verlag GmbH & Co. KGaA.

Streitner, C. et al., 2012. An hnRNP-like RNA-binding protein affects alternative splicing by in vivo interaction with transcripts in Arabidopsis thaliana. *Nucleic Acids Research*, 40(22), pp.11240–11255.

Streitner, C. et al., 2008. The small glycine-rich RNA binding protein AtGRP7 promotes floral transition in Arabidopsis thaliana. *The Plant Journal*, 56(2), pp.239–250.

Suetake, I. et al., 2004. DNMT3L stimulates the DNA methylation activity of Dnmt3a and Dnmt3b through a direct interaction. *Journal of Biological Chemistry*, 279(26), pp.27816–27823.

Suzuki, M.M. & Bird, A., 2008. DNA methylation landscapes: provocative insights from epigenomics. *Nature Reviews Genetics*, 9(6), pp.465–476.

Takeuchi, T. et al., 1995. Gene trap capture of a novel mouse gene, jumonji, required for neural tube formation. *Genes & Development*, 9(10), pp.1211–1222.

Takeuchi, T. et al., 2006. Roles of jumonji and jumonji family genes in chromatin regulation and development. *Developmental Dynamics*, 235(9), pp.2449–2459.

Tan, M. et al., 2010. Identification of 67 Histone Marks and Histone Lysine Crotonylation as a New Type of Histone Modification. *Cell*, 146(6), pp.1016–1028.

Tanner, N.K. & Linder, P., 2001. DExD/H box RNA helicases: From generic motors to specific dissociation functions. *Molecular Cell*, 8(2), pp.251–262.

Tarakhovsky, A.A., 2010. Tools and landscapes of epigenetics. *Nature Immunology*, 11(7), pp.565–568.

Taverna, S.D. et al., 2007. How chromatin-binding modules interpret histone modifications: lessons from professional pocket pickers. *Nature Structural & Molecular Biology*, 14(11), pp.1025–1040.

Tessarz, P. & Kouzarides, T., 2014. Histone core modifications regulating nucleosome structure and dynamics. *Nature Publishing Group*, 15(11), pp.703–708.

Thorstensen, T., Grini, P.E. & Aalen, R.B., 2011. SET domain proteins in plant development. *BBA - Gene Regulatory Mechanisms*, 1809(8), pp.407–420.

Toyoda, M. et al., 2002. jumonjiDownregulates Cardiac Cell Proliferation by Repressingcyclin D1Expression. *Developmental Cell*, 5(1), pp.85–97.

Trewick, S.C., McLaughlin, P.J. & Allshire, R.C., 2005. Methylation: lost in hydroxylation? *EMBO reports*, 6(4), pp.315–320.

Trojer, P. & Reinberg, D., 2007. Facultative heterochromatin: Is there a distinctive molecular signature? *Molecular Cell*, 28(1), pp.1–13.

Tsukada, Y.-I.Y. et al., 2006. Histone demethylation by a family of JmjC domain-containing proteins. *Nature*, 439(7078), pp.811–816.

Tucker, S.L. et al., 2010. Evolutionary history of plant multisubunit RNA polymerases IV and V: subunit origins via genome-wide and segmental gene duplications, retrotransposition, and lineage-specific subfunctionalization. *Cold Spring Harbor Symposia on Quantitative Biology*, 75(0), pp.285–297.

Uetz, P. et al., 2000. A comprehensive analysis of protein-protein interactions in Saccharomyces cerevisiae. *Nature*, 403(6770), pp.623–627.

Van de Vosse, D.W. et al., 2011. Role of the nuclear envelope in genome organization and gene expression. *Wiley interdisciplinary reviews. Systems biology and medicine*, 3(2), pp.147–166.

Völkel, P. & Angrand, P.-O., 2006. The control of histone lysine methylation in epigenetic regulation. *Biochimie*, 89(1), pp.1–20.

Waddington, C.H., 1942. *An Introduction to Modern Genetics*, Routledge.

Wang, J., Jia, S.T. & Jia, S., 2016. New Insights into the Regulation of Heterochromatin. pp.1–11.

Wang, X. et al., 2007. SKB1-mediated symmetric dimethylation of histone H4R3 controls flowering time in Arabidopsis. *EMBO Journal*, 26(7), pp.1934–1941.

Woo, H.R., Dittmer, T.A. & Richards, E.J., 2008. Three SRA-Domain Methylcytosine-Binding Proteins Cooperate to Maintain Global CpG Methylation and Epigenetic Silencing in Arabidopsis T. Kakutani, ed. *PLoS Genetics*, 4(8), p.e1000156.

Wu, H. et al., 2010. Structural biology of human H3K9 methyltransferases. N. Gay, ed. *PLoS ONE*, 5(1), p.e8570.

Xu, Y., Wang, B.-C. & Zhu, Y.-X., 2007. Identification of proteins expressed at extremely low level in Arabidopsis leaves. *Biochemical and Biophysical Research Communications*, 358(3), pp.808–812.

Yamane, K. et al., 2006. JHDM2A, a JmjC-Containing H3K9 Demethylase, Facilitates Transcription Activation by Androgen Receptor. *Cell*, 125(3), pp.483–495.

Yasuhara, J.C. & Wakimoto, B.T., 2006. Oxymoron no more: the expanding world of heterochromatic genes. *Trends in genetics : TIG*, 22(6), pp.330–338.

Yu, T.-Y. et al., 2016. The Arabidopsis Receptor Kinase ZAR1 Is Required for Zygote Asymmetric Division and Its Daughter Cell Fate. G. P. Copenhaver, ed. *PLoS Genetics*, 12(3), p.e1005933.

Zemach, A. et al., 2013. The Arabidopsis Nucleosome Remodeler DDM1 Allows DNA Methyltransferases to Access H1-Containing Heterochromatin. *Cell*, 153(1), pp.193–205.

Zhang, H & Zhu, J.K., 2013. Active DNA Demethylation in Plants and Animals. *Cold Spring Harbor Symposia on Quantitative Biology*, 77(0), pp.161–173.

Zhang, Kangling et al., 2007. Distinctive core histone post-translational modification patterns in Arabidopsis thaliana. *PLoS ONE*, 2(11), p.e1210.

Zhang, Xiaoyu et al., 2006. Genome-wide high-resolution mapping and functional analysis of DNA methylation in arabidopsis. *Cell*, 126(6), pp.1189–1201.

Zhang, Xing et al., 2003. Structural basis for the product specificity of histone lysine methyltransferases. *Molecular Cell*, 12(1), pp.177–185.

Zhang, Y & Reinberg, D., 2001. Transcription regulation by histone methylation: interplay between different covalent modifications of the core histone tails. *Genes & Development*, 15(18), pp.2343–2360.

Zhang, Zhaoliang et al., 2011. Arabidopsis floral initiator SKB1 confers high salt tolerance by regulating transcription and pre-mRNA splicing through altering histone H4R3 and small nuclear ribonucleoprotein LSM4 methylation. *The Plant cell*, 23(1), pp.396–411.

Zhao, Q. et al., 2009. PRMT5-mediated methylation of histone H4R3 recruits DNMT3A, coupling histone and DNA methylation in gene silencing. *Nature Structural & Molecular Biology*, 16(3), pp.304–311.

Zheng, X. et al., 2008. ROS3 is an RNA-binding protein required for DNA demethylation in Arabidopsis. *Nature*, 455(7217), pp.1259–1262.

Zhou, H. et al., 2012. Ubiquitin-specific protease16 modulates salt tolerance in Arabidopsis by regulating Na(+)/H(+) antiport activity and serine hydroxymethyltransferase stability. *The Plant cell*, 24(12), pp.5106–5122.

Zofall, M. & Grewal, S., 2006. Swi6/HP1 recruits a JmjC domain protein to facilitate transcription of heterochromatic repeats. *Molecular Cell*, 22(5), pp.681–692.

7 List of Abbreviations:

180CEN:	180bp centromeric repeat
5meC:	5-methylcytosine
ARID:	AT-rich interaction domain
ASH1:	Absent, small or homeotic disks
BiFC:	Bimolecular fluorescence complementation
CenH3:	Centromeric histone 3 variant
ChIP:	Chromatin immunoprecipitation
DAPI:	4′,6′-diamidino-2-phenylindole
E(z):	Enhancer of zeste
EMS:	Ethyl methanesulfonate
FISH:	Fluorescence *in situ* hybridization
GFP:	Green fluorescent protein
H2B:	Histone 2B
H3:	Histone 3
H3K4me:	Histone 3 lysine 4 methylation
H3K9me2:	Histone 3 lysine 9 dimethylation
H4R3sme2	Histone 4 arginine 3 symmetric dimethylation
HAT:	Histone acetyl transferase
HDAC:	Histone deacetylase
HDM:	Histone demethylase
HKMT:	Histone lysine methyltransferase
HMT:	Histone methyl transferase
HOX:	Homeobox
HP1:	Heterochromatin binding protein
JmjC:	Jumonji C domain
LSD1:	Lysine-specific histone demethylase 1A
MS:	Mass spectrometry
NMD:	Nonsense-mediated decay
NOR:	Nucleolus organization region
PBS:	Phosphate buffered saline
PcG:	Polycomb group
PTM:	Post-translational modification
RdDM:	RNA directed DNA methylation

rDNA:	Ribosomal DNA
RFP:	Red fluorescent protein
RING:	Really interesting new gene
RRM:	RNA recognition motif
SDS:	Sodium dodecyl sulfate
SSC:	Saline-sodium citrate buffer
ssRNA:	Single strand RNA
Su(var):	Suppressor of variegation
TE:	Transposable element
TRX:	Trithorax
TrxG:	Trithorax group
VAR1:	45S rDNA variant 1
YFP:	Yellow fluorescent protein
Zinc-finger:	ZnF

8 Appendix

8.1 List of proteins identified in mass spectrometry

Appendix table 1: A total of 116 proteins, in both control and sample groups, were identified by mass spectrometry analysis. A) Relative peptide intensities were computed using mass spectra peak areas and indicated under the "Area" columns with no peptide discovery, positive discovery and the highest discovery are signified by red, yellow and the green cell(s), respectively. B) Peptide coverage percentages of mass spectrometry-identified proteins from both control and sample groups were calculated. C) Gene descriptions of identified proteins with their corresponding number of amino acid residues and molecular weights are listed.

A)

Accession	Area Control 1	Area Control 2	Area Control 3	Area Control 4	Area Control 5	Area Control 6	Area Control 7	Area Control 8	Area Sample 1	Area Sample 2	Area Sample 3	Area Sample 4	Area Sample 5	Area Sample 6	Area Sample 7	Area Sample 8
AT1G67090.1	8,310E7	6,224E7	5,408E7	3,440E7	4,381E7	3,681E7	5,339E7	4,533E7	5,408E7	3,859E7	3,245E7	3,578E7	3,566E7	4,818E7	4,139E7	6,717E7
AT5G38410.1	6,656E7	1,007E8	4,403E7	8,358E7	7,022E7	3,021E7	4,477E7	5,629E7	8,819E7	6,716E7	8,241E7	4,345E7	5,770E7	7,466E7	1,017E8	6,717E7
AT5G09810.1	3,191E7	1,211E7	5,362E6	5,424E6	2,165E7	2,993E6	1,455E6	1,056E7	1,372E7	5,487E6	7,538E6	2,920E6	1,365E7	5,855E6	4,195E6	1,959E6
AT1G80270.1	1,990E7	1,016E7	0,000E0	2,482E6	1,101E7	2,927E6	0,000E0	2,065E6	1,791E7	0,000E0	5,187E6	3,142E6	3,146E6	0,000E0	0,000E0	0,000E0
ATCG00480.1	1,736E7	2,085E7	9,162E6	6,412E6	1,952E7	1,034E6	5,299E6	6,008E6	2,825E6	0,000E0	8,504E5	1,023E7	0,000E0	1,333E7	1,865E6	1,238E7

AT4G05320.2	1,649E7	8,652E6	0,000E0	0,000E0	0,000E0	0,000E0	0,000E0	0,000E0	2,496E7	0,000E0	1,346E6	0,000E0	7,507E6	0,000E0	0,000E0	0,000E0
ATCG00490.1	1,236E7	1,598E7	2,942E7	2,429E7	1,279E7	9,764E6	5,304E6	9,032E6	7,194E6	0,000E0	1,199E7	1,329E7	3,999E6	1,141E7	1,215E7	2,325E7
AT1G07930.2	1,110E7	5,157E6	3,482E6	5,495E6	4,317E6	1,670E6	3,045E6	9,524E6	7,990E6	5,791E6	3,937E6	2,520E6	4,449E6	4,040E6	8,151E6	2,390E6
AT1G06680.2	1,073E7	1,079E7	8,433E6	7,150E6	4,632E6	7,472E6	8,080E6	1,131E7	6,564E6	4,222E6	6,783E6	6,865E6	4,541E6	9,991E6	4,911E6	5,139E6
AT2G36360.1	9,778E6	6,529E6	2,317E6	0,000E0	5,045E6	2,114E6	0,000E0	0,000E0	1,007E7	2,738E6	4,354E6	0,000E0	3,120E6	0,000E0	1,558E6	1,377E6
AT4G05180.1	9,657E6	7,777E6	6,537E6	3,265E6	3,802E6	3,830E6	4,697E6	5,690E6	6,489E6	5,501E6	4,541E6	4,509E6	2,843E6	6,528E6	3,610E6	3,166E6
AT1G22790.1	9,589E6	0,000E0	0,000E0	1,276E6	3,763E6	0,000E0	0,000E0	0,000E0	6,112E6	0,000E0	0,000E0	0,000E0	2,409E6	0,000E0	0,000E0	0,000E0
AT2G38810.1	9,412E6	0,000E0	0,000E0	0,000E0	0,000E0	0,000E0	0,000E0	0,000E0	0,000E0	0,000E0	0,000E0	0,000E0	0,000E0	0,000E0	0,000E0	0,000E0
AT5G10450.2	9,322E6	0,000E0	0,000E0	0,000E0	0,000E0	0,000E0	0,000E0	7,034E5	0,000E0	0,000E0	0,000E0	0,000E0	0,000E0	0,000E0	0,000E0	0,000E0
AT2G38540.1	9,152E6	5,440E6	5,522E6	4,770E6	6,061E6	3,158E6	5,331E6	6,084E6	0,000E0	3,474E6	5,536E6	4,780E6	0,000E0	5,457E6	5,917E6	4,479E6
AT4G21280.1	8,972E6	6,795E6	3,661E6	2,438E6	2,614E6	2,537E6	3,725E6	3,231E6	3,837E6	3,634E6	3,697E6	2,245E6	1,598E6	3,358E6	3,004E6	2,485E6
AT3G14880.2	7,190E6	0,000E0	0,000E0	0,000E0	0,000E0	0,000E0	0,000E0	0,000E0	0,000E0	0,000E0	0,000E0	0,000E0	0,000E0	0,000E0	0,000E0	0,000E0
AT5G65350.1	7,104E6	0,000E0	0,000E0	2,761E6	0,000E0	0,000E0	0,000E0	8,855E6	0,000E0	3,857E6	0,000E0	0,000E0	0,000E0	0,000E0	0,000E0	0,000E0
AT2G36530.1	6,891E6	0,000E0	0,000E0	2,226E6	0,000E0	0,000E0	0,000E0	6,652E6	0,000E0	0,000E0	0,000E0	0,000E0	0,000E0	0,000E0	0,000E0	0,000E0
AT1G16030.1	6,699E6	3,339E6	0,000E0	1,637E6	0,000E0	0,000E0	0,000E0	4,294E6	0,000E0	0,000E0	4,947E6	0,000E0	0,000E0	3,555E6	1,551E6	0,000E0

AT1G07660.1	6,211E6	5,072E6	2,097E6	3,386E6	0,000E0	0,000E0	9,768E5	5,354E6	0,000E0	3,766E6	1,661E6	2,109E6	2,092E6	1,792E6	2,684E6	1,652E6
ATCG00680.1	5,325E6	2,474E6	3,913E6	2,489E6	7,046E6	4,114E7	1,707E6	4,183E6	3,331E6	2,470E6	3,229E6	2,701E6	3,529E6	5,041E7	7,377E5	1,149E6
AT3G13920.3	5,323E6	1,832E6	1,224E6	1,729E6	2,120E6	0,000E0	1,186E6	2,573E6	0,000E0	1,737E6	2,078E6	1,139E6	2,007E6	1,740E6	9,261E5	0,000E0
AT3G62030.3	5,114E6	2,625E6	0,000E0	0,000E0	0,000E0	2,554E6	1,688E6	1,757E6	0,000E0	0,000E0	2,700E6	0,000E0	0,000E0	0,000E0	1,387E6	0,000E0
ATCG00270.1	4,773E6	3,246E6	3,851E6	4,467E6	4,684E6	2,418E6	2,474E6	3,892E6	2,475E6	2,453E6	3,542E6	6,306E6	5,073E6	3,586E6	2,127E6	2,029E6
AT1G42970.1	4,156E6	4,804E6	3,885E6	4,404E6	2,448E7	1,299E7	3,341E6	4,108E6	3,675E6	3,693E6	4,485E6	4,414E6	2,298E7	2,218E7	5,041E6	0,000E0
AT3G26650.1	4,156E6	4,804E6	3,885E6	4,404E6	1,973E7	1,612E7	3,341E6	4,108E6	3,675E6	3,693E6	4,485E6	4,414E6	1,715E7	2,620E7	5,041E6	0,000E0
AT4G14960.1	4,148E6	2,688E6	2,599E6	2,114E6	2,392E6	1,811E6	3,029E6	2,422E6	5,317E6	2,493E6	1,989E6	1,714E6	1,744E6	0,000E0	1,646E6	0,000E0
AT3G12580.1	4,132E6	1,382E6	0,000E0	0,000E0	9,395E5	0,000E0	0,000E0	2,276E6	1,903E6	0,000E0	2,976E6	0,000E0	0,000E0	0,000E0	1,949E6	1,542E6
AT1G56410.1	4,132E6	1,382E6	0,000E0	0,000E0	9,395E5	0,000E0	0,000E0	2,276E6	1,903E6	0,000E0	2,337E6	0,000E0	6,316E5	1,191E6	1,949E6	1,542E6
AT3G50820.1	3,892E6	2,100E6	1,174E6	1,925E6	0,000E0	1,516E6	1,604E6	2,202E6	0,000E0	0,000E0	1,034E6	1,204E6	0,000E0	1,671E6	9,986E5	0,000E0
AT1G13440.2	3,219E6	2,442E6	0,000E0	2,932E6	4,272E6	1,248E7	0,000E0	2,362E6	3,131E6	0,000E0	2,517E6	0,000E0	0,000E0	1,768E7	0,000E0	0,000E0
AT1G80960.3	3,176E6	0,000E0	0,000E0	0,000E0	0,000E0	0,000E0	0,000E0	0,000E0	0,000E0	4,084E6	0,000E0	0,000E0	0,000E0	0,000E0	0,000E0	0,000E0
AT4G09320.1	2,478E6	0,000E0	0,000E0	0,000E0	0,000E0	0,000E0	8,593E5	0,000E0	3,230E6	0,000E0	0,000E0	0,000E0	0,000E0	0,000E0	0,000E0	0,000E0
ATCG00020.1	1,536E6	0,000E0	0,000E0	9,766E5	0,000E0	0,000E0	0,000E0	6,468E5	0,000E0	0,000E0	5,099E5	1,276E6	9,255E5	0,000E0	0,000E0	0,000E0

AT1G27840.2	1,461E6	2,162E6	2,063E6	1,234E6	7,705E6	8,823E6	0,000E0	0,000E0	0,000E0	0,000E0	0,000E0	0,000E0	0,000E0	0,000E0	0,000E0	0,000E0
AT3G08580.1	1,333E6	8,928E5	4,471E5	1,813E6	0,000E0	0,000E0	0,000E0	0,000E0	0,000E0	0,000E0	2,578E5	3,476E5	0,000E0	5,934E5	9,089E5	0,000E0
AT4G39260.3	6,965E5	0,000E0	0,000E0	0,000E0	0,000E0	0,000E0	0,000E0	0,000E0	0,000E0	0,000E0	0,000E0	0,000E0	0,000E0	0,000E0	0,000E0	0,000E0
AT1G05450.2	0,000E0	1,212E7	0,000E0	0,000E0	0,000E0	0,000E0	0,000E0	0,000E0	0,000E0	0,000E0	0,000E0	0,000E0	0,000E0	0,000E0	0,000E0	0,000E0
ATCG00120.1	0,000E0	1,625E6	1,446E6	4,177E7	0,000E0	8,650E5	9,169E5	8,032E5	0,000E0	0,000E0	1,587E6	1,483E8	3,261E6	3,668E6	1,758E6	2,118E6
AT4G35710.1	0,000E0	1,553E6	0,000E0	0,000E0	0,000E0	7,836E5	1,099E6	1,076E6	0,000E0	0,000E0	0,000E0	0,000E0	0,000E0	1,451E6	0,000E0	0,000E0
AT4G13310.2	0,000E0	8,827E5	0,000E0	0,000E0	2,181E6	0,000E0	0,000E0	0,000E0	1,578E6	0,000E0	0,000E0	0,000E0	0,000E0	0,000E0	0,000E0	0,000E0
AT1G10630.1	0,000E0	7,213E5	0,000E0	0,000E0	0,000E0	0,000E0	1,121E6	2,090E6	0,000E0	0,000E0	3,484E5	0,000E0	1,760E6	0,000E0	1,669E6	0,000E0
AT5G62690.1	0,000E0	6,722E5	0,000E0	3,456E6	0,000E0	0,000E0	0,000E0	0,000E0	2,516E6	0,000E0	0,000E0	1,270E6	0,000E0	0,000E0	3,968E5	0,000E0
ATCG00280.1	0,000E0	0,000E0	6,165E6	7,007E6	1,821E7	1,690E7	3,433E6	6,211E6	0,000E0	0,000E0	6,055E6	3,910E6	1,138E7	3,112E7	3,250E6	3,540E6
AT5G46110.2	0,000E0	0,000E0	2,766E6	0,000E0	0,000E0	0,000E0	2,876E6	4,489E6	0,000E0	0,000E0	0,000E0	1,457E6	0,000E0	0,000E0	1,474E6	0,000E0
AT2G39730.3	0,000E0	0,000E0	2,347E6	1,960E6	4,026E6	1,305E6	1,278E6	1,350E6	0,000E0	0,000E0	1,744E6	1,244E6	8,714E6	1,783E6	1,836E6	1,836E6
ATCG00350.1	0,000E0	0,000E0	1,631E6	4,078E6	0,000E0	0,000E0	0,000E0	0,000E0	0,000E0	0,000E0	0,000E0	0,000E0	0,000E0	0,000E0	0,000E0	0,000E0
AT5G14740.2	0,000E0	0,000E0	1,318E6	1,029E6	0,000E0	0,000E0	0,000E0	2,227E6	0,000E0	0,000E0	0,000E0	0,000E0	0,000E0	0,000E0	0,000E0	1,214E6
ATMG01190.1	0,000E0	0,000E0	0,000E0	1,223E7	0,000E0	0,000E0	1,490E6	1,592E6	0,000E0	0,000E0	2,151E6	4,238E7	4,925E6	6,140E6	0,000E0	2,288E6

AT5G08670.1	0,000E0	0,000E0	0,000E0	4,806E6	0,000E0	0,000E0	0,000E0	3,709E6	2,825E6	0,000E0	0,000E0	9,398E6	0,000E0	0,000E0	0,000E0	0,000E0
AT5G12860.2	0,000E0	0,000E0	0,000E0	4,715E6	0,000E0	1,802E7	4,929E6	6,060E6	0,000E0	0,000E0	0,000E0	0,000E0	0,000E0	2,950E7	0,000E0	0,000E0
AT3G46780.1	0,000E0	0,000E0	0,000E0	4,409E6	0,000E0	0,000E0	0,000E0	0,000E0	0,000E0	0,000E0	0,000E0	1,577E6	0,000E0	0,000E0	0,000E0	0,000E0
AT4G35090.2	0,000E0	0,000E0	0,000E0	2,759E6	0,000E0	0,000E0	0,000E0	0,000E0	2,307E6	0,000E0	0,000E0	0,000E0	0,000E0	0,000E0	0,000E0	0,000E0
ATCG00340.1	0,000E0	0,000E0	0,000E0	2,280E6	1,109E7	0,000E0	1,633E6	0,000E0	0,000E0	0,000E0	0,000E0	0,000E0	4,258E6	0,000E0	1,240E6	0,000E0
AT4G38970.1	0,000E0	0,000E0	0,000E0	1,168E6	0,000E0	1,434E6	6,124E5	6,868E5	0,000E0	0,000E0	0,000E0	0,000E0	5,190E5	2,951E6	7,520E5	0,000E0
AT2G21330.3	0,000E0	0,000E0	0,000E0	1,113E6	0,000E0	1,229E6	6,124E5	6,868E5	0,000E0	0,000E0	0,000E0	0,000E0	5,190E5	3,981E6	6,074E5	0,000E0
AT3G53420.1	0,000E0	0,000E0	0,000E0	1,082E6	7,839E6	0,000E0	0,000E0	1,287E6	0,000E0	0,000E0	0,000E0	0,000E0	0,000E0	0,000E0	0,000E0	0,000E0
AT5G60660.1	0,000E0	0,000E0	0,000E0	1,082E6	4,256E6	0,000E0	0,000E0	1,587E6	0,000E0	0,000E0	0,000E0	0,000E0	0,000E0	0,000E0	0,000E0	0,000E0
AT1G13930.1	0,000E0	0,000E0	0,000E0	1,052E6	0,000E0	7,041E5	1,069E6	1,330E6	0,000E0	0,000E0	1,127E6	1,007E6	0,000E0	1,597E6	0,000E0	0,000E0
AT4G01050.1	0,000E0	0,000E0	0,000E0	8,337E5	0,000E0	0,000E0	0,000E0	0,000E0	0,000E0	0,000E0	0,000E0	1,002E6	0,000E0	0,000E0	0,000E0	0,000E0
AT3G21210.1	0,000E0	0,000E0	0,000E0	0,000E0	2,889E7	0,000E0	0,000E0	0,000E0	0,000E0	0,000E0	0,000E0	0,000E0	0,000E0	0,000E0	0,000E0	0,000E0
AT3G14210.1	0,000E0	0,000E0	0,000E0	0,000E0	1,623E7	0,000E0	0,000E0	0,000E0	0,000E0	0,000E0	0,000E0	0,000E0	9,490E6	0,000E0	0,000E0	0,000E0
ATCG01110.1	0,000E0	0,000E0	0,000E0	0,000E0	3,985E6	0,000E0	0,000E0	0,000E0	0,000E0	0,000E0	0,000E0	0,000E0	7,288E5	0,000E0	0,000E0	0,000E0
AT1G01620.2	0,000E0	0,000E0	0,000E0	0,000E0	3,484E6	7,727E5	0,000E0	0,000E0	0,000E0	0,000E0	0,000E0	0,000E0	0,000E0	0,000E0	0,000E0	0,000E0

AT4G14670.1	0,000E0	0,000E0	0,000E0	0,000E0	2,554E6	0,000E0	0,000E0	0,000E0	0,000E0	0,000E0	0,000E0	0,000E0	0,000E0	0,000E0	3,915E6	0,000E0
AT1G71695.1	0,000E0	0,000E0	0,000E0	0,000E0	2,429E6	0,000E0	0,000E0	0,000E0	0,000E0	0,000E0	0,000E0	0,000E0	0,000E0	0,000E0	0,000E0	0,000E0
AT5G64290.1	0,000E0	0,000E0	0,000E0	0,000E0	2,226E6	0,000E0	0,000E0	0,000E0	0,000E0	0,000E0	0,000E0	0,000E0	0,000E0	0,000E0	0,000E0	0,000E0
AT2G39010.1	0,000E0	0,000E0	0,000E0	0,000E0	1,928E6	0,000E0	0,000E0	9,911E5	0,000E0	0,000E0	0,000E0	0,000E0	0,000E0	0,000E0	0,000E0	0,000E0
AT4G10040.1	0,000E0	0,000E0	0,000E0	0,000E0	1,820E6	0,000E0	2,352E6	1,090E6	0,000E0	0,000E0	0,000E0	0,000E0	0,000E0	0,000E0	0,000E0	0,000E0
AT1G30380.1	0,000E0	0,000E0	0,000E0	0,000E0	1,479E6	0,000E0	7,719E5	0,000E0	0,000E0	0,000E0	0,000E0	0,000E0	0,000E0	0,000E0	0,000E0	0,000E0
AT4G18360.2	0,000E0	0,000E0	0,000E0	0,000E0	1,420E6	0,000E0	0,000E0	0,000E0	0,000E0	0,000E0	0,000E0	0,000E0	0,000E0	3,685E6	0,000E0	0,000E0
AT4G04640.1	0,000E0	0,000E0	0,000E0	0,000E0	0,000E0	3,502E6	0,000E0	0,000E0	0,000E0	0,000E0	0,000E0	0,000E0	0,000E0	2,718E7	0,000E0	0,000E0
AT5G52470.2	0,000E0	0,000E0	0,000E0	0,000E0	0,000E0	3,026E6	0,000E0	0,000E0	0,000E0	0,000E0	0,000E0	0,000E0	0,000E0	2,755E6	0,000E0	0,000E0
AT4G27440.1	0,000E0	0,000E0	0,000E0	0,000E0	0,000E0	1,085E6	0,000E0	0,000E0	0,000E0	0,000E0	0,000E0	0,000E0	0,000E0	1,276E6	0,000E0	0,000E0
AT5G12470.1	0,000E0	0,000E0	0,000E0	0,000E0	0,000E0	5,347E5	0,000E0	0,000E0	0,000E0	0,000E0	0,000E0	0,000E0	0,000E0	1,700E6	0,000E0	0,000E0
AT5G24780.1	0,000E0	0,000E0	0,000E0	0,000E0	0,000E0	0,000E0	8,080E5	7,603E5	0,000E0	0,000E0	6,366E5	7,746E5	0,000E0	7,059E5	0,000E0	0,000E0
AT5G35530.1	0,000E0	0,000E0	0,000E0	0,000E0	0,000E0	0,000E0	0,000E0	4,708E6	0,000E0	0,000E0	0,000E0	0,000E0	0,000E0	0,000E0	0,000E0	0,000E0
AT3G07770.1	0,000E0	0,000E0	0,000E0	0,000E0	0,000E0	0,000E0	0,000E0	3,736E6	0,000E0	0,000E0	0,000E0	0,000E0	0,000E0	0,000E0	0,000E0	0,000E0
AT4G28520.3	0,000E0	0,000E0	0,000E0	0,000E0	0,000E0	0,000E0	0,000E0	2,318E6	0,000E0	0,000E0	0,000E0	0,000E0	0,000E0	0,000E0	0,000E0	0,000E0

AT3G46740.1	0,000E0	0,000E0	0,000E0	0,000E0	0,000E0	0,000E0	0,000E0	2,078E6	0,000E0	0,000E0	0,000E0	0,000E0	0,000E0	0,000E0	0,000E0	5,224E6
AT5G44120.1	0,000E0	0,000E0	0,000E0	0,000E0	0,000E0	0,000E0	0,000E0	1,468E6	0,000E0	0,000E0	0,000E0	0,000E0	0,000E0	0,000E0	0,000E0	0,000E0
AT3G13860.1	0,000E0	0,000E0	0,000E0	0,000E0	0,000E0	0,000E0	0,000E0	1,145E6	0,000E0	0,000E0	0,000E0	0,000E0	0,000E0	0,000E0	0,000E0	0,000E0
AT5G42270.1	0,000E0	0,000E0	0,000E0	0,000E0	0,000E0	0,000E0	0,000E0	5,714E5	0,000E0	0,000E0	0,000E0	0,000E0	0,000E0	0,000E0	0,000E0	0,000E0
AT5G27720.1	0,000E0	0,000E0	0,000E0	0,000E0	0,000E0	0,000E0	0,000E0	0,000E0	4,791E7	0,000E0	0,000E0	0,000E0	0,000E0	0,000E0	0,000E0	0,000E0
AT4G00990.1	0,000E0	0,000E0	0,000E0	0,000E0	0,000E0	0,000E0	0,000E0	0,000E0	3,809E7	1,279E7	0,000E0	0,000E0	0,000E0	0,000E0	2,609E7	0,000E0
AT3G20250.1	0,000E0	0,000E0	0,000E0	0,000E0	0,000E0	0,000E0	0,000E0	0,000E0	2,298E7	0,000E0	0,000E0	0,000E0	0,000E0	0,000E0	0,000E0	0,000E0
AT5G63560.1	0,000E0	0,000E0	0,000E0	0,000E0	0,000E0	0,000E0	0,000E0	0,000E0	1,416E7	0,000E0	0,000E0	0,000E0	0,000E0	0,000E0	0,000E0	0,000E0
AT3G01540.1	0,000E0	0,000E0	0,000E0	0,000E0	0,000E0	0,000E0	0,000E0	0,000E0	8,486E6	0,000E0	0,000E0	0,000E0	0,000E0	0,000E0	0,000E0	0,000E0
AT5G20950.1	0,000E0	0,000E0	0,000E0	0,000E0	0,000E0	0,000E0	0,000E0	0,000E0	6,761E6	0,000E0	0,000E0	0,000E0	0,000E0	0,000E0	0,000E0	0,000E0
AT1G15690.2	0,000E0	0,000E0	0,000E0	0,000E0	0,000E0	0,000E0	0,000E0	0,000E0	5,005E6	0,000E0	0,000E0	0,000E0	0,000E0	0,000E0	0,000E0	0,000E0
AT5G03170.1	0,000E0	0,000E0	0,000E0	0,000E0	0,000E0	0,000E0	0,000E0	0,000E0	3,648E6	0,000E0	0,000E0	0,000E0	0,000E0	0,000E0	0,000E0	0,000E0
AT3G45140.1	0,000E0	0,000E0	0,000E0	0,000E0	0,000E0	0,000E0	0,000E0	0,000E0	1,705E6	0,000E0	0,000E0	0,000E0	0,000E0	0,000E0	1,210E6	0,000E0
AT5G50920.1	0,000E0	0,000E0	0,000E0	0,000E0	0,000E0	0,000E0	0,000E0	0,000E0	0,000E0	1,660E6	0,000E0	0,000E0	0,000E0	0,000E0	7,370E5	0,000E0
AT5G49910.1	0,000E0	0,000E0	0,000E0	0,000E0	0,000E0	0,000E0	0,000E0	0,000E0	0,000E0	0,000E0	8,280E6	0,000E0	0,000E0	0,000E0	0,000E0	0,000E0

AT4G24280.1	0,000E0	0,000E0	0,000E0	0,000E0	0,000E0	0,000E0	0,000E0	0,000E0	0,000E0	0,000E0	7,172E6	0,000E0	0,000E0	0,000E0	0,000E0	0,000E0
AT3G60750.2	0,000E0	0,000E0	0,000E0	0,000E0	0,000E0	0,000E0	0,000E0	0,000E0	0,000E0	0,000E0	3,212E6	0,000E0	0,000E0	0,000E0	1,138E6	1,267E6
AT5G42020.1	0,000E0	0,000E0	0,000E0	0,000E0	0,000E0	0,000E0	0,000E0	0,000E0	0,000E0	0,000E0	2,803E6	0,000E0	0,000E0	0,000E0	8,200E5	0,000E0
AT5G26742.3	0,000E0	0,000E0	0,000E0	0,000E0	0,000E0	0,000E0	0,000E0	0,000E0	0,000E0	0,000E0	1,274E6	0,000E0	0,000E0	0,000E0	0,000E0	0,000E0
AT1G09080.2	0,000E0	0,000E0	0,000E0	0,000E0	0,000E0	0,000E0	0,000E0	0,000E0	0,000E0	0,000E0	5,263E5	0,000E0	0,000E0	0,000E0	0,000E0	0,000E0
AT5G26630.1	0,000E0	0,000E0	0,000E0	0,000E0	0,000E0	0,000E0	0,000E0	0,000E0	0,000E0	0,000E0	0,000E0	3,546E7	0,000E0	0,000E0	0,000E0	0,000E0
AT4G37930.1	0,000E0	0,000E0	0,000E0	0,000E0	0,000E0	0,000E0	0,000E0	0,000E0	0,000E0	0,000E0	0,000E0	1,773E6	0,000E0	0,000E0	0,000E0	0,000E0
AT1G48030.1	0,000E0	0,000E0	0,000E0	0,000E0	0,000E0	0,000E0	0,000E0	0,000E0	0,000E0	0,000E0	0,000E0	7,526E5	0,000E0	0,000E0	0,000E0	0,000E0
AT2G21660.2	0,000E0	0,000E0	0,000E0	0,000E0	0,000E0	0,000E0	0,000E0	0,000E0	0,000E0	0,000E0	0,000E0	5,831E5	0,000E0	0,000E0	6,269E5	0,000E0
AT1G56190.2	0,000E0	0,000E0	0,000E0	0,000E0	0,000E0	0,000E0	0,000E0	0,000E0	0,000E0	0,000E0	0,000E0	0,000E0	3,524E6	0,000E0	0,000E0	0,000E0
AT1G03630.2	0,000E0	0,000E0	0,000E0	0,000E0	0,000E0	0,000E0	0,000E0	0,000E0	0,000E0	0,000E0	0,000E0	0,000E0	0,000E0	1,233E6	0,000E0	0,000E0
AT4G25050.1	0,000E0	0,000E0	0,000E0	0,000E0	0,000E0	0,000E0	0,000E0	0,000E0	0,000E0	0,000E0	0,000E0	0,000E0	0,000E0	6,075E5	0,000E0	0,000E0
AT2G01210.1	0,000E0	0,000E0	0,000E0	0,000E0	0,000E0	0,000E0	0,000E0	0,000E0	0,000E0	0,000E0	0,000E0	0,000E0	0,000E0	0,000E0	1,284E10	0,000E0
AT2G25140.1	0,000E0	0,000E0	0,000E0	0,000E0	0,000E0	0,000E0	0,000E0	0,000E0	0,000E0	0,000E0	0,000E0	0,000E0	0,000E0	0,000E0	1,695E6	0,000E0
AT4G13940.4	0,000E0	0,000E0	0,000E0	0,000E0	0,000E0	0,000E0	0,000E0	0,000E0	0,000E0	0,000E0	0,000E0	0,000E0	0,000E0	0,000E0	1,569E6	0,000E0

AT3G52960.1	0,000E0	0,000E0	0,000E0	0,000E0	0,000E0	0,000E0	0,000E0	0,000E0	0,000E0	0,000E0	0,000E0	0,000E0	0,000E0	0,000E0	5,946E5	0,000E0
AT5G17920.1	0,000E0	0,000E0	0,000E0	0,000E0	0,000E0	0,000E0	0,000E0	0,000E0	0,000E0	0,000E0	0,000E0	0,000E0	0,000E0	0,000E0	4,424E5	0,000E0
AT2G37270.1	0,000E0	0,000E0	0,000E0	0,000E0	0,000E0	0,000E0	0,000E0	0,000E0	0,000E0	0,000E0	0,000E0	0,000E0	0,000E0	0,000E0	3,329E5	0,000E0
AT2G04842.1	0,000E0	0,000E0	0,000E0	0,000E0	0,000E0	0,000E0	0,000E0	0,000E0	0,000E0	0,000E0	0,000E0	0,000E0	0,000E0	0,000E0	0,000E0	8,554E5
AT1G24020.1	0,000E0	0,000E0	0,000E0	0,000E0	0,000E0	0,000E0	0,000E0	0,000E0	0,000E0	0,000E0	0,000E0	0,000E0	0,000E0	0,000E0	0,000E0	0,000E0
AT1G71100.1	0,000E0	0,000E0	0,000E0	0,000E0	0,000E0	0,000E0	0,000E0	0,000E0	0,000E0	0,000E0	0,000E0	0,000E0	0,000E0	0,000E0	0,000E0	0,000E0

B)

Accession	Control 1	Control 2	Control 3	Control 4	Control 5	Control 6	Control 7	Control 8	Sample 1	Sample 2	Sample 3	Sample 4	Sample 5	Sample 6	Sample 7	Sample 8
AT1G67090.1	8,33	8,33	8,33	15,00	8,33	8,33	8,33	15,00	8,33	8,33	15,00	15,00	8,33	8,33	15,00	4,44
AT5G38410.1	11,05	4,42	11,05	4,42	4,42	11,05	11,05	11,05	4,42	4,42	4,42	11,05	4,42	4,42	4,42	4,42
AT5G09810.1	10,34	10,34	7,43	7,43	13,26	7,43	2,65	12,20	7,43	10,34	10,34	7,43	19,36	10,34	2,65	2,65
AT1G80270.1	1,01	1,01		1,01	1,01	1,01		1,01	1,01		1,01	1,01	1,01			
ATCG00480.1	5,42	2,61	2,61	20,88	2,61	2,61	2,61	4,82	2,21		2,61	26,71		2,61	2,61	2,61
AT4G05320.2	11,82	19,69							11,82		21,01		11,82			
ATCG00490.1	9,19	12,94	22,76	15,45	11,27	13,57	10,65	11,27	4,18		16,70	11,27	8,56	11,27	10,86	16,28
AT1G07930.2	10,22	7,80	5,65	10,22	5,65	5,65	2,96	10,22	8,06	2,96	5,65	5,65	5,65	5,65	2,96	5,65
AT1G06680.2	4,57	10,50	10,50	10,50	10,96	10,50	10,50	10,50	4,57	4,57	10,50	10,50	10,50	10,50	10,50	10,50
AT2G36360.1	1,41	1,41	1,41		1,41	1,41			1,41	1,41	1,41		1,41		1,41	1,41
AT4G05180.1	14,78	24,35	29,57	18,70	14,35	20,00	24,35	24,35	10,43	14,35	14,35	20,00	14,35	10,00	14,35	15,65
AT1G22790.1	2,78			2,78	2,78				2,78				2,78			
AT2G38810.1	6,62															

AT5G10450.2	7,32							4,07	4,07							
AT2G38540.1	8,47	8,47	8,47	8,47	8,47	8,47	8,47	8,47		8,47	8,47	8,47		8,47	8,47	8,47
AT4G21280.1	41,70	26,01	23,77	14,35	16,14	9,87	34,53	34,08	10,76	8,52	47,09	18,39	13,45	19,28	34,08	9,87
AT3G14880.2	2,53															
AT5G65350.1	5,04			5,04				9,35		5,04						
AT2G36530.1	1,35			1,35				1,35								
AT1G16030.1	2,01	2,01		2,01				4,49			7,12			2,01	4,49	
AT1G07660.1	21,36	21,36	9,71	9,71			9,71	33,01		9,71	9,71	9,71	33,01	9,71	9,71	9,71
ATCG00680.1	2,17	4,72	4,92	8,07	10,43	13,78	2,17	2,17	2,17	2,17	2,17	2,17	6,89	12,40	2,17	2,17
AT3G13920.3	2,49	2,49	2,49	2,49	2,49		2,49	5,72		2,49	5,72	2,49	2,49	2,49	5,72	
AT3G62030.3	4,63	2,32				4,63	2,32	2,32			4,63				3,09	
ATCG00270.1	6,52	6,52	6,52	6,52	6,52	6,52	6,52	6,52	2,83	2,83	6,52	6,52	6,52	6,52	6,52	6,52
AT1G42970.1	3,36	3,36	3,36	4,92	22,15	8,05	3,36	3,36	3,36	3,36	3,36	3,36	25,50	8,05	3,36	
AT3G26650.1	3,79	3,79	3,79	5,56	11,87	13,89	3,79	3,79	3,79	3,79	3,79	3,79	9,09	13,64	3,79	
AT4G14960.1	3,51	3,51	3,51	5,85	3,51	3,51	3,51	3,51	3,51	3,51	3,51	3,51	3,51		3,51	

AT3G12580.1	2,77	1,08			1,08			5,23	1,08		10,46				2,46	2,00
AT1G56410.1	2,92	1,13			1,13			5,51	1,13		10,53		1,94	1,94	2,59	2,11
AT3G50820.1	4,53	2,11	3,63	5,74		5,74	3,63	5,74			3,63	3,63		5,74	3,63	
AT1G13440.2	4,52	4,84		4,84	4,84	15,48		4,84	4,52		9,35			12,58		
AT1G80960.3	1,73									1,73						
AT4G09320.1	5,33						5,33		5,33							
ATCG00020.1	3,12			3,68				3,12			3,68	10,20	3,68			
AT1G27840.2	1,27	1,27	1,27	1,27	1,27	1,27										
AT3G08580.1	4,72	2,10	2,10	2,10							2,10	2,10		2,10	2,10	
AT4G39260.3	10,87															
AT1G05450.2		3,90														
ATCG00120.1		1,78	1,78	27,61		2,37	5,52	4,14			5,52	35,50	3,16	9,66	5,92	7,89
AT4G35710.1		2,47				2,47	2,47	2,47						2,47		
AT4G13310.2		1,54			1,54				1,54							
AT1G10630.1		5,52					6,08	11,60			5,52		6,08		6,08	

AT5G62690.1		2,22		4,44					2,22			6,89			2,22	
ATCG00280.1			2,96	2,96	11,21	11,21	2,96	2,96			2,96	4,65	8,03	8,03	2,96	2,96
AT5G46110.2			7,41				7,41	7,41				7,41			7,41	
AT2G39730.3			3,40	8,62	8,16	3,40	3,40	5,67			3,40	5,67	9,07	3,40	3,40	3,40
ATCG00350.1			0,93	2,00												
AT5G14740.2			5,02	5,02				4,25								5,02
ATMG01190.1				5,52			1,38	1,97			1,38	6,90	1,38	1,38		1,38
AT5G08670.1				4,14				1,98	1,98			1,98				
AT5G12860.2				1,26		4,50	1,26	3,06						3,06		
AT3G46780.1				9,61								2,35				
AT4G35090.2				2,32					1,69							
ATCG00340.1				1,63	1,63		1,63						3,54		1,63	
AT4G38970.1				5,78		5,78	2,51	2,51					2,51	8,04	2,51	
AT2G21330.3				2,57		4,88	2,57	2,57					2,57	10,54	4,88	
AT3G53420.1				3,14	11,15			3,14								

AT5G60660.1			4,12	3,09	7,22			7,22								
AT1G13930.1				7,10		7,10	7,10	7,10			7,10	7,10		7,10		
AT4G01050.1				2,79								2,79				
AT3G21210.1					0,87											
AT3G14210.1					10,71								5,61			
ATCG01110.1					2,04								2,29			
AT1G01620.2					4,67	4,67										
AT4G14670.1					1,12										1,12	
AT1G71695.1					2,79											
AT5G64290.1					2,13											
AT2G39010.1					4,15			4,15								
AT4G10040.1					6,25		6,25	13,39								
AT1G30380.1					6,92		6,92									
AT4G18360.2					3,18									3,18		
AT4G04640.1						5,63								24,93		

AT5G52470.2						4,03							4,03			
AT4G27440.1						2,99							1,75			
AT5G12470.1						2,59							2,85			
AT5G24780.1							3,70	6,30			2,59	3,70	2,59			
AT5G35530.1								5,24								
AT3G07770.1								1,50								
AT4G28520.3								2,21								
AT3G46740.1								3,79								8,68
AT5G44120.1								4,56								
AT3G13860.1								1,57								
AT5G42270.1								2,13								
AT5G27720.1									5,43							
AT4G00990.1									13,69	4,76				13,93		
AT3G20250.1									1,04							
AT5G63560.1									2,35							

AT3G01540.1									0,97							
AT5G20950.1									1,44							
AT1G15690.2									1,71							
AT5G03170.1									3,66							
AT3G45140.1									1,00						1,00	
AT5G50920.1										1,40					1,40	
AT5G49910.1											16,30					
AT4G24280.1											14,07					
AT3G60750.2											4,86				2,03	2,03
AT5G42020.1											2,54				1,20	
AT5G26742.3											1,68					
AT1G09080.2											2,11					
AT5G26630.1												2,75				
AT4G37930.1												3,87				
AT1G48030.1												2,17				

AT2G21660.2												6,29			6,29	
AT1G56190.2													2,22			
AT1G03630.2														4,76		
AT4G25050.1														11,68		
AT2G01210.1															1,12	
AT2G25140.1															1,35	
AT4G13940.4															4,31	
AT3G52960.1															3,42	
AT5G17920.1															1,31	
AT2G37270.1															3,86	
AT2G04842.1																1,69
AT1G24020.1						7,74										
AT1G71100.1								2,25								

C)

Accession	Description	# AAs	MW [kDA]
AT1G67090.1	Symbols: RBCS1A ribulose bisphosphate carboxylase small chain 1A chr1:25048465-25049249 REVERSE LENGTH=180	180	20,2
AT5G38410.1	Symbols: Ribulose bisphosphate carboxylase (small chain) family protein chr5:15377501-15378306 REVERSE LENGTH=181	181	20,3
AT5G09810.1	Symbols: ACT7 actin 7 chr5:3052809-3054220 FORWARD LENGTH=377	377	41,7
AT1G80270.1	Symbols: PPR596 PENTATRICOPEPTIDE REPEAT 596 chr1:30181265-30183331 FORWARD LENGTH=596	596	67,2
ATCG00480.1	Symbols: ATPB, PB ATP synthase subunit beta chrC:52660-54156 REVERSE LENGTH=498	498	53,9
AT4G05320.2	Symbols: UBQ10 polyubiquitin 10 chr4:2718559-2719932 FORWARD LENGTH=457	457	51,2
ATCG00490.1	Symbols: RBCL ribulose-bisphosphate carboxylases chrC:54958-56397 FORWARD LENGTH=479	479	52,9
AT1G07930.2	Symbols: GTP binding Elongation factor Tu family protein chr1:2459014-2460458 FORWARD LENGTH=372	372	41,3
AT1G06680.2	Symbols: PSBP-1, OEE2, PSII-P photosystem II subunit P-1 chr1:2048076-2049186 FORWARD LENGTH=219	219	23,7
AT2G36360.1	Symbols: Galactose oxidase/kelch repeat superfamily protein chr2:15243461-15247523 REVERSE LENGTH=496	496	55,0
AT4G05180.1	Symbols: PSBQ, PSBQ-2, PSII-Q photosystem II subunit Q-2 chr4:2672093-2673170 REVERSE LENGTH=230	230	24,6

AT1G22790.1	Symbols: unknown protein chr1:8070271-8071292 FORWARD LENGTH=216	216	23,5
AT2G38810.1	Symbols: HTA8 histone H2A 8 chr2:16219444-16220679 REVERSE LENGTH=136	136	14,4
AT5G10450.2	Symbols: GRF6, AFT1, 14-3-3lambda G-box regulating factor 6 chr5:3284452-3286261 REVERSE LENGTH=246	246	27,7
AT2G38540.1	Symbols: LP1, LTP1, ATLTP1 lipid transfer protein 1 chr2:16130418-16130893 FORWARD LENGTH=118	118	11,7
AT4G21280.1	Symbols: PSBQ, PSBQA, PSBQ-1 photosystem II subunit QA chr4:11334446-11335587 FORWARD LENGTH=223	223	23,8
AT3G14880.2	Symbols: FUNCTIONS IN: molecular_function unknown; INVOLVED IN: response to karrikin; BEST *Arabidopsis thaliana* protein match is: transcription factor-related (TAIR:AT4G18650.1) chr3:5006565-5007689 FORWARD LENGTH=237	237	27,3
AT5G65350.1	Symbols: HTR11 histone 3 11 chr5:26119406-26119825 REVERSE LENGTH=139	139	15,6
AT2G36530.1	Symbols: LOS2, ENO2 Enolase chr2:15321081-15323786 REVERSE LENGTH=444	444	47,7
AT1G16030.1	Symbols: Hsp70b heat shock protein 70B chr1:5502386-5504326 REVERSE LENGTH=646	646	70,9
AT1G07660.1	Symbols: Histone superfamily protein chr1:2369212-2369523 FORWARD LENGTH=103	103	11,4
ATCG00680.1	Symbols: PSBB photosystem II reaction center protein B chrC:72371-73897 FORWARD LENGTH=508	508	56,0
AT3G13920.3	Symbols: EIF4A1, RH4, TIF4A1 eukaryotic translation initiation factor 4A1 chr3:4592635-4594094 REVERSE LENGTH=402	402	45,7
AT3G62030.3	Symbols: ROC4 rotamase CYP 4 chr3:22973708-22975139 FORWARD LENGTH=259	259	28,1

ATCG00270.1	Symbols: PSBD photosystem II reaction center protein D chrC:32711-33772 FORWARD LENGTH=353	353	39,5
AT1G42970.1	Symbols: GAPB glyceraldehyde-3-phosphate dehydrogenase B subunit chr1:16127552-16129584 FORWARD LENGTH=447	447	47,6
AT3G26650.1	Symbols: GAPA, GAPA-1 glyceraldehyde 3-phosphate dehydrogenase A subunit chr3:9795226-9796848 FORWARD LENGTH=396	396	42,5
AT4G14960.1	Symbols: TUA6 Tubulin/FtsZ family protein chr4:8548753-8550319 REVERSE LENGTH=427	427	47,2
AT3G12580.1	Symbols: HSP70, ATHSP70 heat shock protein 70 chr3:3991487-3993689 REVERSE LENGTH=650	650	71,1
AT1G56410.1	Symbols: ERD2, HSP70T-1 heat shock protein 70 (Hsp 70) family protein chr1:21117147-21119241 FORWARD LENGTH=617	617	68,3
AT3G50820.1	Symbols: PSBO2, PSBO-2, OEC33 photosystem II subunit O-2 chr3:18891008-18892311 REVERSE LENGTH=331	331	35,0
AT1G13440.2	Symbols: GAPC-2, GAPC2 glyceraldehyde-3-phosphate dehydrogenase C2 chr1:4608465-4610494 REVERSE LENGTH=310	310	33,9
AT1G80960.3	Symbols: F-box and Leucine Rich Repeat domains containing protein chr1:30416065-30418220 FORWARD LENGTH=462	462	53,1
AT4G09320.1	Symbols: NDPK1 Nucleoside diphosphate kinase family protein chr4:5923424-5924366 FORWARD LENGTH=169	169	18,8
ATCG00020.1	Symbols: PSBA photosystem II reaction center protein A chrC:383-1444 REVERSE LENGTH=353	353	38,9
AT1G27840.2	Symbols: ATCSA-1 Transducin/WD40 repeat-like superfamily protein chr1:9693332-9696257 REVERSE LENGTH=393	393	43,2
AT3G08580.1	Symbols: AAC1 ADP/ATP carrier 1 chr3:2605706-2607030 REVERSE LENGTH=381	381	41,4

AT4G39260.3	Symbols: CCR1, ATGRP8, GR-RBP8, GRP8 cold, circadian rhythm, and RNA binding 1 chr4:18274166-18274958 REVERSE LENGTH=92	92	10,2
AT1G05450.2	Symbols: Bifunctional inhibitor/lipid-transfer protein/seed storage 2S albumin superfamily protein chr1:1600004-1601086 FORWARD LENGTH=205	205	20,6
ATCG00120.1	Symbols: ATPA ATP synthase subunit alpha chrC:9938-11461 REVERSE LENGTH=507	507	55,3
AT4G35710.1	Symbols: *Arabidopsis* protein of unknown function (DUF241) chr4:16925301-16926152 FORWARD LENGTH=283	283	31,6
AT4G13310.2	Symbols: CYP71A20 cytochrome P450, family 71, subfamily A, polypeptide 20 chr4:7750453-7751856 FORWARD LENGTH=390	390	44,4
AT1G10630.1	Symbols: ATARFA1F, ARFA1F ADP-ribosylation factor A1F chr1:3513189-3514230 REVERSE LENGTH=181	181	20,6
AT5G62690.1	Symbols: TUB2 tubulin beta chain 2 chr5:25181560-25183501 FORWARD LENGTH=450	450	50,7
ATCG00280.1	Symbols: PSBC photosystem II reaction center protein C chrC:33720-35141 FORWARD LENGTH=473	473	51,8
AT5G46110.2	Symbols: APE2, TPT Glucose-6-phosphate/phosphate translocator-related chr5:18698019-18700212 FORWARD LENGTH=297	297	32,7
AT2G39730.3	Symbols: RCA rubisco activase chr2:16571174-16573345 REVERSE LENGTH=441	441	48,5
ATCG00350.1	Symbols: PSAA Photosystem I, PsaA/PsaB protein chrC:39605-41857 REVERSE LENGTH=750	750	83,2
AT5G14740.2	Symbols: CA2, CA18, BETA CA2 carbonic anhydrase 2 chr5:4760536-4762382 FORWARD LENGTH=259	259	28,3
ATMG01190.1	Symbols: ATP1 ATP synthase subunit 1 chrM:302166-303689 REVERSE LENGTH=507	507	54,9

AT5G08670.1	Symbols: ATP synthase alpha/beta family protein chr5:2818395-2821149 REVERSE LENGTH=556	556	59,6
AT5G12860.2	Symbols: DiT1 dicarboxylate transporter 1 chr5:4059850-4061919 REVERSE LENGTH=556	556	59,0
AT3G46780.1	Symbols: PTAC16 plastid transcriptionally active 16 chr3:17228766-17231021 FORWARD LENGTH=510	510	54,3
AT4G35090.2	Symbols: CAT2 catalase 2 chr4:16701105-16703215 REVERSE LENGTH=474	474	55,0
ATCG00340.1	Symbols: PSAB Photosystem I, PsaA/PsaB protein chrC:37375-39579 REVERSE LENGTH=734	734	82,4
AT4G38970.1	Symbols: FBA2 fructose-bisphosphate aldolase 2 chr4:18163714-18165659 REVERSE LENGTH=398	398	43,0
AT2G21330.3	Symbols: FBA1 fructose-bisphosphate aldolase 1 chr2:9128416-9130152 REVERSE LENGTH=389	389	41,8
AT3G53420.1	Symbols: PIP2A, PIP2, PIP2;1 plasma membrane intrinsic protein 2A chr3:19803906-19805454 REVERSE LENGTH=287	287	30,5
AT5G60660.1	Symbols: PIP2F, PIP2;4 plasma membrane intrinsic protein 2;4 chr5:24375673-24376939 REVERSE LENGTH=291	291	30,9
AT1G13930.1	Symbols: Involved in response to salt stress. Knockout mutants are hypersensitive to salt stress. chr1:4761091-4761558 FORWARD LENGTH=155	155	16,2
AT4G01050.1	Symbols: TROL thylakoid rhodanese-like chr4:455874-458175 FORWARD LENGTH=466	466	49,4
AT3G21210.1	Symbols: zinc ion binding chr3:7438241-7440756 REVERSE LENGTH=804	804	91,8
AT3G14210.1	Symbols: ESM1 epithiospecifier modifier 1 chr3:4729886-4731562 FORWARD LENGTH=392	392	44,0
ATCG01110.1	Symbols: NDHH NAD(P)H dehydrogenase subunit H chrC:122011-123192 REVERSE LENGTH=393	393	45,5

AT1G01620.2	Symbols: PIP1C, TMP-B, PIP1;3 plasma membrane intrinsic protein 1C chr1:225986-226960 REVERSE LENGTH=214	214	22,5
AT4G14670.1	Symbols: CLPB2 casein lytic proteinase B2 chr4:8410054-8412557 FORWARD LENGTH=623	623	68,9
AT1G71695.1	Symbols: Peroxidase superfamily protein chr1:26964359-26966557 FORWARD LENGTH=358	358	39,5
AT5G64290.1	Symbols: DCT, DIT2.1 dicarboxylate transport 2.1 chr5:25714495-25716642 REVERSE LENGTH=563	563	60,0
AT2G39010.1	Symbols: PIP2E, PIP2;6 plasma membrane intrinsic protein 2E chr2:16291564-16293746 FORWARD LENGTH=289	289	31,0
AT4G10040.1	Symbols: CYTC-2 cytochrome c-2 chr4:6277083-6278281 FORWARD LENGTH=112	112	12,2
AT1G30380.1	Symbols: PSAK photosystem I subunit K chr1:10722325-10723013 FORWARD LENGTH=130	130	13,2
AT4G18360.2	Symbols: Aldolase-type TIM barrel family protein chr4:10146627-10148386 REVERSE LENGTH=314	314	34,4
AT4G04640.1	Symbols: ATPC1 ATPase, F1 complex, gamma subunit protein chr4:2350761-2351882 REVERSE LENGTH=373	373	40,9
AT5G52470.2	Symbols: FIB1, FBR1, ATFIB1, ATFBR1, SKIP7 fibrillarin 1 chr5:21294290-21296409 FORWARD LENGTH=273	273	29,2
AT4G27440.1	Symbols: PORB protochlorophyllide oxidoreductase B chr4:13725648-13727107 FORWARD LENGTH=401	401	43,3
AT5G12470.1	Symbols: Protein of unknown function (DUF3411) chr5:4044950-4047290 REVERSE LENGTH=386	386	41,3
AT5G24780.1	Symbols: VSP1, ATVSP1 vegetative storage protein 1 chr5:8507783-8508889 REVERSE LENGTH=270	270	30,2
AT5G35530.1	Symbols: Ribosomal protein S3 family protein chr5:13710355-13712192 REVERSE LENGTH=248	248	27,4

AT3G07770.1	Symbols: Hsp89.1, AtHsp90.6, AtHsp90-6 HEAT SHOCK PROTEIN 89.1 chr3:2479611-2483970 FORWARD LENGTH=799	799	90,5
AT4G28520.3	Symbols: CRU3, CRC cruciferin 3 chr4:14087596-14089617 FORWARD LENGTH=453	453	50,0
AT3G46740.1	Symbols: TOC75-III, MAR1 translocon at the outer envelope membrane of chloroplasts 75-III chr3:17216104-17219296 REVERSE LENGTH=818	818	89,1
AT5G44120.1	Symbols: CRA1, ATCRA1, CRU1 RmlC-like cupins superfamily protein chr5:17756460-17757432 REVERSE LENGTH=285	285	31,6
AT3G13860.1	Symbols: HSP60-3A heat shock protein 60-3A chr3:4561704-4565133 REVERSE LENGTH=572	572	60,4
AT5G42270.1	Symbols: VAR1, FTSH5 FtsH extracellular protease family chr5:16902659-16905102 FORWARD LENGTH=704	704	75,2
AT5G27720.1	Symbols: EMB1644/LSM4 Small nuclear ribonucleoprotein family protein chr5:9815904-9817304 FORWARD LENGTH=129	129	14,3
AT4G00990.1	Symbols: Transcription factor jumonji (jmjC) domain-containing protein chr4:427035-431535 FORWARD LENGTH=840	840	96,0
AT3G20250.1	Symbols: APUM5, PUM5 pumilio 5 chr3:7059098-7062660 REVERSE LENGTH=961	961	106,9
AT5G63560.1	Symbols: HXXXD-type acyl-transferase family protein chr5:25449517-25451234 FORWARD LENGTH=426	426	47,1
AT3G01540.1	Symbols: DRH1, ATDRH1 DEAD box RNA helicase 1 chr3:213077-216142 REVERSE LENGTH=618	618	67,6
AT5G20950.1	Symbols: Glycosyl hydrolase family protein chr5:7107609-7110775 REVERSE LENGTH=624	624	67,9
AT1G15690.2	Symbols: AVP1, ATAVP3, AVP-3, AtVHP1;1 Inorganic H pyrophosphatase family protein chr1:5399115-5402185 FORWARD LENGTH=642	642	67,7

AT5G03170.1	Symbols: FLA11, ATFLA11 FASCICLIN-like arabinogalactan-protein 11 chr5:752898-753638 REVERSE LENGTH=246	246	25,6
AT3G45140.1	Symbols: LOX2, ATLOX2 lipoxygenase 2 chr3:16525437-16529233 FORWARD LENGTH=896	896	102,0
AT5G50920.1	Symbols: CLPC, ATHSP93-V, HSP93-V, DCA1, CLPC1 CLPC homologue 1 chr5:20715710-20719800 REVERSE LENGTH=929	929	103,4
AT5G49910.1	Symbols: CPHSC70-2EAT SHOCK PROTEIN 70-2, HSC70-7, cpHsc70-2 chloroplast heat shock protein 70-2 chr5:20303470-20306295 FORWARD LENGTH=718	718	76,9
AT4G24280.1	Symbols: cpHsc70-1 chloroplast heat shock protein 70-1 chr4:12590094-12593437 FORWARD LENGTH=718	718	76,5
AT3G60750.2	Symbols: Transketolase chr3:22454004-22456824 FORWARD LENGTH=740	740	79,8
AT5G42020.1	Symbols: BIP, BIP2 Heat shock protein 70 (Hsp 70) family protein chr5:16807697-16810480 REVERSE LENGTH=668	668	73,5
AT5G26742.3	Symbols: EMB1138 DEAD box RNA helicase (RH3) chr5:9285540-9288618 REVERSE LENGTH=655	655	70,8
AT1G09080.2	Symbols: BIP3 Heat shock protein 70 (Hsp 70) family protein chr1:2929268-2931804 REVERSE LENGTH=665	665	74,0
AT5G26630.1	Symbols: MADS-box transcription factor family protein chr5:9350815-9351471 FORWARD LENGTH=218	218	25,1
AT4G37930.1	Symbols: SHM1, STM, SHMT1 serine transhydroxymethyltransferase 1 chr4:17831891-17834742 REVERSE LENGTH=517	517	57,4
AT1G48030.1	Symbols: mtLPD1 mitochondrial lipoamide dehydrogenase 1 chr1:17717432-17719141 REVERSE LENGTH=507	507	54,0
AT2G21660.2	Symbols: ATGRP7, CCR2 cold, circadian rhythm, and rna binding 2 chr2:9265477-9266316 REVERSE LENGTH=159	159	15,5

AT1G56190.2	Symbols: Phosphoglycerate kinase family protein chr1:21028622-21030454 FORWARD LENGTH=405	405	42,6
AT1G03630.2	Symbols: POR C, PORC protochlorophyllide oxidoreductase C chr1:907699-909245 FORWARD LENGTH=399	399	43,6
AT4G25050.1	Symbols: ACP4 acyl carrier protein 4 chr4:12870178-12871024 FORWARD LENGTH=137	137	14,5
AT2G01210.1	Symbols: Leucine-rich repeat protein kinase family protein chr2:119509-121734 REVERSE LENGTH=716	716	78,3
AT2G25140.1	Symbols: HSP98.7, CLPB-M, CLPB4 casein lytic proteinase B4 chr2:10697877-10701998 REVERSE LENGTH=964	964	108,6
AT4G13940.4	Symbols: HOG1, SAHH1 S-adenosyl-L-homocysteine hydrolase chr4:8054931-8056763 FORWARD LENGTH=325	325	35,5
AT3G52960.1	Symbols: Thioredoxin superfamily protein chr3:19639699-19640403 FORWARD LENGTH=234	234	24,7
AT5G17920.1	Symbols: ATCIMS, ATMETS, ATMS1 Cobalamin-independent synthase family protein chr5:5935771-5939195 FORWARD LENGTH=765	765	84,3
AT2G37270.1	Symbols: ATRPS5B, RPS5B ribosomal protein 5B chr2:15647883-15649042 REVERSE LENGTH=207	207	23,0
AT2G04842.1	Symbols: EMB2761 threonyl-tRNA synthetase, putative / threonine--tRNA ligase, putative chr2:1698466-1701271 REVERSE LENGTH=650	650	74,7
AT1G24020.1	Symbols: MLP423 MLP-like protein 423 chr1:8500653-8501458 REVERSE LENGTH=155	155	17,0
AT1G71100.1	Symbols: RSW10 Ribose 5-phosphate isomerase, type A protein chr1:26814726-26815529 FORWARD LENGTH=267	267	28,3

8.2 JMJ27 peptide coverages detected by mass spectrometry

Appendix table 2: JMJ27 peptides identified in each gel slice via in gel trypsin digestion followed by mass spectrometry analysis are represented by red bold characters. Sequence coverage scores indicate the highest coverages for the two slices from lane positions of expected JMJ27 molecular weight: Sample 1 and 7. No peptides were identified in Samples 4, 6, and 8 and controls groups C1-C8. (YPYDVPDYA: translated HA tag at C').

SAMPLE 1	SAMPLE 2
Sequence Coverage: 16%	**Sequence Coverage: 7%**
1 MEKMRGKRIR PR**DSGELVED GRSESER**KTR KKENDVVSKG RIGRGRGRGE	**1** MEKMRGKRIR PRDSGELVED GRSESERKTR KKENDVVSKG RIGRGRGRGE
51 VSKRSIEIDI SNPEKDIKPD GSRKCLGSTC HHCKILTSES DLIFCSKCNK	**51** VSKRSIEIDI SNPEKDIKPD GSRKCLGSTC HHCKILTSES DLIFCSKCNK
101 KCYCFDCIKR SYSERTHEEV RAACPFCMMT CICRACLRLP LVIKPPSEKD	**101** KCYCFDCIKR SYSERTHEEV RAACPFCMMT CICRACLRLP LVIKPPSEKD
151 TDVKLKQLQY LLVKVLPVLK DIYTEQNREL EIESTI**RGHP VTEANIKR**CK	**151** TDVKLKQLQY LLVKVLPVLK DIYTEQNR**EL EIESTIRGHP VTEANIKR**CK
201 LDPSERIYCD LCR**TSIANFH R**SCPNKNCSV DICLSCCKEL SEGFHQERDG	**201** LDPSERIYCD LCRTSIANFH RSCPNKNCSV DICLSCCKEL SEGFHQERDG
251 KKNAEGKGYE CRIPAGQGKD SDAYVPLHFS TWKLNSDSSI PCPPKECGGC	**251** KKNAEGKGYE CRIPAGQGKD SDAYVPLHFS TWKLNSDSSI PCPPKECGGC
301 GTSTLELRRL WKRDWVEK**LI TNAEK**CTLNF RPTDVDIVHE CSSCSTNSDS	**301** GTSTLELRRL WKRDWVEKLI TNAEKCTLNF RPTDVDIVHE CSSCSTNSDS
351 IRRQAAFRKN AHDNFLYSPN AVDLAEDDIA HFQFHWMKAE PVIVRNVLEK	**351** IRRQAAFRKN AHDNFLYSPN AVDLAEDDIA HFQFHWMKAE PVIVRNVLEK
401 TSGLSWEPMV MWRACREMDP KRKGTEEETT KVKALDCLDW CEVEINLHQF	**401** TSGLSWEPMV MWRACREMDP KRKGTEEETT KVKALDCLDW CEVEINLHQF
451 FEGYLEGRMH KNGWPEMLKL KDWPPSDLFE KRLPRHNAEF IAALPFFDYT	**451** FEGYLEGRMH KNGWPEMLKL KDWPPSDLFE KRLPRHNAEF IAALPFFDYT
501 DPK**SGILNLA TR**FPEGSLKP DLGPK**TYIAY GFHEELNR**GD SVTKLHCDIS	**501** DPK**SGILNLA TR**FPEGSLKP DLGPKTYIAY GFHEELNRGD SVTKLHCDIS
551 DAVNVLTHTA KVEIPPVKYQ NIKVHQK**KYA EAMLQK**QQYS GQVKEASELE	**551** DAVNVLTHTA KVEIPPVKYQ NIKVHQKKYA EAMLQKQQYS GQVKEASELE
601 NKSMKEVDES KKDLKDKAAN EEQSNNSSRP SGSGEAEKVI ISK**EDNPTQP**	**601** NKSMKEVDES KKDLKDKAAN EEQSNNSSRP SGSGEAEKVI ISKEDNPTQP
651 AVSTSVESIQ EQKLDAPKET DGNTNERSKA VHGGAVWDIF RREDVPK**LIQ**	**651** AVSTSVESIQ EQKLDAPKET DGNTNERSKA VHGGAVWDIF RREDVPK**LIQ**
701 FLKRHEHEFR HFNNEPLESV IHPIHDQTMF LSDSQKKQLK EEFDIEPWTF	**701 FLK**RHEHEFR HFNNEPLESV IHPIHDQTMF LSDSQKKQLK EEFDIEPWTF
751 EQHLGEAVFI PAGCPHQVRN RQSCIKVALD FVAPESVEEC LR**LTQEFR**RL	**751** EQHLGEAVFI PAGCPHQVRN RQSCIKVALD FVAPESVEEC LR**LTQEFR**RL
801 PK**DHSSSEDK LELKKIALYA ASSAIREVKG LMQSSR**RSDT DPAFLYKVVY	**801** PKDHSSSEDK LELKK**IALYA ASSAIR**EVKG LMQSSRR**SDT DPAFLYK**VVY
851 PYDVPDYA	**851** PYDVPDYA

SAMPLE 3	SAMPLE 5
Sequence Coverage: 1%	**Sequence Coverage**: **1%**
1 MEKMRGKRIR PRDSGELVED GRSESERKTR KKENDVVSKG RIGRGRGRGE	**1** MEKMRGKRIR PRDSGELVED GRSESERKTR KKENDVVSKG RIGRGRGRGE
51 VSKRSIEIDI SNPEKDIKPD GSRKCLGSTC HHCKILTSES DLIFCSKCNK	**51** VSKRSIEIDI SNPEKDIKPD GSRKCLGSTC HHCKILTSES DLIFCSKCNK
101 KCYCFDCIKR SYSERTHEEV RAACPFCMMT CICRACLRLP LVIKPPSEKD	**101** KCYCFDCIKR SYSERTHEEV RAACPFCMMT CICRACLRLP LVIKPPSEKD
151 TDVKLKQLQY LLVKVLPVLK DIYTEQNR**EL EIESTIR**GHP VTEANIKRCK	**151** TDVKLKQLQY LLVKVLPVLK DIYTEQNREL EIESTIRGHP VTEANIKRCK
201 LDPSERIYCD LCRTSIANFH RSCPNKNCSV DICLSCCKEL SEGFHQERDG	**201** LDPSERIYCD LCRTSIANFH RSCPNKNCSV DICLSCCKEL SEGFHQERDG
251 KKNAEGKGYE CRIPAGQGKD SDAYVPLHFS TWKLNSDSSI PCPPKECGGC	**251** KKNAEGKGYE CRIPAGQGKD SDAYVPLHFS TWKLNSDSSI PCPPKECGGC
301 GTSTLELRRL WKRDWVEKLI TNAEKCTLNF RPTDVDIVHE CSSCSTNSDS	**301** GTSTLELRRL WKRDWVEKLI TNAEKCTLNF RPTDVDIVHE CSSCSTNSDS
351 IRRQAAFRKN AHDNFLYSPN AVDLAEDDIA HFQFHWMKAE PVIVRNVLEK	**351** IRRQAAFRKN AHDNFLYSPN AVDLAEDDIA HFQFHWMKAE PVIVRNVLEK
401 TSGLSWEPMV MWRACREMDP KRKGTEEETT KVKALDCLDW CEVEINLHQF	**401** TSGLSWEPMV MWRACREMDP KRKGTEEETT KVKALDCLDW CEVEINLHQF
451 FEGYLEGRMH KNGWPEMLKL KDWPPSDLFE KRLPRHNAEF IAALPFFDYT	**451** FEGYLEGRMH KNGWPEMLKL KDWPPSDLFE KRLPRHNAEF IAALPFFDYT
501 DPKSGILNLA TRFPEGSLKP DLGPKTYIAY GFHEELNRGD SVTKLHCDIS	**501** DPKSGILNLA TRFPEGSLKP DLGPKTYIAY GFHEELNRGD SVTKLHCDIS
551 DAVNVLTHTA KVEIPPVKYQ NIKVHQKKYA EAMLQKQQYS GQVKEASELE	**551** DAVNVLTHTA KVEIPPVKYQ NIKVHQKKYA EAMLQKQQYS GQVKEASELE
601 NKSMKEVDES KKDLKDKAAN EEQSNNSSRP SGSGEAEKVI ISKEDNPTQP	**601** NKSMKEVDES KKDLKDKAAN EEQSNNSSRP SGSGEAEKVI ISKEDNPTQP
651 AVSTSVESIQ EQKLDAPKET DGNTNERSKA VHGGAVWDIF RREDVPKLIQ	**651** AVSTSVESIQ EQKLDAPKET DGNTNERSKA VHGGAVWDIF RREDVPKLIQ
701 FLKRHEHEFR HFNNEPLESV IHPIHDQTMF LSDSQKKQLK EEFDIEPWTF	**701** FLKRHEHEFR HFNNEPLESV IHPIHDQTMF LSDSQKKQLK EEFDIEPWTF
751 EQHLGEAVFI PAGCPHQVRN RQSCIKVALD FVAPESVEEC LRLTQEFRRL	**751** EQHLGEAVFI PAGCPHQVRN RQSCIKVALD FVAPESVEEC LR**LTQEFR**RL
801 PKDHSSSEDK LELKKIALYA ASSAIREVKG LMQSSRRSDT DPAFLYKVVY	**801** PKDHSSSEDK LELKK**IALYA ASSAIR**EVKG LMQSSRRSDT DPAFLYKVVY
851 PYDVPDYA	**851** PYDVPDYA

SAMPLE 7
Sequence Coverage: **17%**
1 MEKMRGKRIR PR**DSGELVED GRSESERK**TR KKENDVVSKG RIGRGRGRGE
51 VSKR**SIEIDI SNPEK**DIKPD GSRKCLGSTC HHCKILTSES DLIFCSKCNK
101 KCYCFDCIKR SYSERTHEEV RAACPFCMMT CICRACLRLP LVIKPPSEKD
151 TDVKLKQLQY LLVKVLPVLK DIYTEQNR**EL EIESTIRGHP VTEANIKR**CK
201 LDPSERIYCD LCR**TSIANFH R**SCPNKNCSV DICLSCCKEL SEGFHQERDG
251 KKNAEGKGYE CRIPAGQGKD SDAYVPLHFS TWKLNSDSSI PCPPKECGGC
301 GTSTLELRRL WKRDWVEKLI TNAEKCTLNF RPTDVDIVHE CSSCSTNSDS
351 IRRQAAFRKN AHDNFLYSPN AVDLAEDDIA HFQFHWMKAE PVIVRNVLEK
401 TSGLSWEPMV MWRACREMDP KRKGTEEETT KVKALDCLDW CEVEINLHQF
451 FEGYLEGRMH KNGWPEMLKL KDWPPSDLFE KRLPRHNAEF IAALPFFDYT
501 DPK**SGILNLA TRFPEGSLKP DLGPK**TYIAY GFHEELNRGD SVTKLHCDIS
551 DAVNVLTHTA KVEIPPVKYQ NIKVHQK**KYA EAMLQK**QQYS GQVKEASELE
601 NKSMKEVDES KKDLKDKAAN EEQSNNSSRP SGSGEAEKVI ISK**EDNPTQP**
651 **AVSTSVESIQ EQK**LDAPKET DGNTNERSKA VHGGAVWDIF RREDVPK**LIQ**
701 **FLK**RHEHEFR HFNNEPLESV IHPIHDQTMF LSDSQKKQLK EEFDIEPWTF
751 EQHLGEAVFI PAGCPHQVRN RQSCIKVALD FVAPESVEEC LR**LTQEFR**RL
801 PK**DHSSSEDK LELKKIALYA ASSAIR**EVKG LMQSSR**RSDT DPAFLYK**VVY
851 PYDVPDYA

8.3 Proteins detected only in sample group

Appendix table 3: 30 proteins including JMJ27 are filtered out of the initial list of 116 proteins based on their detection in sample groups but not in control groups. Experimental setting for the generation of each sample are denoted on top of each sample column.

		JMJ27-HA SEEDLINGS IP							
		SONICATION						NO SONICATION	
Accession	Description	Sample 1	Sample 2	Sample 3	Sample 4	Sample 5	Sample 6	Sample 7	Sample 8
AT5G27720.1	EMB1644/LSM4	4,791E7	0,000E0	0,000E0	0,000E0	0,000E0	0,000E0	0,000E0	0,000E0
AT4G00990.1	JMJ27	3,809E7	1,279E7	0,000E0	0,000E0	0,000E0	0,000E0	2,609E7	0,000E0
AT3G20250.1	PUM5	2,298E7	0,000E0	0,000E0	0,000E0	0,000E0	0,000E0	0,000E0	0,000E0
AT5G63560.1	HXXXD-type acyl-transferase family protein	1,416E7	0,000E0	0,000E0	0,000E0	0,000E0	0,000E0	0,000E0	0,000E0
AT3G01540.1	DRH1	8,486E6	0,000E0	0,000E0	0,000E0	0,000E0	0,000E0	0,000E0	0,000E0
AT5G20950.1	Glycosyl hydrolase family protein	6,761E6	0,000E0	0,000E0	0,000E0	0,000E0	0,000E0	0,000E0	0,000E0
AT1G15690.2	AVP1	5,005E6	0,000E0	0,000E0	0,000E0	0,000E0	0,000E0	0,000E0	0,000E0
AT5G03170.1	FLA11	3,648E6	0,000E0	0,000E0	0,000E0	0,000E0	0,000E0	0,000E0	0,000E0

AT3G45140.1	LOX2	1,705E6	0,000E0	0,000E0	0,000E0	0,000E0	0,000E0	1,210E6	0,000E0
AT5G50920.1	CLPC	0,000E0	1,660E6	0,000E0	0,000E0	0,000E0	0,000E0	7,370E5	0,000E0
AT5G49910.1	cpHsc70-2	0,000E0	0,000E0	8,280E6	0,000E0	0,000E0	0,000E0	0,000E0	0,000E0
AT4G24280.1	cpHsc70-1	0,000E0	0,000E0	7,172E6	0,000E0	0,000E0	0,000E0	0,000E0	0,000E0
AT3G60750.2	Transketolase	0,000E0	0,000E0	3,212E6	0,000E0	0,000E0	0,000E0	1,138E6	1,267E6
AT5G42020.1	BIP2	0,000E0	0,000E0	2,803E6	0,000E0	0,000E0	0,000E0	8,200E5	0,000E0
AT5G26742.3	EMB1138, DEAD box RNA helicase (RH3)	0,000E0	0,000E0	1,274E6	0,000E0	0,000E0	0,000E0	0,000E0	0,000E0
AT1G09080.2	BIP3	0,000E0	0,000E0	5,263E5	0,000E0	0,000E0	0,000E0	0,000E0	0,000E0
AT5G26630.1	MADS-box transcription factor family protein	0,000E0	0,000E0	0,000E0	3,546E7	0,000E0	0,000E0	0,000E0	0,000E0
AT4G37930.1	SHM1	0,000E0	0,000E0	0,000E0	1,773E6	0,000E0	0,000E0	0,000E0	0,000E0
AT1G48030.1	mtLPD1	0,000E0	0,000E0	0,000E0	7,526E5	0,000E0	0,000E0	0,000E0	0,000E0
AT2G21660.2	ATGRP7, CCR2	0,000E0	0,000E0	0,000E0	5,831E5	0,000E0	0,000E0	6,269E5	0,000E0
AT1G56190.2	Phosphoglycerate kinase family protein	0,000E0	0,000E0	0,000E0	0,000E0	3,524E6	0,000E0	0,000E0	0,000E0
AT1G03630.2	POR C	0,000E0	0,000E0	0,000E0	0,000E0	0,000E0	1,233E6	0,000E0	0,000E0
AT4G25050.1	ACP4	0,000E0	0,000E0	0,000E0	0,000E0	0,000E0	6,075E5	0,000E0	0,000E0

AT2G01210.1	Leucine-rich repeat protein kinase family protein	0,000E0	0,000E0	0,000E0	0,000E0	0,000E0	0,000E0	1,28E+10	0,000E0
AT2G25140.1	HSP98.7	0,000E0	0,000E0	0,000E0	0,000E0	0,000E0	0,000E0	1,695E6	0,000E0
AT4G13940.4	HOG1, SAHH1	0,000E0	0,000E0	0,000E0	0,000E0	0,000E0	0,000E0	1,569E6	0,000E0
AT3G52960.1	Thioredoxin superfamily protein	0,000E0	0,000E0	0,000E0	0,000E0	0,000E0	0,000E0	5,946E5	0,000E0
AT5G17920.1	ATCIMS	0,000E0	0,000E0	0,000E0	0,000E0	0,000E0	0,000E0	4,424E5	0,000E0
AT2G37270.1	RPS5B	0,000E0	0,000E0	0,000E0	0,000E0	0,000E0	0,000E0	3,329E5	0,000E0
AT2G04842.1	EMB2761, threonyl-tRNA synthetase, putative/threonine-tRNA ligase	0,000E0	0,000E0	0,000E0	0,000E0	0,000E0	0,000E0	0,000E0	8,554E5